



UCGE Reports
Number 20329

Department of Geomatics Engineering

In-Orbit Performance of the CanX-2 Nanosatellite's GPS Receiver

(URL: <http://www.geomatics.ucalgary.ca/graduatetheses>)

by

Erin Kahr

May 2011



UNIVERSITY OF CALGARY

In-Orbit Performance of the CanX-2 Nanosatellite's GPS Receiver

by

Erin Kahr

A THESIS

SUBMITTED TO THE FACULTY OF GRADUATE STUDIES
IN PARTIAL FULFILMENT OF THE REQUIREMENTS FOR THE
DEGREE OF MASTER OF SCIENCE

DEPARTMENT OF GEOMATICS ENGINEERING

CALGARY, ALBERTA

MAY, 2011

© Erin Kahr 2011

Abstract

The CanX-2 Nanosatellite is a student built satellite launched into orbit April 28th, 2008. Among its scientific payloads, CanX-2 is carrying a commercial off the shelf dual frequency geodetic grade GPS receiver. The receiver, a NovAtel OEM4-G2L, is operated intermittently and has been used for the collection of both radio occultation data and orbit determination data.

This thesis presents an empirical study of the acquisition properties of the OEM4-G2L under orbital dynamics. A method has been designed for rapidly acquiring a position fix in spite of CanX-2's orbital velocity. First hand experiences of acquisition successes and challenges in orbit have helped refine the method, ultimately cutting the average acquisition time down from 20 minutes to 3.5 minutes, at the cost of operational complexity. An algorithm enabling the same rapid acquisition without ground support has been designed based on the constraints of nanosatellite operations, and validated using CanX-2 data.

Preface

The research carried out for this thesis represents several firsts. It is the first time a dual frequency commercial GPS receiver has been successfully flown on board a student cubesat and collected scientific data. It is also the first time a NovAtel receiver has flown in space, despite earlier studies indicating that it was suitable for the application. As such, the CanX-2 radio occultation experiment has been a significant forerunner for current and future missions such as AISSat, RAX, JC2Sat, CASSIOPE and CanX-4/5, all of which are carrying or plan to carry NovAtel receivers into space.

In order to share the CanX-2 orbital experiences with the scientific community, results from operating the GPS receiver onboard CanX-2 have been previously published in two conference papers with a third in preparation:

1. Kahr, E., K. O’Keefe and S. Skone (2010) “Optimizing Tracking and Acquisition Capabilities for the CanX-2 Nanosatellite’s COTS GPS Receiver in Orbit,” *Proceedings of ION GNSS 2010*, September 21-24, Portland, Oregon.
2. Kahr, E., S. Skone and K. O’Keefe (2010) “Orbit Determination for the CanX-2 Nanosatellite Using Intermittent GPS Data,” *Proceedings of ION GNSS 2010*, September 21-24, Portland, Oregon.
3. Kahr E., O. Montenbruck, K. O’Keefe, S. Skone, J. Urbanek, L. Bradbury, and P. Fenton (2011) “GPS Tracking of a Nanosatellite – the CanX-2 Flight Experience”, in *Proceedings of the 8th International ESA Conference on Guidance, Navigation and Control Systems*, June 5-11, Carlsbad, Czech Republic.

The first two papers represent work which was carried out almost exclusively by the first author, while the third represents a collaboration of data collected by the University of Calgary and processing tools and expertise from the German Space Operations Centre.

The author’s research work from the first conference paper has been almost entirely reproduced in this thesis, with permission of the co-authors. The work represents a

significant portion of the figures and text in chapter three. The later two conference papers represent research work which only superficially overlaps with the topics of the thesis, and the papers have therefore been fully referenced in the text any place that their ideas and materials have been used.

Acknowledgements

I could not possibly have written this thesis without the support and input of a great number of people.

First, I would like to thank of my supervisor, Dr. Kyle O’Keefe, who in addition to always being willing to help with a technical question, ultimately trusted in me enough to give me complete freedom in what and where I researched. It was having the flexibility to continuously change the course of my work, to seek out expertise across the country and abroad, and to make my own judgement calls based on my experiences which made this work what it is. It is extremely rare that a graduate student be given so much freedom to pursue their own academic interests and it has made working on this project an absolute pleasure.

I would also like to acknowledge Dr. Susan Skone, the primary investigator of the CanX-2 Radio Occultation payload, whose work in setting up the experiment was the first step in making any of this research possible.

Certainly deserving of thanks are the students and staff of the University of Toronto Institute for Aerospace Studies Space Flight Lab, who put in all the time and effort I could possibly ask running experiments for me, fielding all my ignorant questions and unrealistic requests, and on numerous occasions explaining in small words that a non-aerospace engineer can understand why what I want to do won’t work. You’ve been an essential part of my learning curve, thank you.

A special thanks goes to Dr. Oliver Montenbruck, for inviting me to DLR for a hectic but extremely helpful week of data processing, and for answering my many questions since. The guidance, feedback and opportunity to play with real orbit determination software have been absolutely essential to the quality of this work.

Next I would like to thank both the JC2Sat team at the Canadian Space Agency and the professors at University of Stuttgart, each for hosting me for a semester. Both

experiences were incredible and enriching. In particular, thanks to Matthias Weigelt for repeatedly explaining inertial coordinate systems to me: TEME and I have finally settled our differences.

I would like to acknowledge the scholarship support I received during my studies from the Natural Science and Engineering Research Council of Canada, from Alberta's Informatics Circle of Research Excellence, and from the University of Calgary, which provided me the opportunity to pursue the project of my choosing.

Finally I would like to acknowledge my friends, who made sure that even in times of extreme academic stress I didn't get too deprived of vitamins B and W (beer and wings), and who came along for some healthy doses of vitamin S (skiing) as well.

At long last I would like to thank my family for their continual support, both during all of my far flung adventures and during all the times when I've been unbelievably busy with university. I apologize for any times that I've tested your patience and understanding; it is at precisely those times when your backing has meant the most to me.

Dedication

*I would like to dedicate this work to my parents Jill and Harry, and to my sister Paula.
You three more than anyone else have made me who I am today.*

Table of Contents

Approval Page.....	ii
Abstract.....	iii
Preface	iv
Acknowledgements	vi
Dedication.....	viii
Table of Contents	ix
List of Tables	xi
List of Figures and Illustrations	xii
List of Symbols, Abbreviations and Nomenclature	xvi
CHAPTER ONE: INTRODUCTION.....	1
1.1 CanX-2 GPS Research Objectives	2
1.2 A Brief Introduction to GPS	2
1.3 A Brief Introduction to GPS in Low Earth Orbit	5
1.4 Thesis Outline	7
CHAPTER TWO: THE CANX-2 MISSION	9
2.1 Launch and Orbital Parameters	10
2.2 The Radio Occultation Experiment	12
2.3 The Scientific Payload	14
2.3.1 The GPS Receiver	15
2.3.2 Qualification for Space.....	17
2.3.3 The Antenna	18
2.3.4 Antenna Mounting.....	20
2.4 Operations Onboard CanX-2.....	22
2.4.1 Power Budget	22
2.4.2 Ground Contact	24
2.4.3 Onboard Memory	26
2.4.4 Attitude Control System	26
2.4.5 Experimental Schedule	28
CHAPTER THREE: LESSONS LEARNED IN ORBIT.....	30
3.1 Acquisition Challenge.....	31
3.2 Previous Work.....	32
3.3 Script Generation.....	33
3.4 Script Format.....	35
3.5 Initial Results.....	37
3.6 Improvements.....	39
3.6.1 Pointing Direction	39
3.6.2 Doppler Assignment.....	41
3.6.2.1 Potential Causes of Frequency Drift	42
3.6.2.2 Frequency Drift Modelling.....	44
3.6.3 Antenna Field of View.....	48
3.6.4 Script Formatting.....	52
3.6.5 Memory Usage	54

3.7 Script Generation for Long Data Arcs.....	57
3.8 Effectiveness of Channel Assignment.....	59
CHAPTER FOUR: A PROPOSED METHODOLOGY FOR AUTONOMOUS	
ORBIT PROPAGATION	63
4.1 Fundamentals of Satellite Orbits	64
4.2 Orbital Propagation.....	67
4.2.1 Analytical Orbital Propagators versus Numerical Integrators	67
4.2.2 Why SGP4?.....	69
4.2.3 The SGP4 Algorithm	70
4.3 Estimating Two Line Elements	72
4.3.1 Previous Work.....	72
4.3.2 Least Squares Estimation.....	74
4.3.3 The Least Squares Algorithm.....	75
4.3.3.1 Estimated Parameters	76
4.3.3.2 Observations	77
4.3.3.3 Coordinate Systems.....	80
4.3.3.4 Weight Matrix.....	84
4.3.3.5 Outlier Detection.....	86
4.3.3.6 Design Matrix	88
4.3.3.7 Misclosure Vector	89
4.3.3.8 SGP4 Version.....	89
4.3.3.9 Convergence Criteria.....	90
4.3.3.10 Point of Expansion	90
4.4 Preliminary Results.....	93
CHAPTER FIVE: RESULTS.....	96
5.1 Experimental Setup.....	96
5.2 Initial Results.....	98
5.3 NORAD Assessment	101
5.4 Fixed Drag Results	104
5.5 Optimum Operating Scheme.....	108
5.6 Suitability of Onboard TLE Estimation for Rapid Acquisition	110
CHAPTER SIX: CONCLUSIONS AND FUTURE WORK.....	117
6.1 Conclusions from Operation in Orbit	117
6.2 Suitability of the Proposed Operating Scheme	118
6.3 Current Work.....	120
6.4 Future Work	120
REFERENCES.....	123
APPENDIX A: RECEIVER CONFIGURATION ON BOARD CANX-2.....	130
APPENDIX B: CANX-2 DATA COLLECTIONS	132
APPENDIX C: PRECISE ORBIT DETERMINATION	139

List of Tables

Table 2.1: Version Information for the NovAtel GPS receiver on board CanX-2	15
Table 2.2: Specifications for the NovAtel GPS receiver on board CanX-2 (NovAtel 2003, 2006)	16
Table 2.3: Specifications for the GPS Antenna on board CanX-2 (AeroAntenna 2003)	19
Table 2.4: Excerpt from the contact schedule for NTS and CanX-2, showing contact details for November 27, 2010 (Bradbury 2010)	25
Table 3.1: Time to First Fix Averages from December 2009 to January 2010 radio occultation data collection.....	60
Table 3.2: Time to First Fix Averages from November 2010 long arc data collection	61
Table 4.1: Two Line Elements necessary for SGP4 propagation	72
Table 4.2: Possible parameterisations for the TLE estimation	77
Table 5.1: November-December 2010 data collection campaign.....	97
Table 5.2: Data combinations used for TLE estimation.....	98
Table 5.3: Variability in Time to First Fix at various level of in-track orbit error	115

List of Figures and Illustrations

Figure 2.1: The assembled CanX-2 spacecraft prior to launch (from Sarda et al 2009 used with permission)	10
Figure 2.2: The CanX-2 mission patch (from Sarda et al 2009, used with permission) ...	10
Figure 2.3: CanX-2 along with the rest of the secondary passengers integrated to the upper stage (from Sarda et al 2009, used with permission)	11
Figure 2.4: ISRO PSLV-C9 launched at 03:53 UTC April 28th 2008 carrying CanX-2 (from Sarda et al 2009, used with permission).....	11
Figure 2.5: CanX-2's Position during a descending arc on July 30th, 2010 (from Kahr et al 2010, used with permission)	12
Figure 2.6: Required geometry for atmospheric retrieval using limb sounding	13
Figure 2.7: L1 gain pattern, figure courtesy of UTIAS Space Flight Lab.....	21
Figure 2.8: L2 gain pattern, figure courtesy of UTIAS Space Flight Lab.....	21
Figure 2.9: Timeline of GPS position fixes from April 2008 to February 2011	28
Figure 3.1: Flow chart of the script generation software.....	34
Figure 3.2: Predicted GPS constellation visible to the CanX-2 satellite. The centre of the plot represents the local zenith and the top of the plot is the forward motion direction	37
Figure 3.3: Script corresponding to the January 16, 2009 data collection	37
Figure 3.4: Power level on all trials November 2008 - February 2009.....	39
Figure 3.5: Power level on April 24th, 2009 Trial.....	41
Figure 3.6: Doppler offset on CanX-2's GPS receiver	42
Figure 3.7: Relativistic effects on CanX-2's clock in orbit.....	43
Figure 3.8: Doppler offset during the April 24th trial.....	45
Figure 3.9: Acquired geometry of the April 24th trial	47
Figure 3.10: Predicted geometry of the April 24th trial	48
Figure 3.11: Acquisition pattern with a zenith pointing antenna field of view	50

Figure 3.12: June 12 th , 2009 tracking results with a 45 degree antenna pointing direction and 25 degree antenna elevation mask.....	51
Figure 3.13: All data collected November 28 th , 2008 prior to memory limited shutdown.....	54
Figure 3.14: (above) All data collected January 18th, 2010 prior to memory limited shutdown. The rapid change in color near the end of the trial represents the higher logging rate.....	56
Figure 3.15: (right) Script for the successful January 18th data collection.....	56
Figure 3.16: Sample script for long arc data collection	59
Figure 4.1: Ellipse geometry.....	65
Figure 4.2: Physical meaning of the angular Keplerian elements.....	66
Figure 4.3: Variation in CanX-2's orbital elements over a period of one year	68
Figure 4.4: TLE mean Keplerian elements obtained from GPS data using VEC2TLE....	73
Figure 4.5: Difference between the smooth SGP4 trajectory and the precise position of CanX-2 over 24 hours.....	74
Figure 4.6: Error in the receiver's BESTXYZ position during the August 6, 2010 data collection, logged every 2 seconds	78
Figure 4.7: Error in the receiver's BESTXYZ position during the second November 25, 2010 data collection, logged every 30 seconds	79
Figure 4.8: TEME and ECEF coordinate frames	80
Figure 4.9: Comparison between the receiver's BESTXYZ standard deviations and true position error during the August 6, 2010 data collection, logged every 2 seconds	84
Figure 4.10: Comparison between the receiver's BESTXYZ standard deviations and true position error during the November 25, 2010 data collection, logged every 30 seconds	85
Figure 4.11: Positioning errors (red) are eliminated if the estimated errors (cyan) are above the 20 m threshold. August 6, 2010 data collection, logged every 2 seconds	87
Figure 4.12: Positioning errors (red) are eliminated if the estimated errors (cyan) are above the 20 m threshold. November 25, 2010 data collection, logged every 30 seconds	88

Figure 4.13: Flow chart of the least squares estimation	92
Figure 4.14: Residuals in the fit of five days of GPS data to an SGP4 trajectory	94
Figure 5.1: Long term propagation accuracy of a TLE estimated from all GPS data collected over a 3 hour span, relative to the precise orbit trajectories.....	99
Figure 5.2: Long term propagation accuracy of a TLE estimated from all GPS data collected over a 12 hour span, relative to the precise orbit trajectories.....	100
Figure 5.3: Long term propagation accuracy of a TLE estimated from all GPS data collected over a 48 hour span, relative to the precise orbit trajectories.....	100
Figure 5.4: Long term propagation accuracy of a TLE estimated from all GPS data collected over a week span, relative to the precise orbit trajectories	101
Figure 5.5: Long term propagation accuracy of the November 20 th , 2010 (day 324) NORAD TLE, relative to the precise orbit trajectories	102
Figure 5.6: Long term propagation accuracy of all NORAD TLE sets published from November 9 th to December 3 rd 2010 (days 313 to 337), relative to the precise orbits	103
Figure 5.7: Long term propagation accuracy of the third November 17th, 2010 (day 321) NORAD TLE, relative to the precise orbit trajectories	104
Figure 5.8: Long term propagation accuracy of a TLE estimated from GPS data collected over a 3 hour span and fixed drag, relative to the precise orbits	105
Figure 5.9: Long term propagation accuracy of a TLE estimated from GPS data collected over a 12 hour span and fixed drag, relative to the precise orbits	106
Figure 5.10: Long term propagation accuracy of a TLE estimated from GPS data collected over a 24 hour span and fixed drag, relative to the precise orbits	106
Figure 5.11: Long term propagation accuracy of a TLE estimated from GPS data collected over a 48 hour span and fixed drag, relative to the precise orbits	107
Figure 5.12: Long term propagation accuracy of a TLE estimated from GPS data collected over a week span and fixed drag, relative to the precise orbits.....	107
Figure 5.13: Long term propagation accuracy of all TLE estimated from 24 hour spans of GPS data and fixed drag, relative to the precise orbits	108
Figure 5.14: Long term propagation accuracy of all TLE estimated from 12 hour spans of GPS data and fixed drag, relative to the precise orbits	109
Figure 5.15: Long term propagation accuracy of all TLE estimated from single GPS data sets and fixed drag, relative to the precise orbits	109

Figure 5.16: Predicted Doppler shifts on the visible GPS constellation November 25, 2010 from 19:07 to 20:32 UTC.....	111
Figure 5.17: Error in Doppler induced by a -35 second adjustment to the time of ephemeris	112
Figure 5.18: Error in Doppler induced by a -17.5 second adjustment to the time of ephemeris	112
Figure 5.19: Error in Doppler induced by a 17.5 second adjustment to the time of ephemeris	113
Figure 5.20: Error in Doppler induced by a 20 second adjustment to the time of ephemeris	113
Figure 5.21: Error in Doppler induced by a 35 second adjustment to the time of ephemeris	114
Figure 5.22: Effect of advancing the time of ephemeris on channel assignment	116
Figure 6.1: Timeline of GPS data collection on board CanX-2.....	118
Figure C.1: Comparison with the November 17, 2009 (day 351) arc, created using L1 and L2 data.....	141
Figure C.2: Comparison with the May 6, 2010 (day 126) arc, created using L1 and L2 data.....	142
Figure C.3: Comparison with the December 1, 2010 (day 335) arc, created using L1 and L2 data.....	143

List of Symbols, Abbreviations and Nomenclature

List of Abbreviations

Abbreviation	Definition
AISSat	Automatic Identification System Satellite
CanX-2	Canadian Advanced Nanospace eXperiment 2
CanX-4/5	Canadian Advanced Nanospace eXperiment 4 and 5
CANOE	Canadian Advanced Nanospace Operating Environment
CASSIOPE	CAScade, Smallsat and IOnospheric Polar Explorer
CHAMP	CHAllenging Minisatellite Payload
COTS	Commercial Off the Shelf
COCOM	Coordinating Committee on Multilateral Export Controls
COSMIC	Constellation Observing System for Meteorology, Ionosphere and Climate
CMOS	Complementary metal–oxide–semiconductor
DLR	Deutschen Zentrum für Luft- und Raumfahrt
DMC	Disaster Monitoring Constellation
FOV	Field of View
GMST	Greenwich Mean Sidereal Time
GNSS	Global Navigation Satellite System
GPS	Global Positioning System
IERS	International Earth Rotation and Reference System Service
ION	Institute of Navigation
ISRO	Indian Space Research Organisation
IT	Instantaneous Terrestrial Coordinate Frame
ITRF	International Terrestrial Reference Frame
JC2Sat	Japan Canada 2 Formation Flight Satellites
LEO	Low Earth Orbit
LNA	Low Noise Amplifier
LPT	Low Power Transceiver
MRSE	Mean Radial Spherical Error
NASA	National Aeronautics and Space Administration
NORAD	North American Aerospace Defence Command
NTS	Nanosatellite Tracking Ships
POD	Precise Orbit Determination
PRN	Pseudorandom Noise (codes assigned to uniquely identify each GPS satellite)
PSLV	Polar Satellite Launch Vehicle
RAAN	Right Ascension of the Ascending Node
RAX	Radio Aural Explorer Satellite
RDOD	Reduced Dynamic Orbit Determination
RO	Radio Occultation

RX	Receiver
SFL	Space Flight Laboratory
SGP4	Simplified General Perturbations 4
SGR	Space GPS Receiver
TECU	Total Electron Content Units
TEME	True Equator Mean Equinox
TLE	Two Line Element Set
TOE	Time of Ephemeris
TTF	Time to First Fix
TX	Transmitter
UTC	Universal Time Coordinated
UT1	Universal Time
UTIAS	University of Toronto Institute of Aerospace Studies
VCTCXO	Voltage-Controlled Temperature-Compensated Crystal Oscillator
VEC2TLE	Software generating two line elements from a state vector
WGS84	World Geodetic System 1984

List of Symbols

Symbol	Definition
a	Semi-major axis
A	Least squares design matrix
c	Speed of light
df	Change in frequency
Δr_{iono}	Ionospheric range error
$\Delta r_{multipath}$	Multipath range error
Δr_{orbit}	GPS satellite orbital error
$\Delta r_{rxclock}$	GPS receiver clock error
$\Delta r_{satclock}$	GPS satellite clock error
Δr_{tropo}	Tropospheric range error
Dt	Time elapsed between transmission and reception of a GPS signal
$\Delta t_{n,n-1}$	Time elapsed from epoch n-1 to epoch n
dt_{rx}	Receiver clock offset from GPS time
dx	Least squares update to the estimated parameters
dy	Least squares misclosure vector
e	Eccentricity
e	Noise
f	Frequency
Φ_0	Gravitational Potential
G	Gravitational Constant
$GMST$	Greenwich mean sidereal time as an angle
i	Inclination
i	Least squares subscript indicating a single epoch of GPS data
JD_{UTC}	Julian date in the UTC timescale
JD_{UT1}	Julian date in the UT1 timescale
I_{L1}	L1 wavelength
M	Mean anomaly
m_e	Earth Ratio
M_e	Mass of the Earth
n	Mean motion
N	Least squares normal matrix
n_{obs}	Least squares number of observations
$n_{unknowns}$	Least squares number of unknowns/estimated parameters
v	True anomaly
P	Least squares weight matrix
P_{avg}	Average consumed power of CanX-2 in an orbit

P_{GPS}	Consumed power when the GPS receiver is on
P_{solar}	Average generated power in sunlight
$P_{transmitter}$	Consumed power when the S-band transmitter is on
r	pseudorange
R_1	Euler rotation matrix about the x axis
R_2	Euler rotation matrix about the y axis
R_3	Euler rotation matrix about the z axis
r	Distance
\vec{r}	Position vector
\vec{a}	Acceleration vector
r_c	Orbital radius for a circular orbit
r_{ECEF}	Position in an earth centred earth fixed frame
r_{IT}	Position in the instantaneous terrestrial frame
r_{ITRF}	Position in the ITRF frame
r_{TEME}	Position in the TEME frame
S^2	Least squares a-posteriori variance factor
S_{xOEM4}	OEM4 GPS receiver's estimated standard deviation in x
S_{yOEM4}	OEM4 GPS receiver's estimated standard deviation in y
S_{zOEM4}	OEM4 GPS receiver's estimated standard deviation in z
q	An angle
T	Orbital period
t_{GPS}	Duration of GPS operation per orbit
t_{pass}	Duration of a communications pass window
$t_{sunlight}$	Duration of sunlight per orbit
T_{UT1}	Days of Universal Time elapsed since JD 2451545.0
U	Least squares normal vector
$UT1-UTC$	Published time difference between the UT1 and UTC timescales
v	Least squares residuals
$v_{earthfixedTEME}$	Velocity in the TEME frame before the earth's rotation has been corrected
$v_{inertialTEME}$	Velocity in the TEME frame after correcting for the earth's rotation
v_{IT}	Velocity in the instantaneous terrestrial frame
ω_{earth}	Rotation rate of the earth
ω	Argument of perigee
Ω	Right ascension of the ascending node
x	Least squares vector of the estimated parameters
x_0	Least squares point of expansion for the estimated parameters
x_{GPS}	X component of the GPS satellite's position

x_{OEM4}	X component of the receiver's internal navigation solution
x_p	X component of the polar motion
x_{POD}	X component of the precise orbit determination solution
x_{rx}	X component of the receiver's position
y_{GPS}	Y component of the GPS satellite's position
y_{OEM4}	Y component of the receiver's internal navigation solution
y_p	Y component of the polar motion
y_{POD}	Y component of the precise orbit determination solution
y_{rx}	Y component of the receiver's position
z_{GPS}	Z component of the GPS satellite's position
z_{OEM4}	Z component of the receiver's internal navigation solution
z_{POD}	Z component of the precise orbit determination solution
z_{rx}	Z component of the receiver's position

Chapter One: Introduction

CanX-2, a student designed, built and operated CubeSat mission launched in April 2008, is the first student CubeSat mission to successfully operate a Global Positioning System (GPS) receiver in space. The receiver serves multiple purposes: it is intended for use as a radio occultation experiment for the University of Calgary, it serves as the only means of accurately positioning CanX-2, and it demonstrates the technology for the upcoming CanX-4/5 nanosatellite formation flight mission.

Operation of a GPS receiver in space differs greatly from operation for ground applications. There is a level of complexity associated with operating the technology remotely which simply does not exist when the hardware is easily accessible and can be manipulated, changed out, debugged and set up in person. The receiver's operating environment also differs significantly from the environment for which it was designed. The space environment is harsh in terms of temperature, pressure, and radiation, but beyond the purely environmental factors, the GPS signal environment is altered. To begin with, the sky is not necessarily in the antenna's field of view, and the dynamics of a satellite differ drastically from those of a vehicle, a pedestrian, or a static receiver. The most significant sources of error change as well; troposphere error and to some extent ionospheric error are less important than signal to noise ratio, and multipath is an unknown which can't be re-observed daily or quantified using a static receiver with a known position. Operationally, there are restrictive limits on the power and memory available to the receiver on board a small satellite, and a limited amount of contact time with the ground station during which experiments can be scheduled and data downloaded. Continuous data collection may not be possible, and a constant balance must be achieved during operations to get the best scientific results within the practical limitations of the experiment and satellite.

1.1 CanX-2 GPS Research Objectives

CanX-2 is unique in that, compared to larger missions with larger power budgets, its GPS receiver is operated intermittently. Even other missions with intermittent GPS operation generally follow a regular schedule of operation, either several times daily or for a given number of minutes during each orbit, rather than the sporadic experiments run onboard CanX-2 (Zhou 2003, Ebinuma et al 2005). CanX-2 is also unique because it attempts to collect radio occultation data using a single GPS antenna, forcing a compromise between positioning geometry and scientific results. Using a single antenna has only previously been done on a few missions (Zhou 2003, GENESIS 2011). The objective of the CanX-2 radio occultation payload is to collect GPS data of sufficient quality to extract atmospheric profiles working within these two constraints, and in doing so demonstrate that a nanosatellite is a suitable platform for a scientific radio occultation experiment.

In order to achieve the data collection objective, the capability to warm start the receiver and begin logging scientific data within a few minutes from powering on, with the antenna pointed towards the horizon rather than zenith, is essential. Fulfilling this key criterion for the radio occultation experiment has been the motivation behind this work.

1.2 A Brief Introduction to GPS

The Global Positioning System (GPS) consists of a constellation of between 24 and 32 active satellites orbiting the earth at an orbital altitude of approximately 20200 km in six orbital planes (Leick 2004, Lachapelle 2009). The satellites carry precise atomic clocks, adjusted to a standard time system, and transmit navigation and timing messages.

The system allows for absolute positioning of a GPS receiver within the constellation of GPS satellites based on the travel time of the transmitted signals. The timing difference between when a signal is transmitted from a GPS satellite and received by the user, Δt , can be multiplied by the speed of light, c , to get a pseudorange, r . The observations are

pseudoranges rather than ranges because the receiver clock is not perfectly synchronised with GPS time.

$$r = c\Delta t \quad \text{eq. 1.1}$$

The user triangulates their position based on pseudoranges from four or more GPS satellites. Three pseudorange observations are required for 3D positioning, (x_{rx}, y_{rx}, z_{rx}) , plus a fourth to correct for the offset of the receiver's clock from GPS time (dt_{rx}). The observation equation for a single pseudorange measurement is below, where, in addition to the above symbols, $(x_{GPS}, y_{GPS}, z_{GPS})$ is the known 3D Cartesian position of the GPS satellite and c is the speed of light in a vacuum. The required four GPS measurements allow a series of four equations in four unknowns to be formed and solved. Tracking additional GPS satellites allows for improved positioning accuracy by providing redundant measurements.

$$r = \sqrt{(x_{GPS} - x_{rx})^2 + (y_{GPS} - y_{rx})^2 + (z_{GPS} - z_{rx})^2} + cdt_{rx} \quad \text{eq. 1.2}$$

While equation 1.1 represents the ideal ranging situation, there are several errors which degrade the quality of GPS positioning. A more representative equation for the pseudorange, containing the most significant of the GPS measurement errors, is given below:

$$r = c\Delta t + \Delta r_{iono} + \Delta r_{tropo} + \Delta r_{orbit} + \Delta r_{satclock} + \Delta r_{rxclock} + \Delta r_{multipath} + e \quad \text{eq. 1.3}$$

The most significant GPS measurement errors are:

- Ionospheric error, Δr_{iono} , which is caused by the frequency dependent delay caused by charged particles in the earth's ionosphere. CanX-2's orbit is above the ionosphere's peak effect.

- Tropospheric error, Δr_{tropo} , which is caused by the non-dispersive delay caused by the lower atmosphere, and is dependent on temperature, pressure and water vapour content. CanX-2's orbit is well above any residual tropospheric effects.
- Orbital error, Δr_{orbit} , which is the error in the known position of the GPS satellite.
- Satellite clock error, $\Delta r_{satclock}$, which is the error in the GPS satellite's clock compared to true GPS time. It should be noted that the clocks on board the GPS satellites have a factory offset from the nominal GPS frequency, which compensates for the change in frequency due to relativistic effects at their orbital speed and altitude assuming circular orbits. This error is therefore not a systematic bias but a random error in the clock of each GPS satellite.
- Receiver clock error, $\Delta r_{rxclock}$, is the error in the receiver's clock compared to true GPS time. This error is, again, a random error in the clock, and even in the case of CanX-2 is not as a result of relativistic effects because the receiver clock is steered to closely follow GPS time when the requisite four GPS satellites are being tracked.
- Multipath, $\Delta r_{multipath}$, is the error caused by signals reflecting off of surfaces near the receiving antenna or otherwise following paths other than the geometric straight lines between the GPS satellites' transmitters and the receiving antenna's phase centre.
- Noise, e , is white noise on the pseudorange measurements.

In addition to the errors on individual measurements, the accuracy achievable using GPS is heavily dependent on the geometry of the observed constellation of GPS satellites. Optimal geometry would see an equal distribution of the GPS satellites on all sides of the receiver. The estimated vertical component of the position solution for a receiver on the ground, for example, is always worse than the horizontal components because of the one-sided geometry. While there are likely measurements from above, north, south, east and west of the receiver, there can never be a visible GPS satellite below the receiver to statistically cancel biases from above. Poor geometry can be a very significant factor for

a receiver in low earth orbit, because in addition to GPS satellite being blocked behind the earth, the antenna may have a reduced view of the sky due to the satellite's attitude.

1.3 A Brief Introduction to GPS receivers in Low Earth Orbit

The first GPS receiver to fly in Low Earth Orbit (LEO) was the GPSPAC instrument onboard LandSat-4 (Birmingham et al 1983). It was launched on July 16, 1982. The GPSPAC instrument had only two channels, either one each for L1 and L2, or a single channel with one for backup, depending on the mode of operation. GPSPAC alternated between observations of each of the required four GPS satellites for six seconds, combining the observations through the use of a Kalman filter. The receiver weighed 40 pounds and consumed up to 45 watts of power. The instrument faced a multitude of challenges and problems, most significantly that charged particles in space would occasionally flip a bit in software, causing days of down time to rectify the problem, and that there was less than a full constellation of operational GPS satellites in the early days of the mission leading to significant periods without even the possibility of a GPS positioning solution. In spite of the problems encountered, it was clear even at this early stage that a system capable of real time navigation and precise timing, without the requirement for an extensive network of ground support, was hugely advantageous for an orbiting spacecraft.

At present, GPS is used onboard many satellite missions in Low Earth Orbit, as well as some missions operating above the GPS constellation (Montenbruck et al 2007). The use of GPS onboard spacecraft has evolved into two distinct categories, GPS as a means of navigation and GPS as a scientific instrument (Kramer 2002). GPS for navigation includes applications such as orbit determination, relative navigation (Kroes 2006), precise timing for payloads (Spangelo et al 2010), attitude determination (Langer et al 1994), and to provide real time navigation necessary for other subsystems such as attitude determination and control (De Ruiter et al 2009). GPS as a scientific instrument has been used for atmospheric sounding (Rocken et al 1997, Hwang et al 2009) and for geodesy missions (Montenbruck & Kroes 2003). The use of GPS signals reflected off the earth as

a method for passive remote sensing is also a growing area of research (Gleason et al 2005).

Specialized space receivers have been developed in many cases to overcome the challenges of operation in orbit (Montenbruck et al 2006). Among the modifications made to GPS receivers for space are (Montenbruck & Kroes 2003, Gerner et al 2000):

- Radiation hardening or shielding
- Multiple channels for parallel search and rapid acquisition of GPS signals
- Ability to combine input from multiple antennas
- Higher logging rates for scientific data collection
- Position estimation using a Kalman filter and orbital dynamics model rather than single epoch least squares
- Software which can be updated in small increments during ground contacts
- Spare processor capability for other spacecraft tasks
- Reduced size and power draw where possible
- Extensive test programs to determine survivability in space

The results of these modifications are highly specialized products which are not mass produced (Montenbruck et al 2006). Consequently, the cost of a specialized space receiver exceeds the entire CanX-2 budget, and in many cases the weight, dimensions and power draw also exceed the physical limitations of the CubeSat. CanX-2's chosen GPS receiver and antenna combination, selected long before launch based on the circumstances of the project rather than their suitability for space, have nonetheless enabled performance from CanX-2 on the level of specialized space hardware.

1.4 Thesis Outline

This thesis describes the first three years of the University of Calgary CanX-2 GPS experiment and is organised following the time line of the CanX-2 mission. Each chapter presents the ongoing research, results and conclusions of a phase of the mission.

Chapter two of this thesis presents a detailed discussion of the CanX-2 mission and GPS payload, within the context of the radio occultation experiment for which it was designed. It also summarizes previous work done in qualifying the commercial receiver for use in space. Essentially, this chapter sets out the background of the satellite as it was designed and launched into space on April 28, 2008.

Chapter three presents the first two years of operation of the receiver for radio occultation and navigation data collection. The methodology originally developed for rapid position fixes under orbital dynamics is presented, along with the initial failure of this technique, the months of debugging and refinements, and the final successful data acquisition in late 2009. Also presented is the acquisition of longer data arcs, collected as the focus of the onboard experimentation shifted from atmospheric research to orbit determination in 2010.

Chapter four builds on the experiences and discoveries made throughout the CanX-2 experiment to suggest an improved operation scheme. Current operations have the drawback of involving a lot of ground support; this chapter presents a method of improving on the autonomy of GPS operations for future satellite missions. A simplified approach to orbit determination is presented. The algorithm developed is intended to run onboard satellite missions, ideally as part of the GPS receiver firmware, to enable onboard prediction of the satellite location after long GPS outages and ultimately speed the reacquisition of a GPS position fix.

Chapter five presents the results of the suggested operation scheme. It compares the simplified trajectories of chapter four to precise orbit determination trajectories, in order

to demonstrate that the simplified orbit determination results are sufficiently accurate to warm start the GPS receiver. It also presents the results of an experiment carried out onboard CanX-2 in late 2010 and 2011 in order to establish the required orbit determination accuracy for rapid acquisition.

Chapter six concludes the research work and contains suggestions for future work. While the operating scheme suggested in chapter four would present a significant advantage for a satellite with CanX-2's orbital parameters, this is only one case among the vast spectrum of satellite missions currently being operated or planned, and the same algorithm may not be as well suited to other cases.

Chapter Two: The CanX-2 Mission

Nanosatellites have been growing in popularity in the last decades, as they present significant advantages over large satellites. They are smaller, and therefore lighter and cheaper to launch, they cost less to build, they can be developed more quickly by a reduced team of people, and they represent a significantly lower risk if they should fail. Small satellites are above all making space accessible to universities and commercial enterprises, when historically it was an exclusive arena for national space agencies with the large budgets necessary to support high cost missions (Fleeter 2000). As a trade off, there are significant limitations on what can be achieved on the nanosatellite scale, as physically smaller satellites have less space for payloads and less available power to run them.

The Canadian Advanced Nanospace eXperiment 2 (CanX-2) is a nanosatellite designed and built by a team of students at the Space Flight Laboratory (SFL) in the University of Toronto's Institute for Aerospace Studies (UTIAS). It measures only 10 cm by 10 cm by 34 cm, weighs approximately 3.5 kg, and is considered a "triple CubeSat" based on the standard established by Stanford University and California Polytechnic State University (Sarda et al 2006). Figure 2.1 is a photograph of the spacecraft prior to launch, and Figure 2.2 shows the CanX-2 mission patch.

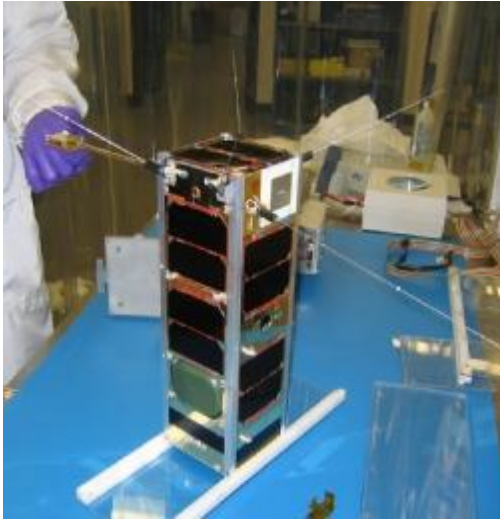


Figure 2.1: The assembled CanX-2 spacecraft prior to launch (from Sarda et al 2009 used with permission)



Figure 2.2: The CanX-2 mission patch (from Sarda et al 2009, used with permission)

Within this tiny satellite are several scientific payloads from different Canadian universities, as well as satellite subsystems which are made from components being flown in space for the first time as advanced testing or risk mitigation for the upcoming CanX-4/5 formation flight mission. The scientific payloads consist of an atmospheric spectrometer used to characterize greenhouse gases and atmospheric pollution from York University, a space materials experiment from University of Toronto, and finally the University of Calgary's radio occultation experiment. The satellite subsystems on board CanX-2 consist of two high performance computers, a three axis momentum bias coarse pointing attitude control system, a miniature reaction wheel, a nanosatellite propulsion experiment, a high data rate S-band transmitter, two CMOS imagers, a battery and a series of solar panels (Rankin et al 2005, Sarda et al 2009).

2.1 Launch and Orbital Parameters

CanX-2 was launched on April 28th, 2008 at 03:53 UTC from a site in Sriharikota, India (Sarda et al, 2009). It was one of ten satellites to share the same launch, with nine small

satellites clustered around the CartoSat-2A prime passenger (Kahr et al 2011). Figure 2.3 shows the small satellites, CanX-2 among them, mounted on the PSLV launch vehicle, and Figure 2.4 shows the launch.

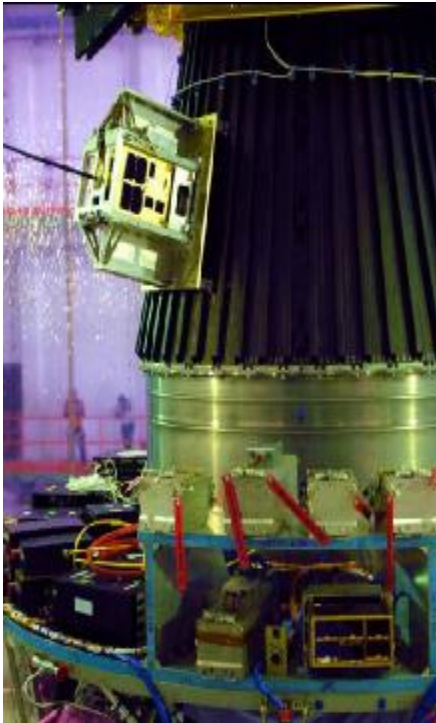


Figure 2.3: CanX-2 along with the rest of the secondary passengers integrated to the upper stage (from Sarda et al 2009, used with permission)



Figure 2.4: ISRO PSLV-C9 launched at 03:53 UTC April 28th 2008 carrying CanX-2 (from Sarda et al 2009, used with permission)

CanX-2 was launched into a near circular orbit with an orbital altitude of 635 km above the ground, which classifies it as being in low earth orbit (LEO). Its orbit is near polar, with an inclination of 98° . CanX-2's orbit is also sun-synchronous, which means that the orbital plane precesses around the earth at a rate of one revolution per year, and also means that the satellite always crosses the equator at the same local solar time, in this case with a descending node of 9:30 am. The orbital velocity of CanX-2 is approximately 7 km/s. Figure 2.5 displays the path of CanX-2 on a descending arc relative to the earth's surface.

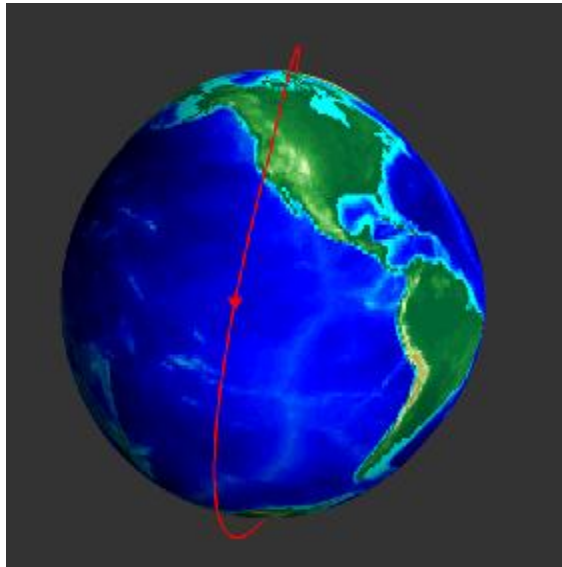


Figure 2.5: CanX-2's Position during a descending arc on July 30th, 2010 (from Kahr et al 2010, used with permission)

2.2 The Radio Occultation Experiment

The concept of radio occultation is that a GPS receiver in low earth orbit is sufficiently high in the atmosphere to be positioned accurately by GPS without experiencing significant atmospheric delay. Tropospheric delay is only significant up a maximum of approximately 60 km above ground level (de Jong et al 2002), while according to Garcia-Fernandez and Montenbruck (2006) a receiver orbiting 1000 km above ground level experiences negligible ionospheric delay. They determined that when an elevation mask of 10 degrees is employed for tracking GPS satellites, the ionospheric positioning error for a receiver in low earth orbit can be roughly estimated based on the vertical total electron content as 0.52 m/TECU , where 1 TECU is equal to $10^{16} \text{ electrons/m}^2$. A satellite orbiting above the ionospheric maximum, at 300 km to 400 km above the earth's surface, will therefore experience far less delay than a receiver on the ground.

With the improved positioning solution in low earth orbit, it is then possible to determine the atmospheric delay on a single GPS signal as the GPS satellite rises or sets behind the atmosphere as viewed from the LEO. The technique, known as limb sounding, was first

developed to measure the atmospheres of Venus and Mars by measuring the phase advance on signals sent from earth to the Mariner missions as they passed behind the distant planets (Fjelbo et al 1965). Limb sounding using GPS integrates the atmospheric error on the Doppler observation and therefore requires a very high data logging rate and an estimated receiver velocity and clock drift accurate to 0.15 mm/s (König et al 2002).

Depending on how near the signal path of the occulting satellite is to the earth surface, radio occultation data can be used to derive electron density in the ionosphere or temperature and pressure in the troposphere. If sufficiently accurate a priori information about the temperature at the upper boundary of the troposphere is available, tropospheric water vapour pressure can also be derived (DeGroot, 2008).

Radio occultation using GPS signals is a well established technique for gathering meteorological data, and the results of the technique are regularly incorporated into global weather models to increase forecast accuracy (Hajj 2002). CanX-2's radio occultation experiment is novel because it attempts to collect the same valuable data from the restricted platform of a nanosatellite using commercial components.

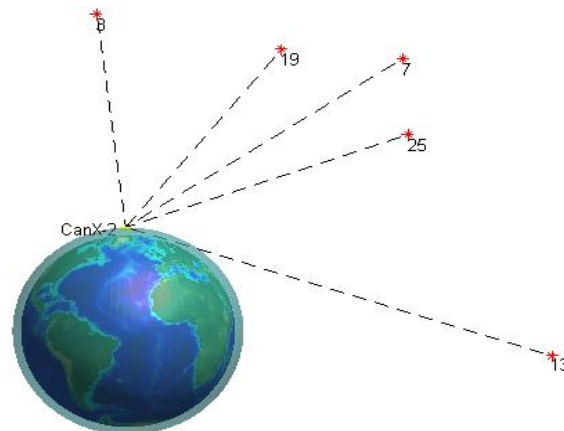


Figure 2.6: Required geometry for atmospheric retrieval using limb sounding

Figure 2.6 is an example of the minimum required GPS constellation geometry for CanX-2 limb sounding experiments, based on an actual data collection on April 24th, 2009. One

GPS satellite, in this example PRN 13, is occulting behind the atmosphere from the point of view of the rear pointing GPS antenna on CanX-2. Atmospheric properties can be derived for the point where the line of sight between CanX-2 and PRN 13 most closely approaches the earth's surface. Four other GPS satellites, here PRNs 3, 19, 7 and 25, meet the minimum requirement for positioning. The use of a single patch antenna imposes a considerable constraint on the experiment, as a balance must be achieved between maximising the signal power on the occulting GPS satellite by pointing the antenna rearward, and still maintaining good geometry in the remaining visible GPS satellites for improved positioning accuracy.

2.3 The Scientific Payload

Among the experimental payloads, the satellite is carrying a NovAtel GPS receiver and an AeroAntenna patch antenna, which are used primarily to carry out the University of Calgary's GPS radio occultation experiment. CanX-2 is the first satellite to carry these particular components into space, which is a significant achievement for the two commercial off the shelf products.

Larger satellite missions will generally only carry space qualified equipment which has been flown in space before or has gone through extensive testing in order to ensure, to the greatest possible extent, that it will be able to survive the rigours of launch, the temperature extremes of space, operation in a vacuum where some materials may either evaporate or electronics may overheat without airflow, and the increased radiation from the sun without the protective shield of the atmosphere (Fleeter, 2000). The motivation for this is the extremely high cost of getting a satellite into space, and the impossibility of fixing any component that fails in orbit. Large satellites are generally also designed to have an extremely high degree of redundancy in critical components.

Nanosatellite projects are; however, in a different category, as a large number of them are amateur projects and lack the funding and resources for this level of certification or testing. Their lower budgets also mean they have less at stake, in that a component failure

has a much lower price tag. This makes them a far more suitable platform for experimental work and less specialized components, as is the case with CanX-2.

2.3.1 The GPS Receiver

The GPS receiver onboard CanX-2 is a NovAtel OEM4-G2L. This is a geodetic grade, dual frequency receiver used primarily in survey applications. It has 24 channels, 12 each dedicated to tracking L1 and semi-codeless L2 signals. It is a commercial off the shelf (COTS) component, with very few modifications made for use in space. The receiver's clock is a 20 MHz voltage-controlled, temperature-compensated crystal oscillator (VCTCXO) (NovAtel 2003). The data specific to CanX-2's receiver, obtained from logging the version information onboard the spacecraft, is given in Table 2.1 below, and the manufacturer's specifications, from the user manual, are given in Table 2.2.

Table 2.1: Version Information for the NovAtel GPS receiver on board CanX-2

Component type	GPSCARD
Model	L1L2100H
Product Serial Number	SVG03470111
Hardware Version	OEM4g2L-2.02-2T
Firmware Software Version	2.140S3
Boot Code Version	2.100
Firmware Compile Date	2003/Dec/11
Firmware Compile Time	15:37:06

Table 2.2: Specifications for the NovAtel GPS receiver on board CanX-2 (NovAtel 2003, 2006)

Standalone L1 only positioning accuracy	1.8 m CEP
Standalone L1/L2 only positioning accuracy	1.5 m CEP
Post-Processed Positioning Accuracy	5 mm + 1 ppm CEP
Time accuracy	20 ns RMS
Velocity accuracy	0.03 m/s RMS
L1 C/A code measurement precision	6 cm RMS
L2 P(Y) code measurement precision	25 cm RMS
L1 carrier phase measurement precision	0.75 mm RMS
L2 carrier phase measurement precision	2 mm RMS
Typical Time To First Fix from Cold Start	50 s
Typical Time To First Fix from Warm Start	40 s
Typical Time To First Fix from Hot Start	30 s
Maximum vibration for sustained tracking	4 G
Operating Temperature	-40 °C to + 85 °C
Storage Temperature	-40 °C to + 95 °C
Humidity	max 95% non-condensing
Size	60 x 100 x 16 mm
Weight	56 g
Voltage	+3.3 +/- 0.15 VDC
Typical Power consumption	1.8 W

The most significant modification to this commercial receiver has been to remove the COCOM (Coordinating Committee on Multilateral Export Controls) limitations, which restrict tracking above an altitude of 18000 m or above a velocity of 515 m/s (NovAtel Inc. 2006), both of which are far exceeded by an object in low earth orbit. A second modification, specific to the radio occultation experiment, was to allow data logging at rates up to 50 Hz, as opposed to the default 20 Hz maximum (NovAtel Inc. 2003, 2005).

In addition to the aforementioned modifications on the firmware level, two of the user defined settings have been changed from the manufacturer's defaults for the space environment. First, the carrier phase smoothing has been reduced to the minimum possible level as recommended in (Montenbruck 2003). The purpose in doing this is to

avoid corruption of the code ranges by ionospheric effects. Using a high degree of carrier phase smoothing would be harmful because the phase data experiences an ionospheric advance while the code data experiences a delay. For a receiver on the ground the change in ionospheric delay over the short time span used for smoothing is generally insignificant, but the rapidly changing geometry as seen at orbital velocity and the gradients in ionospheric delay as a GPS satellite sets behind the atmosphere could introduce significant effects into the raw data.

The second change to the user defined settings was to lower the elevation mask below which the receiver will stop tracking satellites. The default of 5 degrees above the horizon assumes an antenna pointing to zenith somewhere near the earth's surface, but for CanX-2 the elevation mask was opened to 45 degrees below the horizon to enable tracking through the portion of the sky below the nanosatellite, essential for tracking occulting GPS satellites when the antenna's field of view is pointing rearward.

A complete listing of all the receiver's settings for operations in space, obtained from the rxconfig log, has been included in Appendix A.

2.3.2 Qualification for Space

Prior to the selection of the OEM4-G2L receiver for use on board CanX-2, research had been carried out on its potential suitability for use in space. This particular model of receiver had drawn interest from the space community due to its ability to track L1 and L2, its quality as a geodetic grade receiver, its design specification for maintaining lock at high accelerations, its favourably small size and low power draw, and its favourable price compared to existing space-qualified hardware (Montenbruck 2003).

Montenbruck (2003) tested the OEM4-G2 receiver, which is equivalent to the smaller G2L on the software level, for its ability to track in low earth orbit using a GPS simulator, and assessed the signal quality and accuracy of the receiver's internal navigation solution under orbital dynamics. The performance was found to be suitable for

space, although a potential for difficulty in acquiring a position fix with the receiver's default algorithm was identified. The OEM4's search algorithm is designed for Doppler shifts of +/- 10 kHz, although it can track satellites at Doppler shifts of up to +/- 100 kHz. At CanX-2's orbital altitude the Doppler shifts range from +/- 45 kHz, well within the receiver's tracking capability but outside of the acquisition algorithm's search range. Montenbruck also discovered the aforementioned carrier phase smoothing problem, as well as a bias in the radial component of the receiver's calculated position on the order of 17 m. The bias is in all likelihood due to the incorrect implementation of the Hopfield tropospheric correction in receiver's firmware (NovAtel 2005). Logging the ionospheric and tropospheric corrections at orbital altitude has revealed that the implementation does not take into account the receiver's elevation above sea level. The raw carrier phase and pseudorange measurements were found to be unbiased.

In addition to the qualification work on a signal tracking level, Markgraf & Montenbruck (2004) carried out radiation testing of three OEM4-G2L receivers, and Langley et al (2004) carried out thermal vacuum testing. The motivation for these tests came from the planned use of the same receiver onboard the Canadian CASSIOPE satellite. During the radiation testing it was discovered that a component used to reset the receiver if insufficient input power was available failed at doses of 5-7 krad, but overall the receiver's ability to survive under radiation was greater than anticipated, and in fact the oscillator stability under radiation conditions was better than some space qualified receivers. In the thermal vacuum tests it was discovered that the receiver functioned normally in a vacuum at temperatures ranging from -40°C to +50°C.

2.3.3 The Antenna

The GPS antenna chosen for use on board CanX-2 is an AeroAntenna AT2775-1030-SMAF-000-03-26-NM. Some of the manufacturer specifications for the antenna are summarized in Table 2.3 below.

Table 2.3: Specifications for the GPS Antenna on board CanX-2 (AeroAntenna 2003)

Frequencies	1227 MHz +/- 10 MHz, 1575 MHz +/- 10 MHz
Polarization	Right hand circular
Gain with amplifier	26 dB +/- 2 dB (38 mA)
Axial Ratio	3 dB max at bore sight*
Voltage	3 VDC
Voltage Standing Wave Ratio	<= 2.0:1
Impedance	50 Ohms
Operating Temperature	-50 °C to + 70 °C
Storage Temperature	-57 °C to + 70 °C
Altitude	20000 feet
Size	55 x 76 x 23 mm
Weight	127 g

* Taken from the AT2775-203 specifications in the GPS World Antenna Survey (2011)

Discussion with the manufacturer has revealed that the antenna is a military model and was sold without the radome sealed to the base. As such, there is no published or available manufacturer gain pattern (Valdes 2010). It has been revealed that the AT2775-203 is the civilian equivalent antenna, and therefore information for the 203 has been used to supplement the available information for the 103 based on the assumption that they are identical.

CanX-2's patch antenna was originally designed for use on land vehicles, or as a supplemental antenna to a handheld GPS receiver. The antenna's radome is made from a polycarbonate and polybutylene terephthalate blend (PC/PBT Alloy) (Guitteau 2010). The antenna, being a vehicle antenna and not qualified for space, has the potential to fail in the space environment. A specific concern which has been raised by Montenbruck (2010) is that the plastic outer shell may begin to change its properties under constant exposure to solar radiation and eventually become opaque to L band radiation, degrading the signal to noise ratio of the incoming GPS signals. This is however only a matter of

speculation in that there has been no noticeable change in the signal to noise ratio since launch. Although it is less than ideal for the application, the chosen antenna does fit within the budget and size constraints for the nanosatellite, and has allowed for collection of GPS data.

2.3.4 Antenna Mounting

A launch system design requirement prevented satellite components from protruding outside of a tight envelope. The antenna is therefore mounted such that the antenna patch is level with the outer aluminum shell of the satellite, with the antenna fastened beneath the satellite's surface (Bradbury 2011). A 30 cm coax cable is used to connect the antenna and receiver (Orr 2009).

Testing was carried out four years prior to launch in order to characterize the gain pattern of the antenna when mounted to the satellite. The design of the satellite was subsequently changed from a double to a triple CubeSat, but in that the method of mounting the antenna has not changed the test results are still expected to be representative (Bradbury 2011). Figure 2.7 and Figure 2.8 show the test results for L1 and L2 respectively. The gain patterns include the LNA.

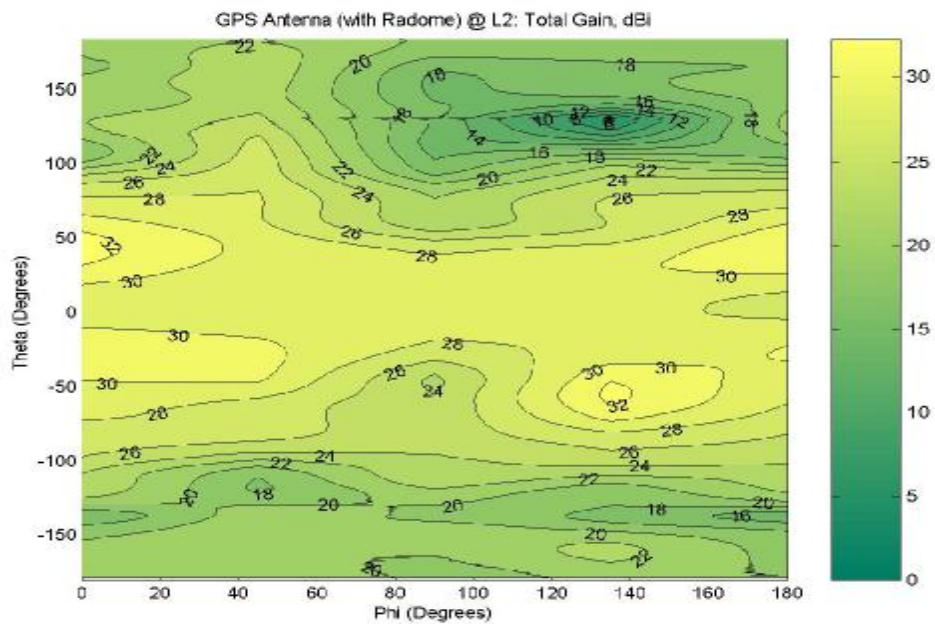


Figure 2.7: L1 gain pattern, figure courtesy of UTIAS Space Flight Lab

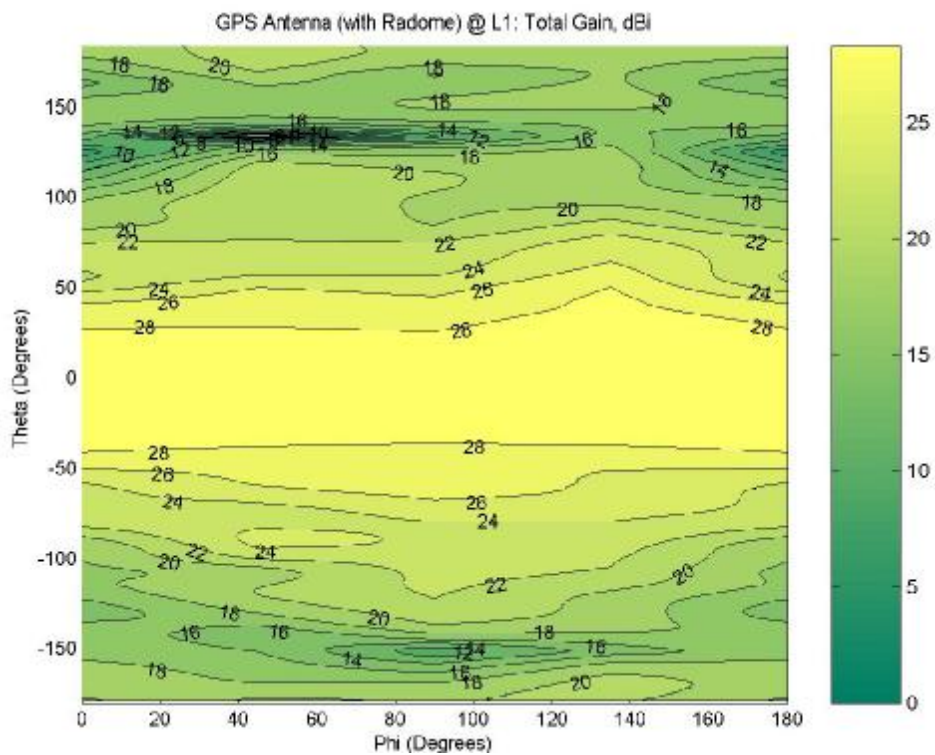


Figure 2.8: L2 gain pattern, figure courtesy of UTIAS Space Flight Lab

2.4 Operations Onboard CanX-2

There are a number of technical limitations specific to operations on board CanX-2, based on the design of the satellite. These operational constraints have been the basis for many design decisions and are explained in detail below.

2.4.1 Power Budget

All satellites face a limited amount of available power because they operate autonomously in space. The needs of the onboard electronics are typically met by a power subsystem consisting of solar panels and batteries. The amount of power available on a satellite is generally directly proportional to its size, as larger outer surfaces allow for larger solar panels, and the size and weight of batteries is more easily accommodated. A larger satellite may also allow for complex systems of deployable solar panels with the ability to track the sun. For a nanosatellite, one of the most significant design constraints is therefore to perform useful science on a very tight power budget.

Being a secondary payload on its launch vehicle, CanX-2 had to be designed in way that would work for a variety of orbits in order to open up the number of potential launch opportunities (Rankin et al 2005). As a result the power subsystem could not be optimized for any one particular orbit. Measuring only 10 by 10 by 34 cm, it also has very limited surface area available for solar panels. The power onboard CanX-2 is provided by 20 solar cells, mounted over all six of the satellite's surfaces, and a single lithium-ion battery (Rankin 2005).

The limited power onboard the nanosatellite makes it impossible to continuously operate the GPS receiver. As such, an intermittent operation scheme is used for the radio occultation experiment and collection of navigation data. At various phases of the experiment, the maximum allowable continuous receiver use has changed. It has only been through experience since launch that the full power capabilities of the satellite have become well understood. Prior to launch the radio occultation experiment was designed

for a maximum receiver time of 15 minutes per day, but more recently continuous GPS data sets of up to 85 minutes in duration have been collected.

According to Sarda (2010), managing the power onboard CanX-2 is done through the use of a power budget. Ideally the spacecraft will remain power positive; over a single orbit more power is generated during the time in sunlight than is used over the entire orbit by all the satellite's systems combined. Calculating the allowable receiver time is a matter of equating the power generated with the power drawn over an orbit. The guiding equation for the allowable receiver time without dipping into the battery is

$$P_{solar}t_{sunlight} = P_{avg}T + P_{transmitter}t_{pass} + P_{GPS}t_{GPS} \quad \text{eq. 2.1}$$

where

$$P_{solar} = \text{Average generated power in sunlight} = 5\text{W}$$

$$t_{sunlight} = \text{Sunlight duration per orbit} \approx 60\text{min}$$

$$P_{avg} = \text{Average consumed power of CanX-2 in an orbit} = 1.25\text{W}$$

$$T = \text{Orbital period} = 98\text{min}$$

$$P_{transmitter} = \text{Consumed power when the S-band transmitter is on} = 5\text{W}$$

$$t_{pass} = \text{Communications pass window} = 17\text{min}$$

$$P_{GPS} = \text{Consumed power when the GPS receiver is on} = 1.50\text{W}$$

$$t_{GPS} \approx 60 \text{ min of GPS receiver operation}$$

This 60 minute value is however only a guideline, and has been calculated for an orbit during which there is a ground contact. By scheduling experiments to avoid the ground station passes and making use of some of the stored battery power, longer GPS data collections are possible, and the limiting factor becomes the attitude control system which is described in section 2.4.4 below.

2.4.2 Ground Contact

Contact with the ground is essential for scheduling and running GPS experiments. Each experiment is controlled through a script written in a combination of two scripting languages. The first is CanX-2 specific, and is the language used by the satellite's operating system, CANOE (Canadian Advanced Nanospace Operating Environment) (Sarda et al 2009). The second is the NovAtel scripting language which is well documented in the receiver's manual (NovAtel 2005). Because the successful collection of GPS data depends on the single patch antenna pointing in an appropriately skyward direction, each GPS experiment consists of two scripts, one for the satellite's attitude determination and control system and the other for the receiver itself. The scripts must be transmitted to the satellite from the ground station in Toronto in order to be executed, and limitations in the operating system dictate that a maximum of four scripts can be queued between ground contacts. The bottom line is that only two GPS experiments can be run between ground contacts.

CanX-2 is controlled by a single ground station at the University of Toronto. Because it is in low earth orbit, CanX-2 travels at a high velocity and has a short orbital period. The window of opportunity for contact is quite short as a result, generally lasting on the order of 10 minutes. Each contact opportunity is called a pass. The 9:30 am descending node, sun synchronous orbit allows for two pass blocks daily, one in the morning local time as CanX-2 descends towards the equator in sunlight, and one in the late evening as it ascends towards the pole in eclipse. Each pass block consists generally of three passes, with one of the passes being of shorter duration due to CanX-2 being at low elevation relative to the ground station. As a rule of thumb, two passes in each pass block are available for making contact.

In addition to low elevation passes, during a number of the high elevation passes only poor contact with the satellite is achieved, preventing the download of data and upload of scripts. Also, due to sharing the same launch vehicle, roughly every seven months the orbital harmonics of CanX-2 and the University of Toronto's NTS satellite coincide in

such a way that the contact times overlap, with the unfortunate result that NTS is given priority and only one or two contacts per week with CanX-2 are possible (Sarda 2010). Finally, at various times since launch ground station outages have prevented any contact at all for periods up to a few weeks.

Table 2.4 below is an excerpt from the weekly contact schedule for CanX-2 and NTS. Rows coloured in yellow make up the morning pass block and occur with both the satellite and ground station in sunlight, while cells coloured in blue make up the evening pass block.

Table 2.4: Excerpt from the contact schedule for NTS and CanX-2, showing contact details for November 27, 2010 (Bradbury 2010)

Satellite	Start Time (UTC)	Stop Time (UTC)	Toronto Date	Start Time (EDT)	Stop Time (EDT)	Duration	Gap
NTS (CANX-6)	2010-11-27 13:22:27	2010-11-27 13:26:16	27-Nov-10	9:22	9:26	0:03:49	0:00:00
CANX-2	2010-11-27 13:23:12	2010-11-27 13:26:37	27-Nov-10	9:23	9:26	0:03:25	1:28:39
NTS (CANX-6)	2010-11-27 14:55:16	2010-11-27 15:08:08	27-Nov-10	10:55	11:08	0:12:52	0:00:00
CANX-2	2010-11-27 14:55:50	2010-11-27 15:08:38	27-Nov-10	10:55	11:08	0:12:48	1:23:07
NTS (CANX-6)	2010-11-27 16:31:45	2010-11-27 16:43:40	27-Nov-10	12:31	12:43	0:11:55	0:00:00
CANX-2	2010-11-27 16:32:15	2010-11-27 16:44:12	27-Nov-10	12:32	12:44	0:11:57	7:35:53
NTS (CANX-6)	2010-11-28 00:20:05	2010-11-28 00:26:21	27-Nov-10	20:20	20:26	0:06:16	0:00:00
CANX-2	2010-11-28 00:20:35	2010-11-28 00:26:39	27-Nov-10	20:20	20:26	0:06:04	1:25:10
NTS (CANX-6)	2010-11-28 01:51:49	2010-11-28 02:04:34	27-Nov-10	21:51	22:04	0:12:45	0:00:00
CANX-2	2010-11-28 01:52:11	2010-11-28 02:04:53	27-Nov-10	21:52	22:04	0:12:42	1:23:31
NTS (CANX-6)	2010-11-28 03:28:24	2010-11-28 03:40:36	27-Nov-10	23:28	23:40	0:12:12	0:00:00
CANX-2	2010-11-28 03:28:41	2010-11-28 03:40:56	27-Nov-10	23:28	23:40	0:12:15	9:58:44

Scripts are transmitted from the ground station to CanX-2 in the UHF band at a rate of 4 kbps, and data is downloaded to the ground station in the space-research science S-band at variable rates between 8 and 1024 kbps (Sarda et al 2009).

2.4.3 Onboard Memory

The computational resources onboard CanX-2 consist of two computers. The main computer used for all normal satellite operations such as collecting satellite telemetry, controlling sub-systems such as attitude control, communicating with the ground station and commanding the payloads. A secondary payload computer is being flown to obtain space heritage and can record and store GPS data (Sarda et al 2009).

CanX-2's onboard memory consists of 16 MB of solid state (flash) memory for each on board computer, which is used to store software and experiment data. The operating system makes use of this memory such that a total of 1 MB is available for logging GPS data, meaning that between ground contacts no more than 1 MB of GPS data can be captured. One NovAtel binary compressed range message is approximately 500 Bytes (assuming the average 9 channels are tracking dual frequency GPS data), so the 1 MB of data storage represents roughly 40 seconds of tracking at the receiver's maximum 50 Hz logging rate, or half an hour of tracking at a 1 second logging rate. There is a further restriction, that if the data storage space is divided between multiple experiments (one experiment being one power up of the GPS receiver) the division of the 1 MB is 10% and 90%. As such, only 100 kB of GPS data can be collected during one experiment while the other experiment can capture 900 kB of data (Sarda 2010).

2.4.4 Attitude Control System

Attitude control is essential for successfully obtaining and maintaining a GPS position fix on any orbiting spacecraft. For CanX-2's single patch antenna design in particular, if the single antenna is not pointed skyward no GPS signals can be acquired and positioning is impossible. Furthermore, if the pointing direction cannot be steadily maintained the receiver will lose lock on some or all of the GPS satellites, and gaps in the GPS tracking will occur.

The attitude determination system on the nanosatellite consists of a three axis magnetometer, and a series of six sun sensors (Sarda et al 2009). In sunlight the attitude can be determined as accurately as +/- 1.5 degrees, with the accuracy worsening in eclipse without the use of the sun sensors (Sarda 2010).

The attitude control is carried out by a series of three magnetorquer coils and a momentum wheel, in a three axis momentum bias configuration. Momentum bias means that all or part of the spacecraft has a continuous spin rate (Fortescue et al 2004). In this case only part of CanX-2 is spinning – the momentum wheel. The inner spinning component stabilises the attitude because the entire satellite essentially becomes a gyroscope. An outside torque acting on the satellite only causes a minimal change in the direction of the momentum wheel's spin axis, and consequently the satellite's attitude. When it is in momentum align mode CanX-2 maintains an attitude in which the long 34 cm axis points in the orbit normal direction. Because there is an upper limit on a momentum wheel's spin rate, and therefore a limit on the extent to which it can be used to correct the attitude, the magnetorquers also enable attitude control and momentum management by aligning the satellite with the earth's magnetic field (Fleeter 2000, Sarda 2009).

During experiments the attitude control system's operation is put into wheel pitch mode. The pointing directions of the payloads can then be actively controlled by speeding up or slowing down the momentum wheel, which causes the opposite reaction in the body of the satellite. In this case the long axis pointing in the orbit normal direction is also the rotation axis about which the satellite body spins in order to achieve the desired payload pointing direction.

The desired pointing direction must be set during a ground contact prior to a GPS data collection. Wheel pitch mode is then activated via a script five minutes prior to powering on the GPS receiver. In sunlight, the payloads can be pointed with accuracy on the order of 2-3 degrees, while in eclipse the attitude control worsens to 5-10 degrees without the

help of the sun sensors (Sarda 2010). The attitude alignment of CanX-2 worsens with time when it is being actively controlled, so a maximum duration of 85 minutes for GPS data collection has been set by the team in Toronto (Urbanek 2010).

2.4.5 Experimental Schedule

The final limitation on CanX-2 operations is the payload experiment schedule. In order to share the resources onboard the satellite and to simplify operations, the payload teams alternate experimentation based on a schedule sent out by Toronto. Calgary's radio occultation or navigation data is generally only collected once or twice a day, over a period of a month, followed by an outage lasting several months while other payloads' experiments are run.

The advantage of this experiment schedule is that it allows for longer periods of data collection, which is useful for experiments where a previous week's GPS positions are propagated forward in time, as it provides the opportunity to collect reference data. It also operationally means that settings specific to running the GPS payload, such as desired satellite attitude or the amount of onboard memory space dedicated to the payload data, can be set up consistently for a period of several weeks, which cuts back on the likelihood of errors being made during individual data takes.

The disadvantage of this experiment schedule is the availability of data. There are long outages of several months during which no GPS data is collected, and on occasions where potential bugs in the experiment setup were discovered immediately following GPS experimentation it would often be months before new experiments were run in order to establish if the solution worked.

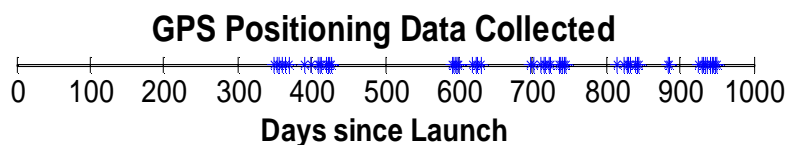


Figure 2.9: Timeline of GPS position fixes from April 2008 to February 2011

Figure 2.9 above displays the timeline of successful GPS data collection over the first 34 months in orbit. This figure represents only data collections resulting in a position fix, although many unsuccessful experiments were run in the year after launch. The following chapter explains in detail the lessons learned in the early days of operating the radio occultation experiment, and their relevance to other missions carrying similar hardware. A chronological listing of all GPS experiments run onboard the CanX-2 nanosatellite as part of the radio occultation experiment, and some of the key parameters used for each, is given in Appendix B.

Chapter Three: Lessons Learned in Orbit

On most large satellite missions carrying GPS, continuous tracking is used for real time positioning of the satellite. As explained in Chapter Two, the design constraints of CanX-2 have made it necessary to operate the GPS receiver intermittently. While the intermittent operations have minimized the receiver's draw on the satellite's power and data storage capabilities, it has added an increased burden in terms pre-planning experiments for the radio occultation data collection campaign. In particular, it is necessary to pre-select specific occultation events for observation, while other satellites carrying radio occultation payloads such as CHAMP and COSMIC observe all daily occultation events as a result of their continuous tracking (König et al 2002, Hwang et al 2009). As a result of only using the receiver during specific events, there is a fundamental requirement that the receiver can be turned on and acquire both a position solution and lock onto the occulting GPS satellite prior to the occultation event starting. Without meeting this requirement the radio occultation experiment is impossible.

The OEM4 receiver, being designed for air and ground applications, uses many assumptions in its acquisition algorithm which are poorly suited to the reality of operation in orbit. A potential for acquisition problems was identified in Montenbruck (2003). Although the report concluded that the receiver's default search algorithm was in fact adequate for orbital operations, it also mentioned the possibility that standard receiver commands could be made use of to aid the acquisition. This chapter explains in depth how standard receiver commands have been employed on CanX-2 in order to meet the strict constraints of nanosatellite operation with the commercial receiver.

Much of the work presented in this chapter has been previously published in the proceedings of the ION GNSS 2010 conference, under the title "Optimizing Tracking and Acquisition Capabilities for the CanX-2 Nanosatellite's COTS GPS Receiver in Orbit."

3.1 Acquisition Challenge

There are a number of reasons that a commercial receiver will have trouble acquiring in space. First, the extreme velocity of a satellite leads to a much broader range of Doppler shifts for incoming signals than a receiver on the ground experiences, which means that the search algorithm takes longer to run and may never find enough signals for a position fix. The Doppler shift at an instant between epochs $n-1$ and n is calculated using the equation below, where $range_{n-1}$ and $range_n$ are the geometric ranges between CanX-2 and a GPS satellite at the two epochs, $Dt_{n,n-1}$ is the elapsed time between the two epochs, and I_{L1} is the L1 wavelength. This equation uses the NovAtel convention of a positive Doppler shift when the two satellites are approaching each other.

$$Doppler_{n,n-1} = \frac{range_{n-1} - range_n}{I_{L1} \Delta t_{n,n-1}} \quad \text{eq. 3.1}$$

For CanX-2, travelling at 7 km/s, the Doppler shifts are typically within a range of +/- 45000 Hz. A stationary receiver on the ground will see shifts within a range of +/- 5000 Hz (Lachapelle 2009), nine times smaller. The NovAtel OEM4 search algorithm covers a range of +/-10000 Hz (NovAtel 2005), which is more than adequate for kinematic ground applications but represents less than a third of the range seen onboard the orbiting CanX-2. For the algorithm to successfully acquire a position fix in space there must therefore be four visible GPS satellites at Doppler shifts within the +/- 10000 Hz window.

The second difficulty in acquisition is that NovAtel receivers narrow the search for GPS satellites by using their last known position and stored almanacs for the GPS constellation to predict which PRNs will be in view. For acquisition in orbit any assumptions about the last known receiver position will be invalid in minutes, and cannot be used to narrow the search to visible PRNs. In particular, with CanX-2's orbital period of 98 minutes and operation typically only once per day if at all, the nanosatellite will have circled the earth multiple times between uses of the GPS receiver, and can be

literally over any place on earth during acquisition. Seeding the search algorithm with its last known position is more likely to hinder than to help acquisition.

Finally, another of the receiver's assumptions when predicting the visible GPS constellation is that the antenna is pointing upward with an unobstructed view of the sky. For CanX-2, the requirement for the radio occultation experiment is that the antenna be pointed rearward in order to maximize the signal power on the setting GPS satellite in order to maintain lock in spite of the atmospheric interference. As a result, only half the sky is in view of the antenna during these experiments, and receiver channels dedicated to searching for PRN's ahead of CanX-2 are a waste of valuable resources.

3.2 Previous Work

Previous satellite missions have applied different techniques in order to acquire under these limitations. The most common are either providing a long acquisition time after cold starting the receiver (Feng et al 2003), making use of a specialized space receiver with additional channels for parallel search (Ebinuma et al 2005), or using an onboard system capable of real time orbit determination in order to propagate the last known position forward and warm start the receiver (Unwin & Sweeting 1995).

Documentation from a combination of existing satellite missions and simulated trials show that cold starting a commercial receiver in space typically takes 7-15 minutes, but can occur in as little as 2 minutes if the right geometry exists (Feng et al 2003, Unwin & Oldfield 2000, Montenbruck et al 2006, Sarda et al 2009). Space receivers with additional channels to speed the search have been found to take an average of 2.5 minutes for the U.S. Space Shuttle's LPT receiver (Page et al 2003), 3 minutes 46 seconds for the Disaster Monitoring Constellation (DMC) satellites' SGR-10 receivers (Ebinuma et al 2005), and typically less than 15 minutes for the Blackjack receiver onboard CHAMP (Montenbruck & Kroes 2003). Warm starting receivers in space using orbital propagators has typically taken 90 seconds (Unwin & Sweeting 1995, Unwin & Oldfield 2000).

Although all of these strategies have been found to be successful, none fit within the power, budget, and operational limitations of CanX-2. Instead, the suggestion of using standard receiver commands to aid acquisition from Montenbruck (2003) has been developed into a working method and implemented.

3.3 Script Generation

The operating scenario for CanX-2 is to generate scripts on the ground containing a series of commands for warm starting the receiver. Each script is specific to a particular occultation event, and must be run at the appropriate time to be effective. The scripts are generated in Calgary, typically once per week during a data collection campaign, and emailed to Toronto. In Toronto scripts are selected based on the timing of the passes, and one or two are uploaded to the satellite daily from the U of T ground station. The experiments are run at the appropriate time by the onboard computer on the satellite, the newly collected GPS data is recorded, and finally the data is downloaded to Toronto during a subsequent pass. The files of experiment results, consisting of raw GPS data from the OEM4, are then emailed back to Calgary at the end of the week for analysis and processing.

An occultation event, for the purposes of data collection, is defined as the period of time that a GPS satellite is occluded from view behind the earth's atmosphere from the point of view of CanX-2. The occultation begins when the GPS satellite passes from the unobstructed sky above CanX-2 into the part of sky obstructed by the atmosphere near the earth, and ends when the GPS satellite sets behind the earth's surface. For simplicity, the "top" of the atmosphere is defined as a spherical shell 500 km above the surface of the earth, and the earth is defined as a sphere of radius 6371 km.

In order to generate scripts, software was developed which predicts all the daily occultation events visible to CanX-2's rear pointing GPS antenna (Kahr 2007). Although commercial missions with multiple GPS antennae are also capable of observing rising occultation events, where GPS satellites ahead of the low earth orbiting satellite begin

behind the earth and rise into view, these are not observed from CanX-2 due to the single antenna and difficulty in first acquiring lock on a GPS satellite while the signal quality and power are degraded by the atmosphere.

During script generation, first the positions of the GPS satellites and the CanX-2 satellite are calculated over an entire day. During this process a record of the PRN number, start and end time is made for each occultation that is seen from CanX-2. The occultations are screened based on occurrence over Canada, on occurrence when the satellite is in sunlight, and on occurrence when a sufficient number of GPS satellites are in view of the rear pointing antenna for the duration of the trial. The daily events meeting these criteria are then ranked based on their geometry, which is assessed using average PDOP during the occultation event. Scripts are only generated for the top occultations daily. Figure 3.1 below is a flow diagram of the predictor software's algorithm.

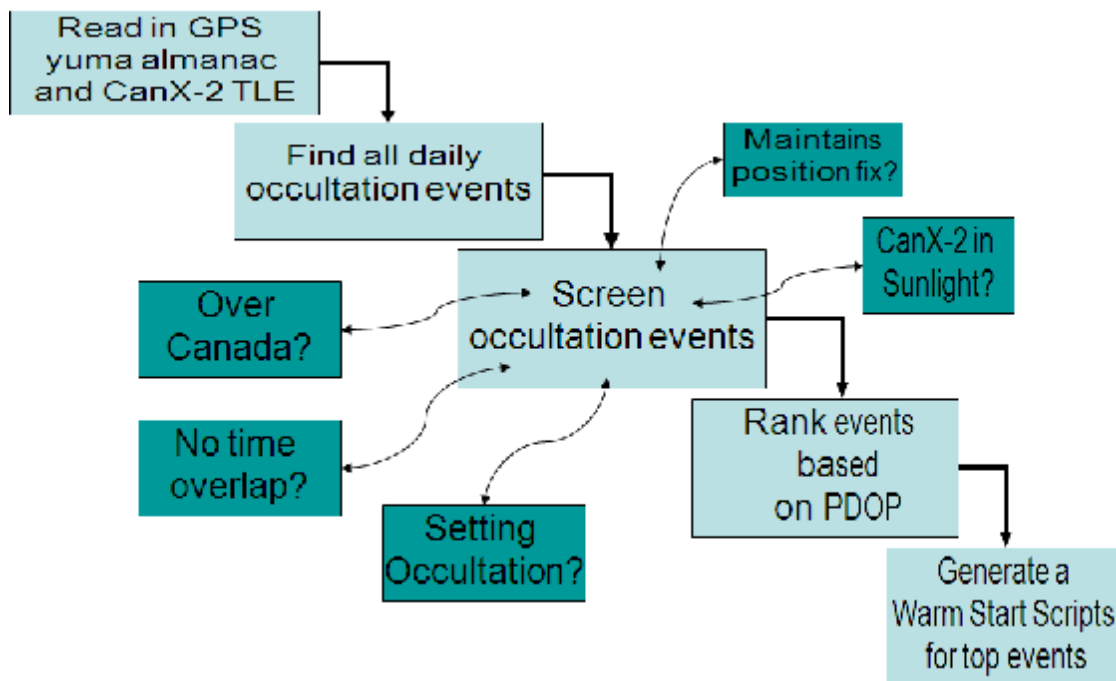


Figure 3.1: Flow chart of the script generation software

3.4 Script Format

Each occultation trial consists of two phases. During the initial acquisition phase the receiver is powered on, a connection to the onboard computer is established, the acquisition commands are issued, and the receiver is given time to begin tracking as many GPS satellites as possible. Data is logged at a low logging rate during this period, to minimize the memory usage while still collecting valuable data about the acquisition process and positions for use in orbit determination. The second phase, lasting six minutes on average, is the observation of the occultation itself. During this phase the logging rate is increased to collect the maximum possible data from the setting GPS satellite. Trials end when either the receiver shut off time is reached or the available memory is filled, whichever occurs first.

The radio occultation experiment scripts consist of three types of commands; basic commands to power on the receiver and connect to it from the onboard computer, warm start commands to set the current time and position in the receiver and assign a particular GPS satellite to each receiver channel, and communication commands to set up the data logging in order to record the results.

The channel assignment is done based on the predicted geometry of CanX-2 and the GPS satellites. NORAD two line elements for CanX-2 and Yuma almanacs for the GPS constellation are used for the prediction. The expected Doppler shifts for each GPS signal are calculated and applied using the NovAtel OEM4 assign command, along with a range of Doppler values to be searched on either side of the assigned value. The example command below assigns channel 0 of the receiver to track PRN 26, with a predicted Doppler shift of -30118 Hz +/- 1500 Hz:

```
assign 0 26 -30118 1500
```

In this way the receiver will search for all GPS satellites in its field view, even if they are in positions that are below the receiver's horizon. Conversely, no channels are wasted on

searching for PRNs that are ahead of CanX-2 and therefore outside the field of view of the rear pointing antenna. Scripts are only generated if there are at least five Doppler assigned channels to provide an initial position fix, the required four and one extra for redundancy.

In addition to the Doppler assigned channels, some channels are assigned to PRNs which will only come into view later in the trial. This can represent half of the available PRNs or more, as the relative speeds of the GPS satellites and low earth orbiter make for extremely rapid changes in geometry. These PRNs are not assigned Doppler values or search windows, based on the assumption that the receiver will find them when they come into view using a stored almanac and its current position and velocity solution. In the case where not all twelve channels are assigned to specific PRNs, the remaining channels are set to 'auto' in order to assist in the search using the receiver's default algorithm.

Figure 3.2 shows the predicted geometry of an occultation event on January 16, 2009, based on a rear pointing antenna with a 15 degree elevation mask. The centre of the figure represents zenith, and the top of the figure is the direction of travel of CanX-2. Based on the figure, PRNs such as 20 and 12, which were in view at the beginning of the trial, were assigned Doppler values. PRNs 4 and 17, which came into view later, were assigned channels but no Dopplers. PRN 14 was the desired occulting PRN for this trial; the trial ends as soon as it sets behind the earth. Figure 3.3 is the corresponding script.

January 16, 2009 from 15:40 to 15:48 UTC
Predicted Visibility of the GPS Constellation

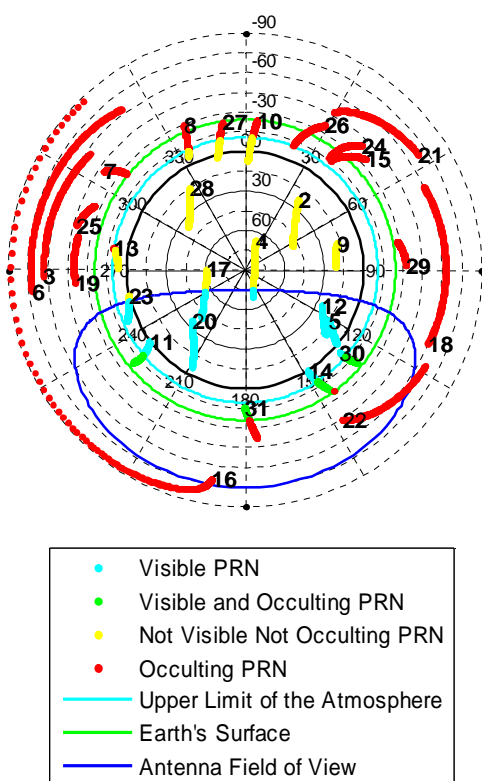


Figure 3.2: Predicted GPS constellation visible to the CanX-2 satellite. The centre of the plot represents the local zenith and the top of the plot is the forward motion direction

```

GPS
34
A N
A N
A N
A N
A N
B 9600
W 10
C com com1 115200 n 8 1 n
W 2
B 115200
W 2
L A
C setapproxpos 53.4328 -78.9167 62
C setapproxtime 490 488472
W 2
C assignall idle
C assign 0 14 -36137 1500
C assign 1 20 -24939 1500
C assign 2 5 -16554 1500
C assign 3 11 -28161 1500
C assign 4 12 -12489 1500
C assign 5 30 -21941 1500
C assign 6 4
C assign 7 17
C assign 8 23
C assign 9 auto
C assign 10 auto
C assign 11 auto
C log rangecmpb ontime 0.02
W 452
C unlogall
U
W 1
A F
E

```

Figure 3.3: Script corresponding to the January 16, 2009 data collection

For each trial compressed range data is logged and later transmitted to the ground, to be post processed and used for both orbit determination and atmospheric retrieval.

3.5 Initial Results

After on orbit commissioning by UTIAS staff, the GPS payload was first made available to researchers at the University of Calgary in November of 2008.

All of the trials run from November 2008 to February 2009 using scripts failed to track sufficient GPS satellites for a position fix. At most three satellites were tracked simultaneously. Investigation into the results showed several patterns which were used in debugging.

First, all GPS satellites tracked in the first four months were acquired at approximately zenith, corresponding to a Doppler shift near zero. It could be concluded that the Doppler assignment was not working.

Second, the time allocated for the acquisition phase of the trials was increased repeatedly, but no improvement was seen in the acquisition. This was particularly notable because cold starting the same receiver had provided a position fix in just under 10 minutes. With an available acquisition time of fifteen minutes, it appeared that Doppler assignment was actually preventing a fix.

Third, the power levels of all the trials were unexpectedly low, with the peak values near 30 dB Hz rather than the expected 50 dB Hz peak for a NovAtel receiver on the ground. Investigating further showed a strong correlation between the positions of the GPS satellites and the observed power levels. Signals at zenith were strongest, with the power level dropping off rapidly as the GPS satellite descended and approached the horizon. No GPS satellites were tracked below the satellite's horizon, making atmospheric observations impossible.

Figure 3.4 shows the combined results of all trials run in the period from November 2008 to February 2009, with the blue line outlining the rear pointing antenna's 15 degree elevation mask, and the GPS satellites coloured based on the L1 signal power. The green and cyan masks show the earth's and atmosphere's upper edges.

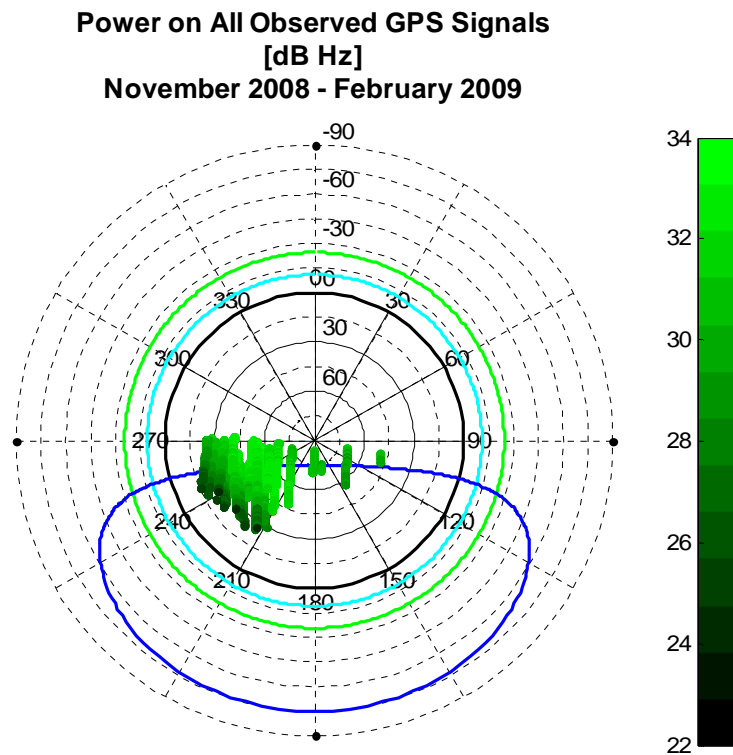


Figure 3.4: Power level on all trials November 2008 - February 2009

3.6 Improvements

Over the period from February to July, 2009, improvements were made to five areas of the experimental setup, which allowed for the eventual successful collection of occultation and positioning data. These were modifying the pointing direction, correcting the Doppler assignment, careful consideration of the antenna's visibility mask, improved formatting of the scripts, and better managing the usage of the available memory.

3.6.1 Pointing Direction

The first significant problem to be solved was the pointing direction of the GPS antenna. It was discovered that through a misinterpretation of the satellite's attitude angles the first set of trials had all been run with the antenna pointing forward instead of rearward. Although a forward pointing antenna can be used to track rising occultations, the acquisition limitations of the OEM4 already discussed and the channels assigned to GPS

satellites behind the receiver prevented tracking of any GPS satellites except those directly overhead. The low power seen in the original trials was also caused in part by the pointing direction, as all satellites tracked were beneath the antenna with elevations ranging from 0 degrees to -10 degrees in the antenna's field of view.

Correcting the pointing direction of the experiment contributed significantly to the future success; however, it did not fully correct the lower than expected power values. Figure 3.5 shows the power levels and PRN distribution seen during a rear pointing occultation trial, which typically range from 29 dB Hz to 39 dB Hz. The cause of the low power remains unknown, but data obtained from an outdoor ground test on live signals prior to launch reveal that the problem already existed and is therefore not a result of either damage during launch or operating conditions in space. Unfortunately the problem was not caught early enough for changes to be possible. While early testing indicated no issue with the antenna mounting or satellite design, changes to the design of the satellite in the intervening years may have resulted in this unsolved tracking problem. The source of the problem however remains a matter of speculation, with the satellite inaccessible in space.

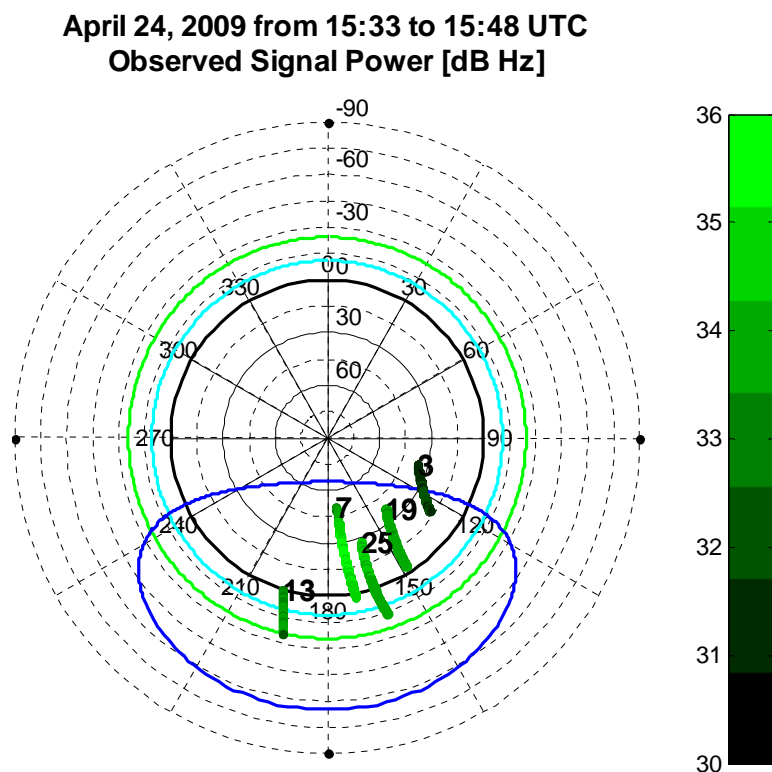


Figure 3.5: Power level on April 24th, 2009 Trial

3.6.2 Doppler Assignment

Investigation into the Doppler assignment showed that there was a significant difference between the predicted and observed Doppler shifts. While the predicted values had been compared to those generated by a Spirent hardware simulator that was used to test the scripting approach before launch (Kahr 2007), one element not accounted for was the initial random bias in the receiver clock frequency on power up. During simulator testing these values were not found to be very significant; however, in contrast to a receiver on the ground it was found that the clock in space had a systematic frequency bias on the order of kHz. Figure 3.6 shows the systematic bias in the receiver clock rate over the course of 15 months in orbit, both in terms of the difference in Doppler as seen on GPS signals, and as a fraction of the nominal L1 frequency of 1575.42 MHz (Lachapelle 2009).

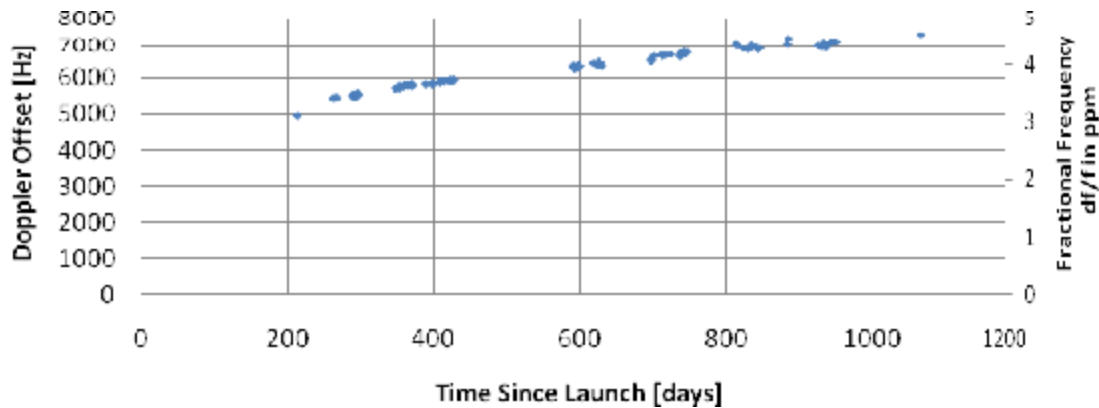


Figure 3.6: Doppler offset on CanX-2's GPS receiver

3.6.2.1 Potential Causes of Frequency Drift

There are several potential causes for the frequency shift in space. Among them are environmental factors such as variation in temperature and pressure, relativistic effects, and the radiation dose experienced in orbit.

The temperatures of components onboard the CanX-2 satellite are monitored, and range between extreme values of 6°C and 45°C (Sarda et al 2009). This is not significantly different than the temperature range an OEM4 GPS receiver might be subjected to in an outdoor survey application, and is well within the manufacturer's specified range of -40 °C to +85 °C (NovAtel 2003). It is unlikely that temperature variation is the cause of such a dramatic offset, in particular because the OEM4-G2L receiver is temperature compensated (NovAtel 2003).

Because quartz crystal has piezoelectric properties, a change in pressure or acceleration will also induce a change in frequency (Vig 2008). For the case of CanX-2, it would, however, be expected that a one-time pressure induced frequency shift would occur at launch with no subsequent frequency drift, which does not correspond to the observed behaviour.

Relativistic effects are a third possible cause. According to Ashby & Spilker (1995) the combined relativistic effects caused by the orbital velocity of a satellite in a circular orbit and its height above the geoid in a spherically symmetric gravity field can be described by the equation below, where m_e is the ratio for the earth of $4.435028687E-3$ metres, r_c is the satellite's orbital radius, and the term $-\Phi_0/c^2$ is the gravitational potential over the speed of light squared with a value of $6.9692842 \times 10^{-10}$.

$$\frac{df}{f} \cong 1 - \frac{3m_e}{2r_c} - \frac{\Phi_0}{c^2} \quad \text{eq. 3.2}$$

Figure 3.7 depicts the magnitude of the relativistic effects at orbital altitudes from low earth orbit to geosynchronous orbit.

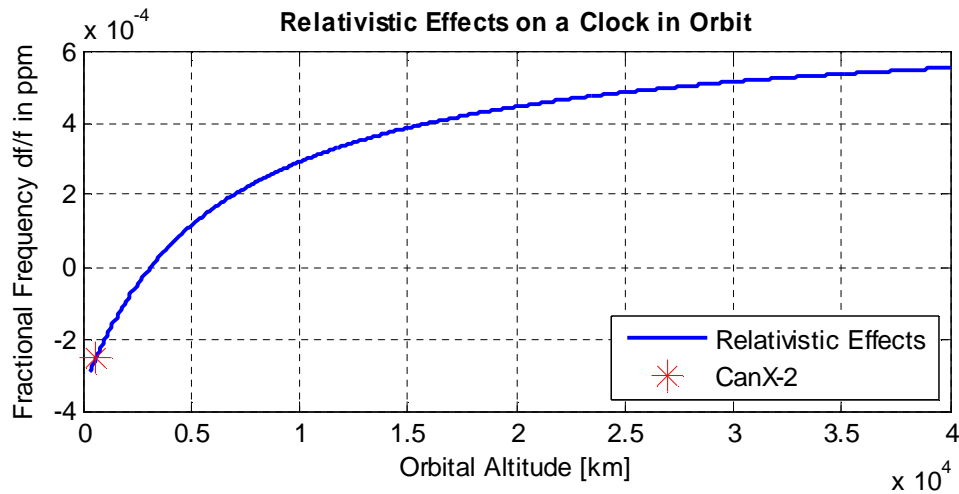


Figure 3.7: Relativistic effects on CanX-2's clock in orbit

It can be seen from the figure that the effect of relativity on the clock frequency in CanX-2's orbit is -2.5165×10^{-4} ppm, four orders of magnitude lower than the observed frequency drift. Relativity can therefore also be ruled out as the cause.

Finally, according to Vig (2008), the impact of radiation above 1 krad on a quartz crystal oscillator is dependent on the purity of the crystal. Pure quartz is able to recover from

radiation effects after time and will not have a sustained frequency shift, while radiation sustained by a crystal with impurities can lead to damage to the crystal's structure. The resulting frequency change can be as large as 10 ppm at a total radiation dose of one Mrad. The frequency shift increases rapidly at lower radiation doses, with a diminishing change in frequency as the dose increases. According to Markgraf & Montenbruck (2004), a satellite in a polar low earth orbit such as CanX-2 would expect a radiation dose on the order of 10 krad. It is not clear if such a low dose of radiation could cause the 3 – 5 ppm shift in CanX-2 clock, but radiation does appear to be the most plausible cause of the frequency drift.

3.6.2.2 Frequency Drift Modelling

It can be seen from Figure 3.6 above that although the magnitude of the clock bias is significant enough to prevent the CanX-2 Doppler assignment from working, it is also reasonably stable and drifts at a predictable rate. Using the first four months of Doppler offsets, linear extrapolation was used to predict the offset in future trials, and to adjust the values assigned in the scripts to compensate. The extrapolated values were generally within 100 Hz of the measured values, which was sufficiently accurate to allow for position fixes even after several months without operating the receiver.

Figure 3.8 shows the difference between the predicted and observed Dopplers during the April 24th experimental trial. It can be seen that the offset has a magnitude of approximately 5700 Hz prior to the fourth PRN being acquired, and then drops near zero when the receiver begins steering its clock. Residual offsets are likely due to inaccuracies in the predicted Dopplers, which are generated based on week old GPS and CanX-2 almanacs.

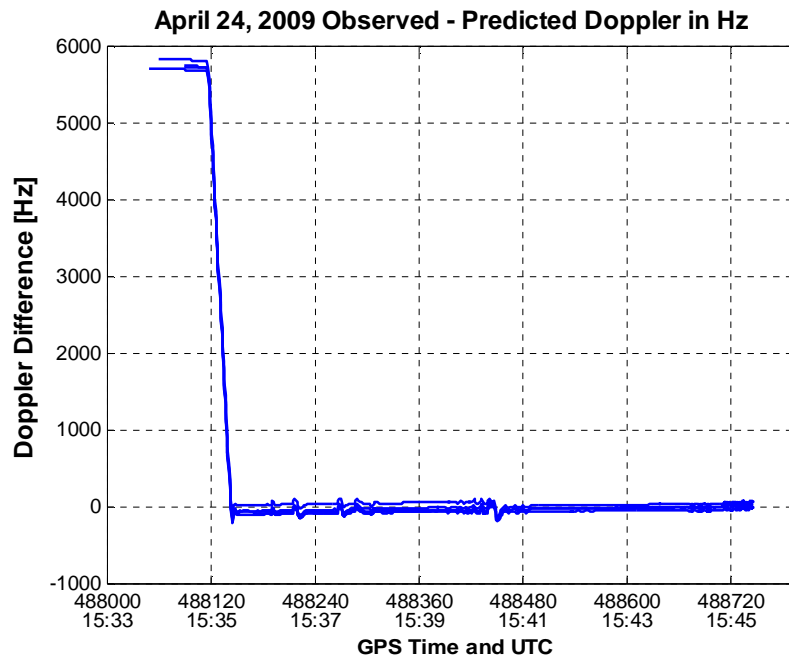


Figure 3.8: Doppler offset during the April 24th trial

In addition to the major correction to the receiver clock, two smaller changes were made to the Doppler channel assignment. First the search window was increased from 1500 Hz to the maximum value of 10000 Hz. The initial value of 1500 Hz, which had been tested successfully using a GPS simulator prior to the launch of CanX-2, was inadequate under real operating conditions. When CanX-2 passes beneath a GPS satellite the Doppler can change by more than 3000 Hz in 45 s. The increased search window has the advantage of containing the true Doppler shift value for much longer. The increased search window also allows the true value to stay within the search range even when clock steering begins and the Doppler shifts being observed by the receiver suddenly jump on the order of 6000 Hz.

The second change was that the initial phase of the occultation experiment, dedicated to receiver start up and acquisition, was shortened. As was previously mentioned, the acquisition phase had been increased repeatedly prior to solving the problem with the clock offset, until acquisition times as long as eleven minutes were scripted. Because of the extreme relative speed of CanX-2 and the GPS satellites, the geometry changes

significantly over the course of minutes. In many trials, after the initial position fix was acquired one of the necessary GPS satellites would set prior to the occultation event beginning. Because the channels are not 'released' in the script but continue to search for the assigned PRNs even after they have set, there are reduced number of channels which are free to seek out new PRNs just coming into view.

For a long trial there are more GPS satellites than receiver channels, and so it is impossible to track them all with the current script format. Releasing channels, although possible, would add significantly to the complexity of the radio occultation scripts. Instead, PRNs which are only in view for a short time are discarded by the script generation software, as they are less likely to be acquired in time to be used. GPS satellites which only come into view near the end of the trial are therefore unlikely to be assigned to channels and tracked.

These late rising GPS satellites are, however, important for the success of the experiment. Their importance stems from the geometry of the situation. Because CanX-2's forward motion, at roughly 7 km/s, is far greater than the speed of the GPS satellites at 4 km/s, all GPS satellites come into view at zenith and set behind CanX-2. Tracking a new satellite late in the event provides a significant improvement to the positioning geometry in most cases, because it will be the only satellite directly overhead. Shortening the acquisition time from eleven minutes down to five minutes effectively bypasses this problem because it reduces the number of satellites that enter the antenna's field of view during the trial. Generally between 8 and 11 of the channels will be assigned for a five minute start up time, depending on the distribution of the GPS constellation.

Figure 3.9 shows the geometry of the satellites tracked on the April 24th, 2009 trial. The antenna elevation mask for this trial was set to -10 degrees, based on the empirical antenna field of view determined during the forward looking trials. It is therefore the area outside the blue line which is visible to the antenna. Each PRN's position is color coded based on time, in order to show the available constellation at each epoch. Although there

is sufficient geometry for positioning initially, PRN 13 sets completely before the desired occultation event on PRN 25 begins. Also, the satellites are all clustered in the same part of the sky.

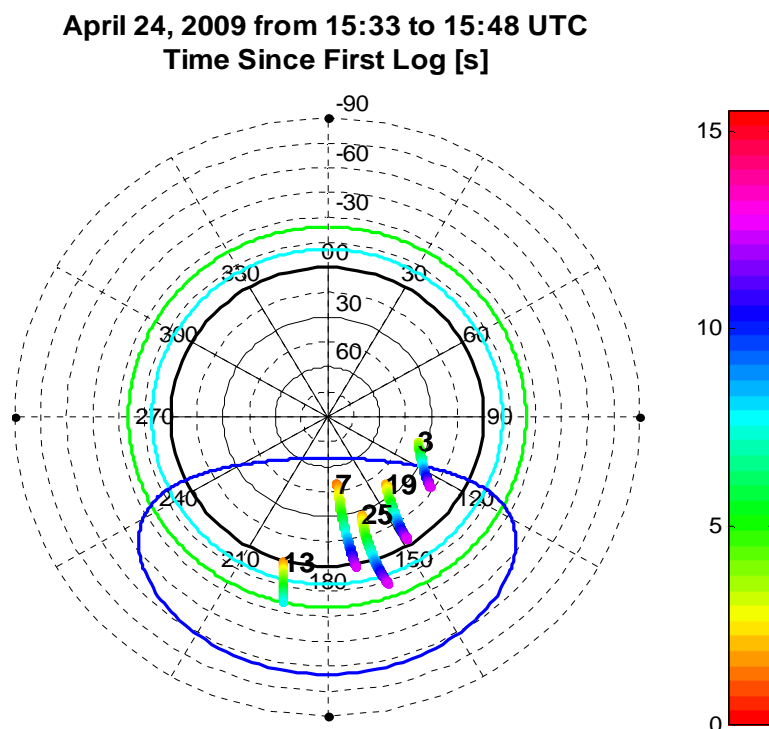


Figure 3.9: Acquired geometry of the April 24th trial

The predicted GPS availability for the same trial is displayed in Figure 3.10, where it can be seen that a total of 15 GPS satellites should have come into view during the trial, and that several of them came into view near zenith and would have significantly improved the geometry had they been acquired. In later trials with shortened acquisition times the distribution of tracked GPS satellites during the occultation event was significantly improved.

**April 24, 2009 from 15:33 to 15:48 UTC
Predicted Visibility of the GPS Constellation**

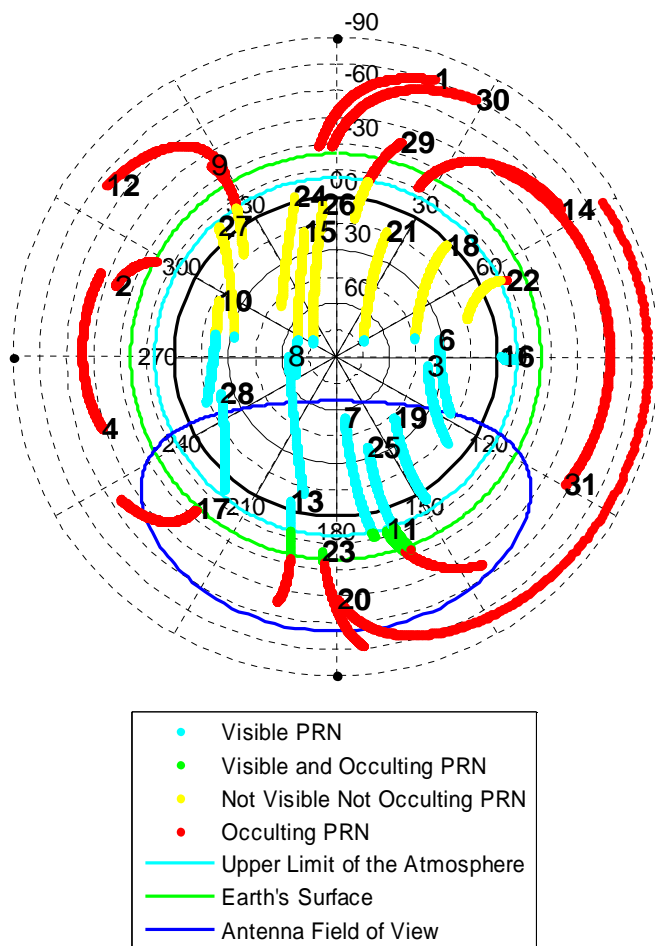


Figure 3.10: Predicted geometry of the April 24th trial

3.6.3 Antenna Field of View

The extent to which the antenna pointing direction is critical to the success of the channel assignment scripts was proven during the forward pointing trials. It has also been proven in subsequent trials that even when the clock drift is properly accounted for in the channel assignment, if the scripts are run without the appropriate attitude control no position fix will be obtained.

Additionally, the initial results with known antenna pointing direction had extremely poor positioning geometry even when sufficient PRNs were tracked, with most of the GPS satellites clustered at the horizon during the occultation event. At most five PRNs were acquired at once, in spite of all twelve channels being assigned values. More detailed investigation into which satellites were acquired from a given script was carried out in an attempt to improve the tracking results. It was found that the signals most likely to be acquired, with or without Doppler assignment, are those closer to the centre of the antenna's field of view. In general, only satellites within an antenna elevation mask of 25 degrees above the antenna's horizon are acquired, even though it had been seen earlier that once acquired they would be tracked down to -10 degrees from the centre of the antenna field of view. This limited elevation mask is likely tied to the low power values. Figure 3.11 depicts the trend in tracking over 5 data collections carried out with the antenna pointing to zenith during November 2010, with the trend of acquiring above 25 degrees (represented by the blue line) and tracking down to negative elevations clearly visible.

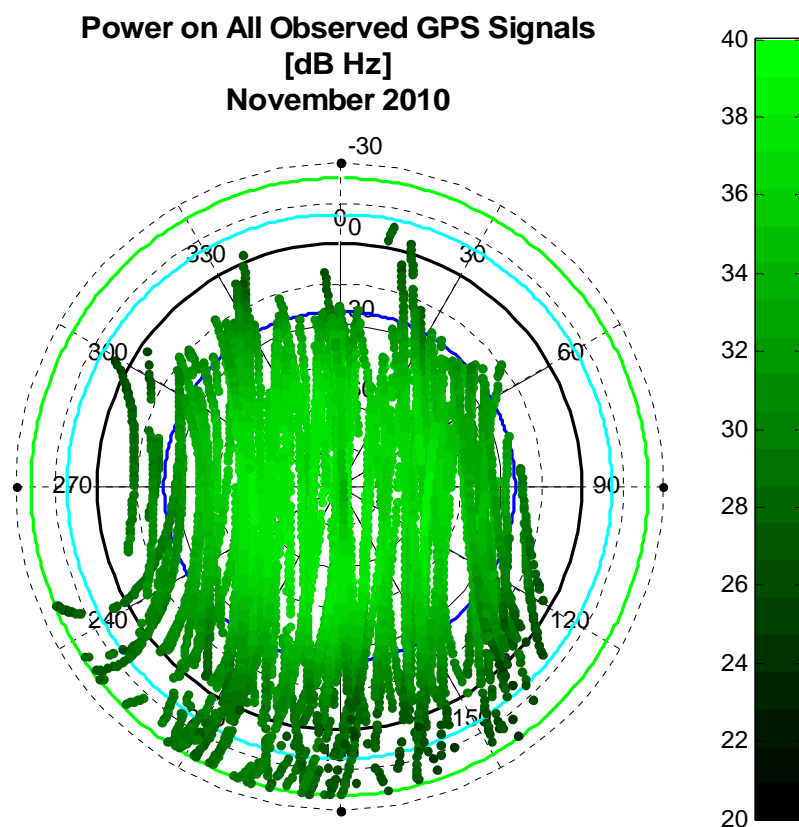


Figure 3.11: Acquisition pattern with a zenith pointing antenna field of view

Two changes were made to the script generator. First, the elevation mask was drastically increased from -10 degrees to 25 degrees in order to limit the field of view for script generation. Although this theoretically limited the number of acceptable occultation events in a day, by eliminating occultation trials which depended on satellites in the edges of the antenna's field of view, it left only the trials with the highest likelihood of success.

At the same time, to get the maximum benefit from the very limited field of view and antenna power, it was requested that future occultation trials be run with the antenna pointing to 45 degrees between zenith and the horizon. This provided a compromise between maximizing the chance of acquiring sufficient satellites to process an occultation event, and maximizing the power on the occulting PRN. The results of a trial collected

with a 25 degree antenna mask and 45 degree antenna pointing angle are displayed in Figure 3.12.

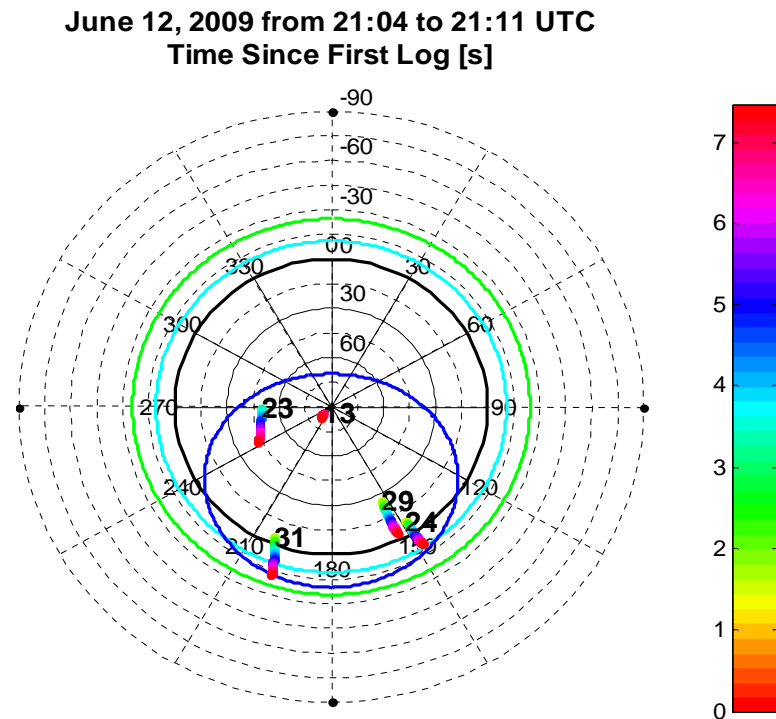


Figure 3.12: June 12th, 2009 tracking results with a 45 degree antenna pointing direction and 25 degree antenna elevation mask

It can be seen that the distribution of the satellites is significantly improved; however, the limited elevation mask prevented tracking of the PRNs all the way to the earth's surface because the stop time for the script was too early. In order to compensate for this undesired side effect the script generation software was modified to provide a second, 5 degree elevation mask for satellites going out of view, while keeping the 25 degree mask used for channel assignment. This combination of antenna pointing direction and elevation masks has been used in many subsequent trials and has met with good results.

3.6.4 Script Formatting

In addition to all the hardware and physical challenges facing the experiment, a few modifications have been made to the scripts themselves in order to solve substantial problems.

The first successful position fix was achieved on April 7th, 2009 after resolving the clock offset and pointing direction problems, but a second set of problems quickly came to light. In more than half of the trials the receiver would either log a few lines of data and stop, log nothing at all, or suddenly behave as though it had been cold started by ‘forgetting’ the approximate time, position and channel assignment. None of these cases allowed for collection of positioning data. Satellite telemetry data showed that the receiver was continuously turned on in all of these cases, and it was originally believed that the receiver was in some way damaged. No pattern was discernable in the trials run from April through to July of 2009 which could be used in either debugging or predicting which future trials would succeed or crash.

Extensive hours spent reading decoded OEM4 output files revealed that in all trials which acquired without crashing, the GPS week changed from the rolled over 0-1024 week assigned in the scripts to the continuous 1024+ GPS week upon acquiring the first signal. The change occurred in the same line as the change in clock status from “approximate” to “coarsesteering”.

Logs from the successful April 24th trial:

```
#RANGEA,COM1,0,88.0,APPROXIMATE,504...
```

```
#RANGEA,COM1,0,84.5,COARSESTEERING,1528...
```

In the few trials that logged data prior to crashing there was no corresponding change in GPS week, and the crash always occurred immediately after the change in clock status.

Logs from just before the crash in a failed April 7th trial:

```
#RANGEA,COM1,0,85.0,APPROXIMATE,502...
```

```
#RANGEA,COM1,0,77.0,COARSESTEERING,502...
```

Scripts using both possible week formats had been tested prior to CanX-2's launch with a GPS simulator; however when the crash occasionally occurred it was attributed to rewinding the simulator scenario and replaying the same GPS times. The OEM4 documentation for the SETAPPROXTIME command is ambiguous, specifying the week format as 0-1024+ which implies that either syntax is acceptable. Insufficient simulator tests were done for the pattern to emerge and be attributed to using the incorrect week format, as the crash only occurs intermittently.

Analysis of the data collected in orbit seems to indicate that the bug in the OEM4's software is only triggered when many satellites are acquired simultaneously, as is the case when accurate Dopplers are assigned to multiple receiver channels. In the early trials only one PRN would be acquired at a time, and the week would be updated with the first PRN's navigation message before any others were acquired. As a result this bug only manifested itself after the clock offset was compensated for. The solution to the problem was changing the time assignment command in future scripts, from "SETAPPROXTIME 504 488002" to "SETAPPROXTIME 1528 488002" which has prevented the problem from reoccurring.

An additional important change to the script format provided by the team in Toronto has been the addition of pauses between each command. Early trials such as the example plotted in Figure 3.9 and Figure 3.10 only acquired approximately half of the satellites which should have been in view. Given the channel assignments, a valid almanac, and a position and velocity fix, the receiver's internal algorithm should have allowed it to begin tracking the remaining satellites. Adding pauses between the script lines has significantly increased the number of satellites acquired, from typically five being tracked before the pauses to as many as nine being tracked afterwards in spite of a smaller constellation of active GPS satellites. It is suspected that some of the channel assignment commands were

formerly being lost, as they were transmitted to the receiver all at once with no time built in for the commands to be individually executed.

3.6.5 Memory Usage

The final area of improvements made to the occultation experiment is better management of the limited memory available for a trial.

Initially, a logging rate of 50 Hz was used for the entire data set in order to collect as much information as possible during the short data collection intervals, and to benefit from any GPS satellites that occulted earlier than the desired occultation event. When the first satellites were tracked it quickly became apparent that the amount of data logged would far exceed the available 1 Megabyte buffer size, even logging in compressed binary format. Figure 3.13 shows the initial data set during which only two satellites were tracked at 50 Hz before the receiver ran out of available memory and shut off.

**November 28, 2008 from 22:23 to 22:29 UTC
Time Since First Log [s]**

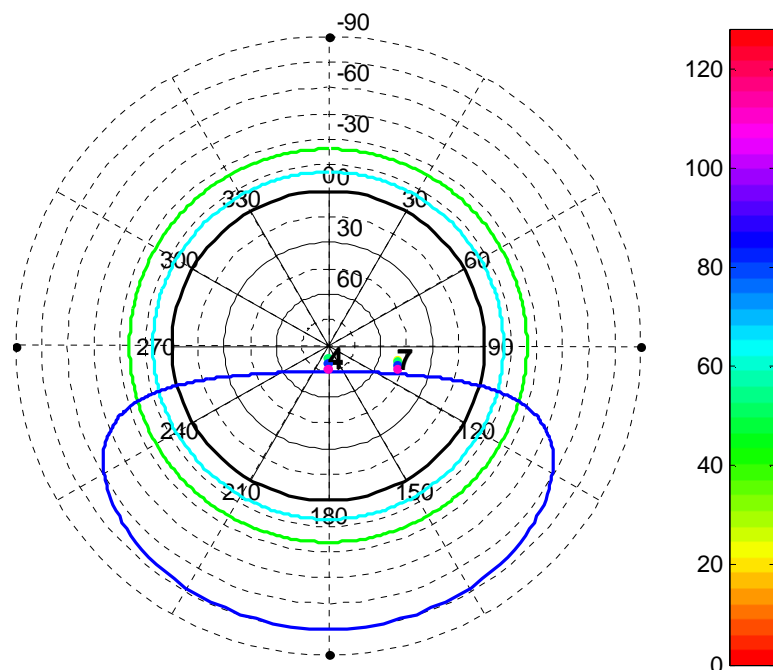


Figure 3.13: All data collected Nov 28th, 2008 prior to memory limited shutdown

To increase the amount of data logged, two logging rates were implemented. A 1 Hz logging rate for the initial startup period allowed for collection of enough data to use for orbit determination and assessment of the acquisition behaviour, and a 50 Hz logging rate during the occultation event itself was ideal for limb sounding. These rates were further reduced to 0.1 Hz during acquisition and 20 Hz during the occultation event as the number of satellites tracked in each trial increased with other script improvements.

In the most recent trials, even at the lower logging rates the buffer fills up prior to the end of the desired occultation event and triggers the early shut down of the receiver. The additional measure of setting unassigned channels to “IDLE” mode, which disables their tracking completely, rather than “AUTO” which used the default search algorithm to aid acquisition was taken, in order to avoid tracking duplicate data from the same GPS satellite. It is a testament to the success of the channel assignment scripts that intentionally disabling some of the channels makes no apparent difference to the number of unique PRNs tracked, and that the available memory is currently still the limiting factor in data collection.

Figure 3.14 shows a more recent trial result, which in spite of the measures taken has maximized the available memory and shut down prior to occulting PRN 20 reaching the earth’s surface. Figure 3.15 is the script used to generate it, in the finalized format for radio occultation data collection.

January 18, 2010 from 16:05 to 16:15 UTC
Time Since First Log [s]

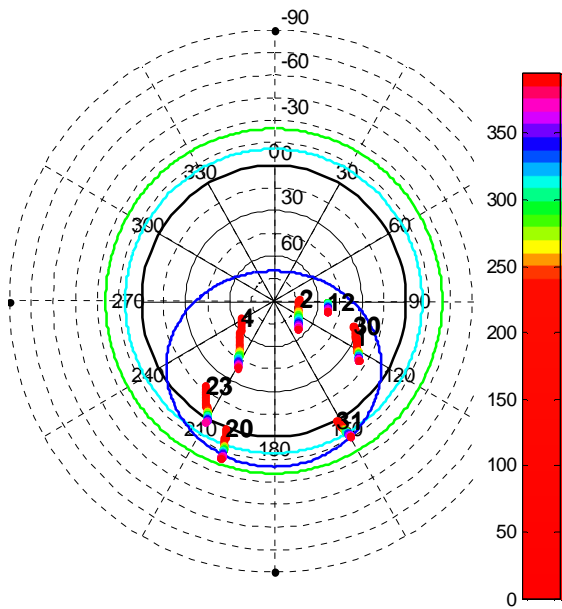


Figure 3.14: (above) All data collected January 18th, 2010 prior to memory limited shutdown. The rapid change in color near the end of the trial represents the higher logging rate.

Figure 3.15: (right) Script for the successful January 18th data collection

```

Slog_week0543_s144660.slg ...
File Edit Format View Help
GPS
53
A N
A N
A N
A N
A N
A N
B 9600
W 10
C com com1 115200 n 8 1 n
W 10
B 115200
W 10
L A
W 1
C setapproxtime 1567 144360
W 1
C setapproxpos 57.9736 -81.1475 629780
W 2
C log rangecmpb ontime 10
W 1
C assignall idle
W 1
C assign 0 20 -33740 10000
W 1
C assign 1 4 922 10000
W 1
C assign 2 1 -2143 10000
W 1
C assign 3 23 -20164 10000
W 1
C assign 4 30 1338 10000
W 1
C assign 5 31 -27508 10000
W 1
C assign 6 2
W 1
C assign 7 12
W 1
C assign 8 13
W 1
C assign 9 idle
W 1
C assign 10 idle
W 1
C assign 11 idle
W 1
W 282
C log rangecmpb ontime 0.05
W 258
C unlogall
W 1
U
W 1
A F
E
    
```

3.7 Script Generation for Long Data Arcs

While the primary goal of the GPS payload is radio occultation, orbit determination is a close second. In order to facilitate the orbit determination work, it was decided to collect some of the longest possible data arcs with the antenna pointing to zenith, as the “best case scenario” GPS data sets. These data sets logged not only raw data, but for the first time also the receiver’s internal position solution, using the BESTXYZ log.

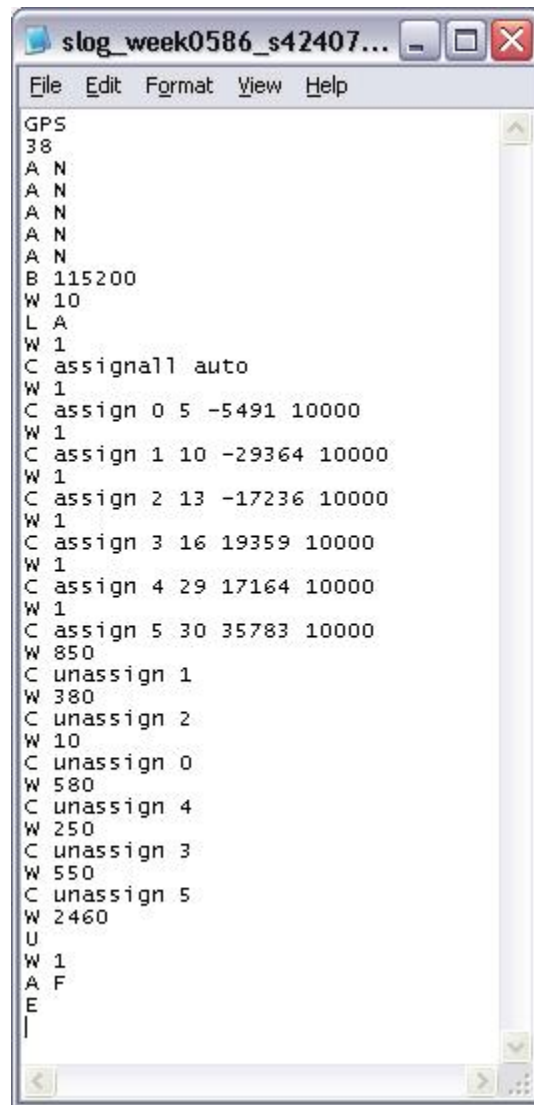
In order to achieve longer data collections an entirely new series of script generation software was required, to create scripts which were not fundamentally based on an occultation event start time, stop time and PRN. This new software makes use of the same algorithms to determine the positions, velocities and inter-visibilitys of CanX-2 and the GPS constellation, but is otherwise based on the schedule of CanX-2 passing from eclipse into sunlight, and the ground contact schedule which must be obtained from the University of Toronto ahead of time.

A script is generated to begin five minutes after CanX-2 passes from shadow into sunlight, based on the attitude control system requirement of five minutes to achieve the desired antenna pointing direction. The data collections last for 85 minutes, based on the restriction of how long the attitude can be accurately maintained. For orbits passing within range of the Toronto ground station the receiver operation times are cut back to fill only the portion of the orbit when CanX-2 is in sunlight but not in contact with the ground, in order to avoid power limitations or corrupt data due to logging and downloading data simultaneously. These shorter scripts are however avoided, as preference is given to the 85 minute data arcs. Based on a week of attempting to collect four to six long arcs daily, it was determined that two per day was the most realistic data collection schedule in order to allow sufficient ground contact time for downloading data and uploading new scripts to the satellite.

Major changes were also made to the structure of the scripts themselves, first to allow for tracking over a long period of time by progressively un-assigning channels as their assigned GPS satellites set, and second to reduce as much as possible the number of commands in the files in order to reduce the transmission burden of uploading new scripts. The changes made included:

- Saving the logging commands and receiver communication settings into the receiver's non-volatile memory and removing the commands from the individual scripts
- Removing the setapproxtime and setapproxpos commands, as the previous mistake of using the wrong year format suggested they made no contribution to acquisition and only the channel assignments were required
- Excluding "assign auto" commands for extra channels, as this is the OEM4's default behaviour and should not require a command
- Releasing each channel after the assigned PRN sets, to allow for default acquisition of newly risen GPS satellites. (If a channel is released before the assigned PRN sets it will "forget" what it was tracking, lose lock, and begin searching with the default search algorithm)

Figure 3.16 below is a sample of the scripts used for collecting long data arcs.



```

slog_week0586_s42407...
File Edit Format View Help
GPS
38
A N
A N
A N
A N
A N
A N
B 115200
W 10
L A
W 1
C assignall auto
W 1
C assign 0 5 -5491 10000
W 1
C assign 1 10 -29364 10000
W 1
C assign 2 13 -17236 10000
W 1
C assign 3 16 19359 10000
W 1
C assign 4 29 17164 10000
W 1
C assign 5 30 35783 10000
W 850
C unassign 1
W 380
C unassign 2
W 10
C unassign 0
W 580
C unassign 4
W 250
C unassign 3
W 550
C unassign 5
W 2460
U
W 1
A F
E
|

```

Figure 3.16: Sample script for long arc data collection

3.8 Effectiveness of Channel Assignment

Because the experimental setup was changed almost weekly during the first year of radio occultation data collection, and again frequently during the long arc data collection, it is difficult to quantify the results with a single number. However, times to various points in the receiver startup have been calculated for 15 radio occultation trials carried out from December 2009 to January 2010, during which the only script parameter to change was idling the extra receiver channels. The same metrics have been measured for 14 long arc

data collections in November 2010. The average times are summarized in Table 3.1 for the radio occultation trials and Table 3.2 for the long arc data collection.

Not included in Table 3.1 is the constant 36 seconds of ‘overhead’, including powering on the receiver, establishing a connection between the on board computer and receiver setting the baud rate for logging GPS data, assigning approximate time and position, and idling all channels immediately prior to assignment. For the data in Table 3.2 the overhead time has been reduced to 12 seconds and is also excluded.

Table 3.1: Time to First Fix Averages from December 2009 to January 2010 radio occultation data collection

Time From First Channel Assignment [seconds]				
Event	Mean	STD	Min	Max
First log	20	1	18	20
First signal tracked	39	15	27	90
Four L1 signals tracked	80	47	34	208
Four L1/L2 signals tracked	99	45	55	224
Valid position solution	164	72	89	326
Valid clock model	211	70	127	338

The table shows that it takes on average 40 seconds for the first signal to be acquired, and an additional 40 seconds for acquisition of four L1 signals. In theory a position could be calculated at this point, although an additional 84 seconds is required for the receiver to acquire L2 signals and process the position solution. The time from receiver start up to a position fix is 3 minutes 20 seconds on average, and from the first channel assignment to a position fix is 2 minutes 44 seconds, which includes 11 seconds of pauses between each channel assignment command in the script.

Table 3.2: Time to First Fix Averages from November 2010 long arc data collection

Time From First Channel Assignment [s]				
Event	Mean	STD	Min	Max
First signal tracked	39	13	30	74
Four L1 signals tracked	106	69	39	281
Four L1/L2 signals tracked	121	68	56	293
Valid position solution	191	86	104	408
Valid clock model	234	64	164	408

The long data arc collection has a slightly worse average time to first fix than the radio occultation trials, at 3 minutes 23 seconds in spite of the shorter overhead time, but based on the standard deviations the differences are insignificant. The longer times to a valid position solution and valid clock model, highlighted above, are biased due to the November data being logged once per 30 seconds as opposed to the 1 second data used for the radio occultations trials. In both cases, a few seconds of synchronisation error also likely exists between the satellite's on board computer clock (used to power on the receiver at the desired epoch) and GPS time used to time stamp the signal acquisition.

The 3.5 minute time to first fix achievable using channel assignment is within the range of values achieved using specialized space receivers in cold start (Page et al 2003, Ebinuma et al 2005). It is significantly better than the time to first fix achieved on CanX-2 with a cold start, which is typically on the order of 20 minutes.

The essential requirements for channel assignment are an estimate of the current time, an estimate of the receiver's clock drift, knowledge of the antenna field of view, and the ability to calculate the relative Doppler shifts between the low earth orbiting satellite and GPS constellation. Ideally, the technique could be incorporated into the receiver and run autonomously in space. Automation would significantly cut back on the operational burden by avoiding the need for script generation and ground contact, but as a trade off requires that either the low earth orbiting satellite or the receiver itself has the ability to estimate its orbital trajectory autonomously in order to compute the expected Doppler shifts of incoming GPS signals. The next chapter presents a method of estimating orbital

parameters from the receiver's navigation solution, in order to propagate the receiver's trajectory through GPS outages autonomously. The chapter following assesses the suitability of this estimated trajectory for warm starting the receiver in orbit, using the CanX-2 receiver's navigation solutions as input and using precise orbit determination solutions as truth data.

Chapter Four: A Proposed Methodology for Autonomous Orbit Propagation

Chapter three outlined the highly effective method of using publicly available ephemeris data for the constellation of GPS satellites and for CanX-2 in order to predict the Doppler shifts on the visible GPS constellation and warm start the receiver. While effective, this method has several drawbacks. First and foremost, it requires a high degree of advance planning, access to public data sources, successful contacts with the ground station, and the experiment must be run at precisely the correct time and satellite attitude for the warm start to work. Additionally, satellites missions which seed the acquisition algorithm using on board orbital propagators have been shown to have a shorter time to first fix in Unwin & Sweeting (1995) and Unwin & Oldfield (2000).

This chapter develops a method in which the GPS data collected on orbit could be used in conjunction with an orbital propagator in order to bridge GPS outages and enable an autonomous warm start when next the receiver is turned on. The five necessary pieces of information for warm starting the receiver are knowledge of the current time, knowledge of the antenna's field of view, knowledge of the receiver's clock drift in space, and finally knowledge of the Doppler shifts on the GPS signals, as calculated from the changing positions of the GPS satellites and the changing position of the low earth orbiter (LEO). An onboard propagator enables the calculation of the LEO's changing position, but there are several fundamental assumptions about the other necessary knowledge.

First, it is assumed that upon start up the receiver would be seeded with the current time and the antenna pointing direction from other satellite sub-systems. The justification for these assumptions is that CanX-2 possesses the necessary sub-systems to provide this information, as do JC2Sat, CASSIOPE, RAX, CanX-4/5, AISSat, ... essentially every other satellite currently carrying or designed to carry a commercial NovAtel receiver (De Ruiter et al 2009, Langley et al 2004, Spangelo et al 2010, Orr et al 2007, UTIAS 2011).

Next, it is assumed that the receiver could autonomously estimate its own clock drift in orbit. The clock drift can be obtained from the velocity solution, calculated from 4 or

more Doppler measurements. The OEM4-G2L receiver will output this value in the “range bias rate” field of the “clockmodel” log. The logged value just needs to be divided by the GPS L1 wavelength to convert the units from m/s to Hz. One critical factor is that the clock drift must be estimated as soon as the first four signals are acquired, prior to the receiver’s clock steering taking effect. The calculation could easily be implemented onboard a satellite. Because the clock drift was found to change slowly and the receiver was found to be insensitive to errors of a few hundred Hz, the most recent clock drift could simply be stored and applied at the next receiver start up, with no need for storage of older data or linear extrapolation to the current epoch.

The final assumption is that the receiver would be run with reasonable frequency. Frequent operation means that the receiver, through tracking GPS satellites, will be able to log the GPS constellation’s almanac from the navigation message and therefore maintain the ability to predict the positions of the GPS constellation reasonably accurately over a period of time. No orbital model is perfect, and the further into the future the satellite’s position must be predicted, the worse the prediction’s accuracy will be. This holds true for both the prediction of the GPS satellites’ positions, and the position of the LEO satellite.

4.1 Fundamentals of Satellite Orbits

According to Kepler’s first law, the motion of an orbiting body can be described as an ellipse, with the central body at one focus (Pail 2005, Sneeuw 2006). If the central body is assumed to be a point mass, the orbiting body’s mass is assumed to be insignificant in comparison, and there are no external forces working on the orbiting body, the equation below fully describes the acceleration acting on it. GM is the gravitational constant multiplied by the central body’s mass, r is the distance from the central body to the satellite, \hat{r} is the position vector from the centre of the central body to the satellite, and \mathbf{a} is the acceleration experienced by the satellite.

$$\mathbf{g} = -\frac{GM}{r^3} \mathbf{r} \quad \text{eq. 4.1}$$

The size and orientation of the elliptical path can be described by a set of six Keplerian elements, which are explained below. The four angular elements are shown in Figure 4.2.

- Right Ascension of the Ascending Node (RAAN), Ω , is the angle from the inertial x axis to the point where the ascending arc of the satellite crosses the equator plane.
- Argument of Perigee, ω , is the angle between the ascending node and the point of closet approach of the satellite to the central body (perigee).
- Inclination, i , is the angle between the equator plane of the central body and the satellite's orbital plane
- Semi-major axis, a , describes the size of the ellipse and is depicted in Figure 4.1

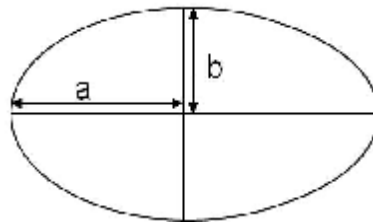


Figure 4.1: Ellipse geometry

- Eccentricity, e , describes the shape of the ellipse and can be calculated from the relation

$$e^2 = \frac{a^2 - b^2}{a^2} \quad \text{eq. 4.2}$$

- True Anomaly, v , is the angle between the perigee and the instantaneous position of the satellite, and is the only time dependent element for the two body problem.

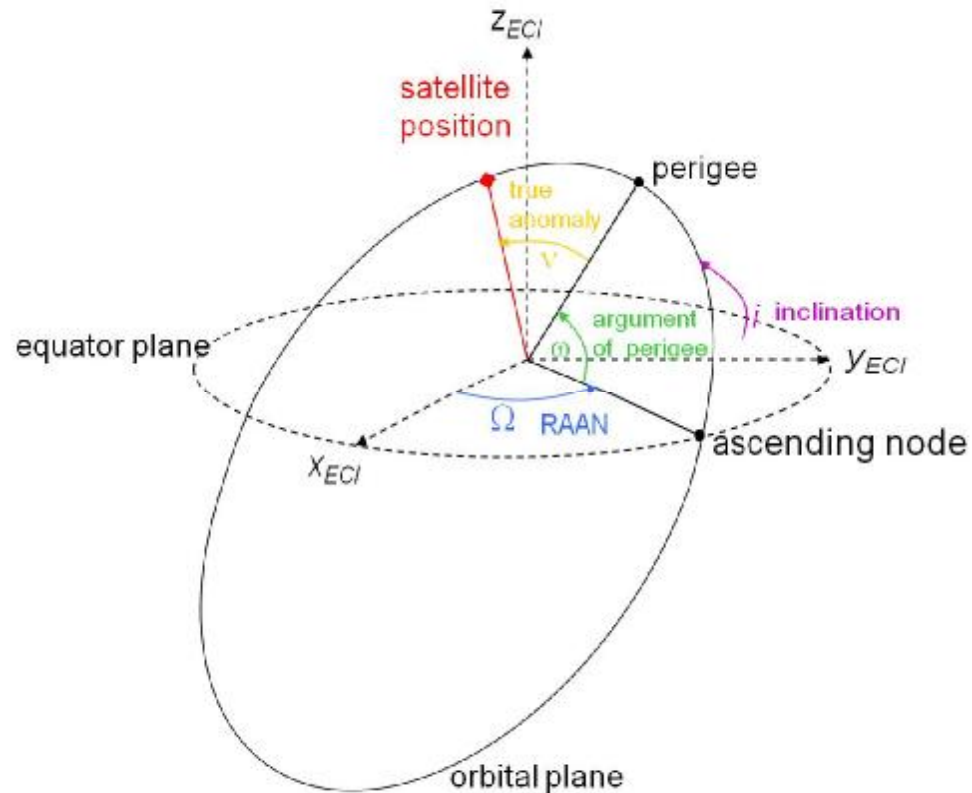


Figure 4.2: Physical meaning of the angular Keplerian elements

A few other quantities are used in this chapter which are closely related to the classic Keplerian elements:

- Mean motion, n , describes the mean velocity of the satellite and is related to the semi-major axis by the relation below, where GM_e are the gravitation constant and the earth's mass.

$$n^2 a^3 = GM_e \quad \text{eq. 4.3}$$

- Mean anomaly, M , is an abstract angle similar to the true anomaly, describing the angle between the perigee and a satellite moving at constant angular velocity n . The quantity has no physical meaning except at the epoch where the satellite is at the perigee, in which case $M=0$.

4.2 Orbital Propagation

Orbit propagation is a vast field of its own. A myriad of perturbing forces act on orbiting bodies, causing their motion to deviate from the ideal case described above. Among them are gravitational forces due to both irregularities in the central body and other bodies in the solar system, and non-conservative forces such as solar radiation pressure or drag. Each of these forces can be modelled more or less precisely, depending on the number of terms and coefficients included in the dynamics modelling, and the availability of information on environmental factors such as the variable atmospheric density or wind speeds at orbital altitudes. Numerical integration methods in conjunction with highly sophisticated dynamics models can be used to propagate a precise spacecraft position into the future, while more computationally efficient analytical models based on mean elements can have a reasonable degree of accuracy over time spans of a few weeks.

The work in this chapter of the thesis focuses on an analytical orbital model, NORAD's Simplified General Perturbations 4 (SGP4) propagator. Although there are far more sophisticated orbital tools available, the inherent limitations of a nanosatellite make SGP4 a good choice for onboard propagation.

4.2.1 Analytical Orbital Propagators versus Numerical Integrators

The basic difference between an analytical orbital propagator and a numerical integrator is that the analytical propagator can calculate the position of a satellite in closed form at any epoch in the past or future, while a numerical integrator must step through time to calculate the satellite's position at the desired epoch.

Because SGP4 is an analytical orbital model, it makes use of the fundamental harmonic motion of an orbiting body to selectively model only the most significant forces (Hoots & Roehrich 1980). High order gravity field coefficients disturb an orbit based on a consistent pattern, but cause no significant net change in the orbital path (Sneeuw 2006).

On the contrary, resonant forces such as the earth's flattening do have a net impact on the orbit, in the case of CanX-2 resulting in a precession of the ascending node around the earth's poles one full revolution per year, allowing for its sun-synchronous orbit, and a drift in the perigee of one full revolution approximately every 100 days. Other non-conservative forces such as drag have the effect of constantly decelerating the satellite in the anti velocity direction, which results in a decrease of the semi-major axis over time and ultimately the decay of the orbit. Figure 4.4 below shows the long term trends in the five of the mean orbital elements and drag for CanX-2 over a year. True anomaly, which changes by 360 degrees each revolution, has been excluded. Note that the irregularity in orbital elements at approximately day 345 is as a result of a propulsion experiment.

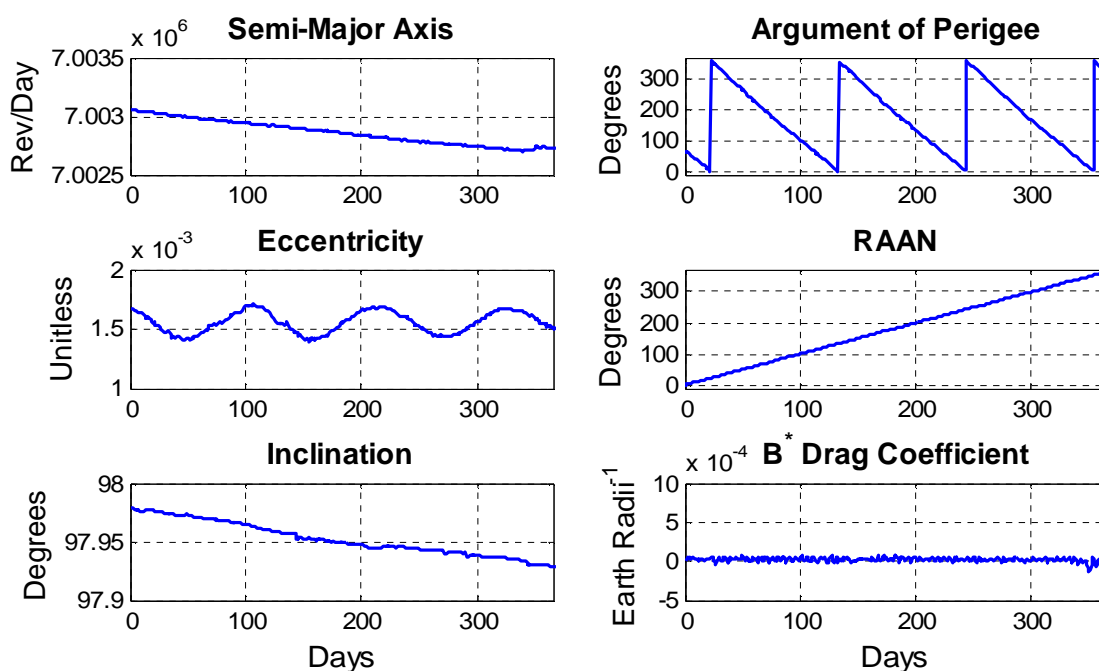


Figure 4.3: Variation in CanX-2's orbital elements over a period of one year

Analytical orbit propagators such as SGP4 work by taking the main disturbing forces and modelling the net change in the satellite's orbit, while neglecting the higher order forces which are either too weak to cause a significant disturbance over a time period of a few days or weeks, or are periodic and therefore have no net effect. Essentially, small

perturbations are ignored in order to achieve good large scale accuracy with a minimum of input parameters or number crunching. The trade off is that for any individual epoch this generalized trajectory will disagree with the satellite's true, perturbed position. For SGP4 the disagreement due to un-modelled perturbations is on the order of hundreds of meters. According to Montenbruck (2000), SGP4 shouldn't be expected to be more accurate than approximately 2 km at any given epoch in time; however, a week later the difference between SGP4 and the satellite's true position may still be on the order of a few kilometres. Essentially, analytical orbit propagators provide a smoothed out trajectory of a satellite's motion, and given a minimum of input data can calculate the satellite's approximate position in closed form for any particular epoch in the past or future.

Alternatively, numerical integrators depend on a very accurate dynamics model and initial position, and step through time, modelling each force acting on the orbiting body at each time step in order to slowly but accurately rebuild or predict the orbital trajectory. This method integrates the acceleration to get velocity and position, and in theory a single epoch of accurate position and velocity information would provide the necessary initial conditions to get good numerical propagator results if all the forces acting on a satellite are well known, and an appropriately small step size is chosen. This single epoch of position and velocity data fully determine the orbit of a satellite as long as there are no un-modelled external forces. The instantaneous results of numerical integration are far more accurate than analytical orbit models, but come at the cost of either a very large processor burden or high data storage requirements for coefficients and constants. For a case such as onboard operations on a nanosatellite, neither of these demands is likely to be achievable.

4.2.2 Why SGP4?

Because the goal is not to achieve high accuracy, but rather high enough accuracy at a relatively low computational cost, an analytical orbit propagator is the obvious choice over numerical integration. Many analytical orbit models have been developed, but SGP4

has been chosen from among them for three reasons. First, while SGP4 is not the most accurate analytical orbital propagator, it is by far one of the most widespread, and can be considered something of an industry standard. Second, NORAD tracks CanX-2 and publishes the data in the form of Two Line Elements (TLE), a format specific to SGP4. As a result, NORAD's tracking network of radar and optical sensors provides a completely independent check for the GPS results. The third reason closely follows from the first two: SGP4 has already been employed in the creation of the warm start scripts for CanX-2 for over two years with good results. As such it is tried, tested, and a proven success.

4.2.3 The SGP4 Algorithm

The SGP4 orbital model was developed in the late 1970's as part of the American effort to track all objects in space during the cold war. The model consists of computer software originally written in the FORTRAN programming language. The trade off between low processing power and reasonable accuracy is a relic of the times: computing power had not evolved enough for a highly sophisticated model to be used, nor had the disturbing forces such as gravity field anomalies been modelled to nearly the accuracy they are today, thanks to modern satellite geodesy missions.

Because NORAD's catalogue of two line element sets is the most complete publicly available resource for objects orbiting the earth, and has been for decades, the use of SGP4 is not limited to American government bodies but is extremely widespread. As a result, there are a vast number of versions of this software in existence, as the software has been frequently updated and improved with little to no tracking of changes and versions. In an effort to standardize the software versions in use, "Spacetrack Report No. 3: Models for Propagation of NORAD Element Sets" was published in 1980; however, since then the multitude of users have continued to apply improvements, bug fixes, and rewrites in various programming languages, with some commercial software such as Analytical Graphics Inc. even having different options allowing the user to choose

between some of the subtleties of the SGP4 coordinate system transformation (Vallado et al 2006).

In 2006 a complete inventory of the versions of the Spacetrack software was carried out by Vallado et al, resulting in the publication of “Revisiting Spacetrack Report #3”, along with the release of four synchronised versions of the SGP4 propagator in C++, FORTRAN, Pascal and Matlab. Although the operational version of the software used by NORAD and NASA are not publicly available, the Revisiting Spacetrack source code has had every possible effort made to compare it to output of the official versions in order to synchronise them, as well as having every effort made to identify and repair bugs or shortcomings in the original algorithm in order to correctly handle all possible orbits.

The forces modelled by SGP4 include the J2, J3 and J4 perturbations, as well as atmospheric drag (Hoots et al 2004). No sectoral or tesseral gravity field coefficients are taken into account, making the orbital model independent of the longitude.

As input, SGP4 requires a reference epoch, six mean Keplerian elements, and a drag coefficient. This information is published for all satellites tracked by NORAD in the format of two line element sets or TLE, which consist of two formatted lines of ascii data containing all the required input parameters. In addition to the essential information for SGP4, the TLE contains some higher order terms, satellite identification data, and checksums, which are not used in the work presented here. Table 4.1 below outlines the format of the TLE fields essential for use with SGP4. An example of a two line element set for CanX-2, published by NORAD through the Celestrak Website (July 31, 2010), is also given. A full description of the TLE format can be found in Vallado et al (2006) and online at Celestrak (2004).

Table 4.1: Two Line Elements necessary for SGP4 propagation

1 32790U 08021H 10211.66515121 -.00000063 00000-0 -12642-5 0 7331
 2 32790 97.8918 275.8894 0015989 140.3639 219.8760 14.81654755121908

<i>Quantity</i>	<i>Line</i>	<i>Fields</i>	<i>Units</i>	<i>Example</i>
Epoch Year	1	19-20	2 digit year	10
Epoch Day	1	21-32	fractional decimal day of year	211.6651512
Bstar Drag Term	1	54-59	Earth radii ⁻¹ , decimal assumed	-12642
Bstar exponent	1	60-61	unitless	-5
Inclination	2	9-16	degrees	97.8918
RAAN	2	18-25	degrees	275.8894
Eccentricity	2	27-33	unitless, decimal assumed	0015989
Argument of Perigee	2	35-42	degrees	140.3639
Mean Anomaly	2	44-51	degrees	219.876
Mean Motion	2	53-63	rev/day	14.81654755

4.3 Estimating Two Line Elements

In order to enable an autonomous warm start of an orbiting GPS receiver, a method is required to form a set of SGP4 Two Line Elements from the GPS data. Operationally, a TLE would be calculated and stored in the receiver's internal memory after each receiver use, and upon start up of the receiver the stored TLE would be retrieved, propagated through SGP4 to calculate the receiver's current orbital position, and along with the receiver's stored GPS almanac used to predict the visible GPS constellation and the Doppler offset of each PRN. Essentially, the existing functionality in the commercial receiver to start up relatively quickly on the ground, based on assumptions of it retaining its last known position, would be extended to the orbital case.

4.3.1 Previous Work

Previous work was done on the topic of estimating TLE from CanX-2 data both by Greene & Zee (2009) in Toronto and by Kahr et al (2010). However, in both of these publications the method of conversion of the GPS data to a two line ephemeris was to use the VEC2TLE program written by Ken Hernandez (1996). The VEC2TLE program takes a

single point GPS position and iterates through the SGP4 propagator until the set of TLE mean Keplerian elements are found which produce an exact match to the input state vector at that single epoch. This method reliably converges to a solution but can give widely varied results as a result of noise in the input GPS data as shown in Figure 4.4 below. The figure represents the output TLE elements for each epoch of GPS data collected at a 2 second logging rate over a period of 48 minutes. These elements are all referenced to the same epoch, so any time dependence of the elements, for example the mean anomaly, has been removed.

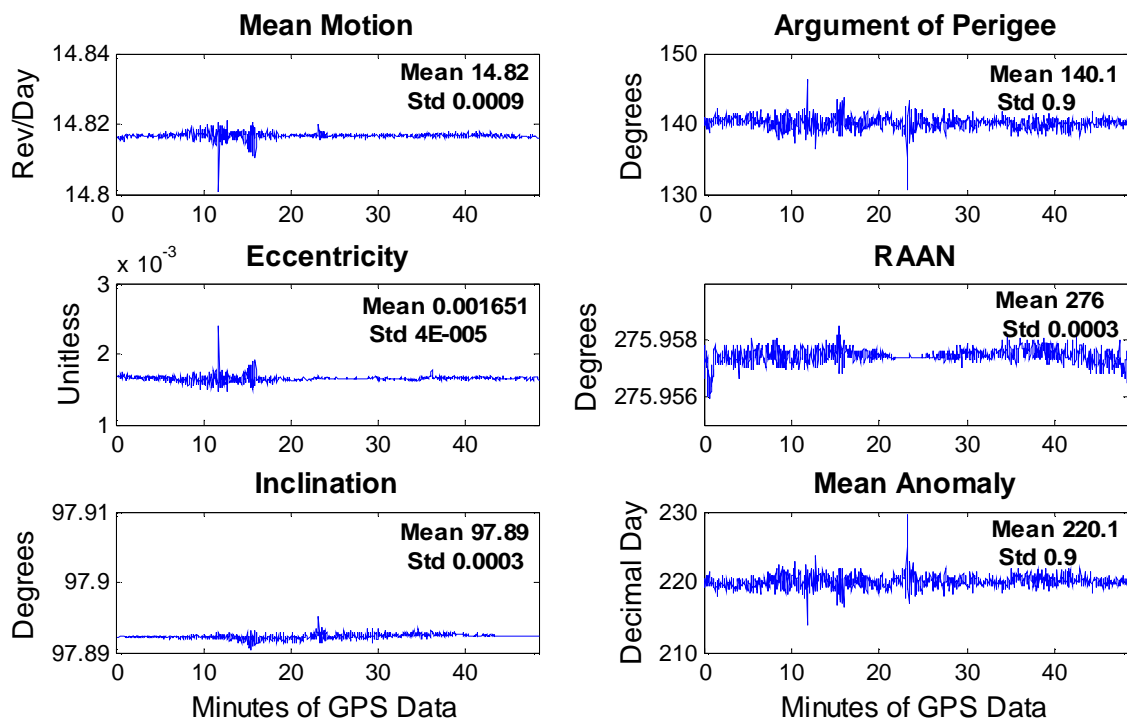


Figure 4.4: TLE mean Keplerian elements obtained from GPS data using VEC2TLE

Although results were obtained using this approach, it has a fundamental weakness. VEC2TLE only uses a single epoch of position and velocity information as input, and finds the TLE to best match the single input state vector. As such, the drag term cannot be estimated and must come from some external source. The bigger problem is illustrated

in Figure 4.5 below. The TLE elements are mean elements, and cannot be accurately estimated from a single epoch of positioning data. This is because the single data point will be very unlikely to fall on the SGP4 arc best fitting the long term trend in the satellite's position. Single epochs of data provide osculating Kepler elements, while mean elements can only be found using longer arcs of input data.

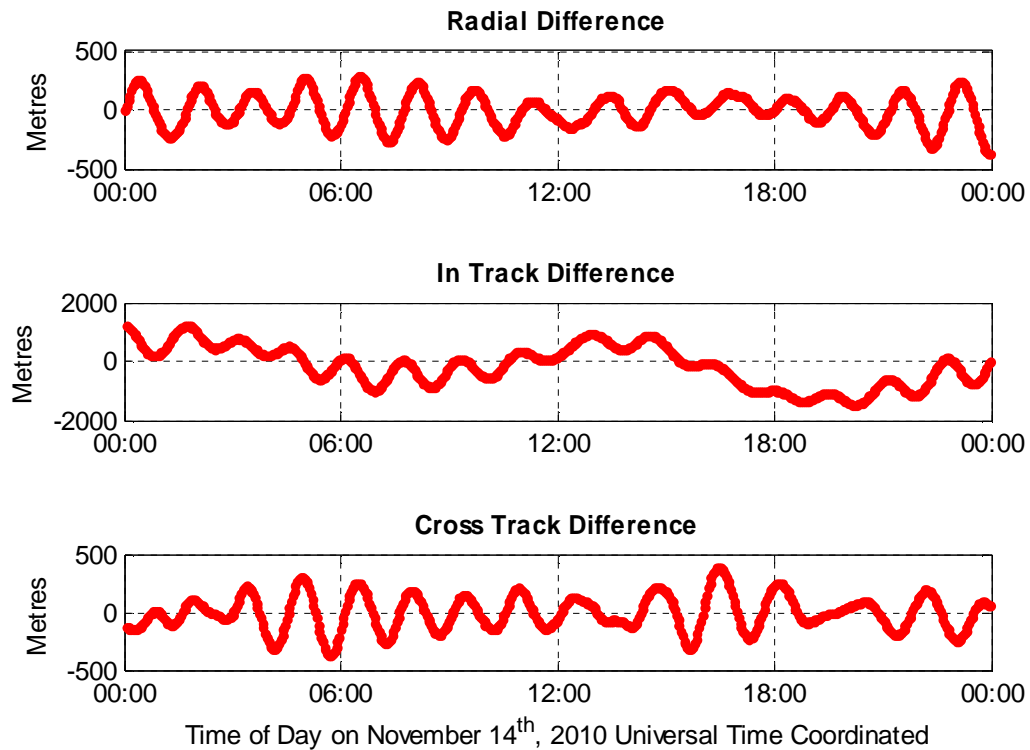


Figure 4.5: Difference between the smooth SGP4 trajectory and the precise position of CanX-2 over 24 hours

4.3.2 Least Squares Estimation

An improved method of estimating has been well documented in Vallado & Crawford (2008), in which a least squares approach to the estimation of TLE was developed, following the same procedure as classic orbit determination. A similar method has been independently developed and implemented by the German Space Centre (DLR), which has been documented in Montenbruck (2000), Jochim et al (1996), Montenbruck et al (1996), and Gill & Montenbruck (2002).

In order to estimate TLE from CanX-2's GPS data, it is this approach which has been taken. Software was developed with a least squares algorithm similar to those of Montenbruck and Vallado, but tailored for use with the CanX-2 data sets.

4.3.3 The Least Squares Algorithm

Because orbit determination is highly non-linear, iterative least squares is imperative to achieve a solution. Of the several mathematically equivalent implementations of least squares, summation of normals has been chosen to enable the input of any number of epochs of GPS measurements while avoiding the inversion of large matrices. The parametric least squares algorithm therefore takes the form below (Leick 2004, El Sheimy 2000):

Until the value of least squares converges

For each epoch of GPS observations, i

$$N_i = A_i^T P_i A_i \quad \text{eq. 4.4}$$

$$U_i = A_i^T P_i dy_i \quad \text{eq. 4.5}$$

$$N = N + N_i \quad \text{eq. 4.6}$$

$$U = U + U_i \quad \text{eq. 4.7}$$

End observation loop

$$dx = -N^{-1}U \quad \text{eq. 4.8}$$

$$x = x_0 + dx \quad \text{eq. 4.9}$$

$$v = A dx + dy \quad \text{eq. 4.10}$$

$$S^2 = \frac{v^T P v}{(n_{obs} - n_{unknowns})} \quad \text{eq. 4.11}$$

End least squares loop

In the above, A is the design matrix containing the partial derivatives of the GPS observations with respect to the unknown TLE parameters, P is the weight matrix of the GPS observations, dy is the misclosure vector between the estimated positions and the GPS observations, x_0 is the initial estimate of the TLE parameters, and x is the improved estimate of the TLE parameters after the iteration, which is subsequently used as the point of expansion (x_0) for the next iteration. The subscripts 1, 2, ..., i indicated epochs of GPS measurements. The a-posteriori variance factor, σ^2 , is calculated from the residuals, v , and serves as the convergence criteria to exit the least squares loop. The following sections provide greater detail about the implementation of the TLE estimation.

4.3.3.1 Estimated Parameters

Seven orbital parameters as well as a time of ephemeris are required as input to SGP4 in order to calculate satellite positions in closed form. The time of ephemeris for the estimated TLE is currently user input, but for on orbit applications the time stamp of the last available GPS measurement would be a reasonable choice. The algorithm has been written such that the seven estimated parameters can take two forms: either as the TLE elements converted to units of radians and minutes, or a Cartesian position and velocity in units of metres and metres/second. In either case the drag parameter retains the SGP4 format, but if the initial Cartesian coordinates are estimated drag is scaled by a factor of 10^5 in order to keep the magnitudes of the parameters similar, and in doing so prevent instability in the least squares during matrix inversion.

The motivation for including Cartesian coordinate estimation as an option was to avoid potential numerical problems such as a negative eccentricity, or problems related to CanX-2's orbit being near-circular and therefore having a poorly defined argument of perigee. The final TLE is identical regardless of which format the estimated parameters take; however a greater sensitivity to the choice of a point of expansion has been found for estimation using Cartesian coordinates, and therefore the results presented in this thesis have all been obtained by estimating the Keplerian elements directly.

Table 4.2: Possible parameterisations for the TLE estimation

<i>TEME Cartesian Coordinates</i>		<i>TLE Elements</i>	
<i>parameter</i>	<i>units</i>	<i>parameter</i>	<i>units</i>
x	metres	revolution rate	rads/minute
y	metres	inclination	radians
z	metres	eccentricity	unitless
vx	metres/second	Argument of Perigee	radians
vy	metres/second	RAAN	radians
vz	metres/second	mean anomaly	radians
B* drag	earth radii ⁻¹	B* drag	earth radii ⁻¹

4.3.3.2 Observations

The input measurements of the spacecraft's position are the GPS receiver's navigation solutions. In order to best simulate autonomous operations in order to determine if onboard orbit determination is viable, the receiver's internal navigation solution, output using the "BESTXYZ" log, has been used as input to the least squares algorithm. BESTXYZ provides the Cartesian WGS84 position and velocity of the receiver, as well as the position and velocity standard deviations in the same frame. For the TLE estimation only the three components of the position solutions have been used as input measurements. The reasoning is that the velocity information obtained inherently by using multiple epochs of GPS positions is more reliable than the single point Doppler velocities estimated in the receiver (Montenbruck 2003, Montenbruck 2000).

Figure 4.6 and Figure 4.7 below compare the BESTXYZ data to a precise orbit determination solution for CanX-2 over the same time spans. The precise orbit determination results are discussed in Appendix C, and are assumed to be accurate at the one metre level where there are GPS measurements and accurate at the tens of metres level otherwise. Here they are used as a truth solution.

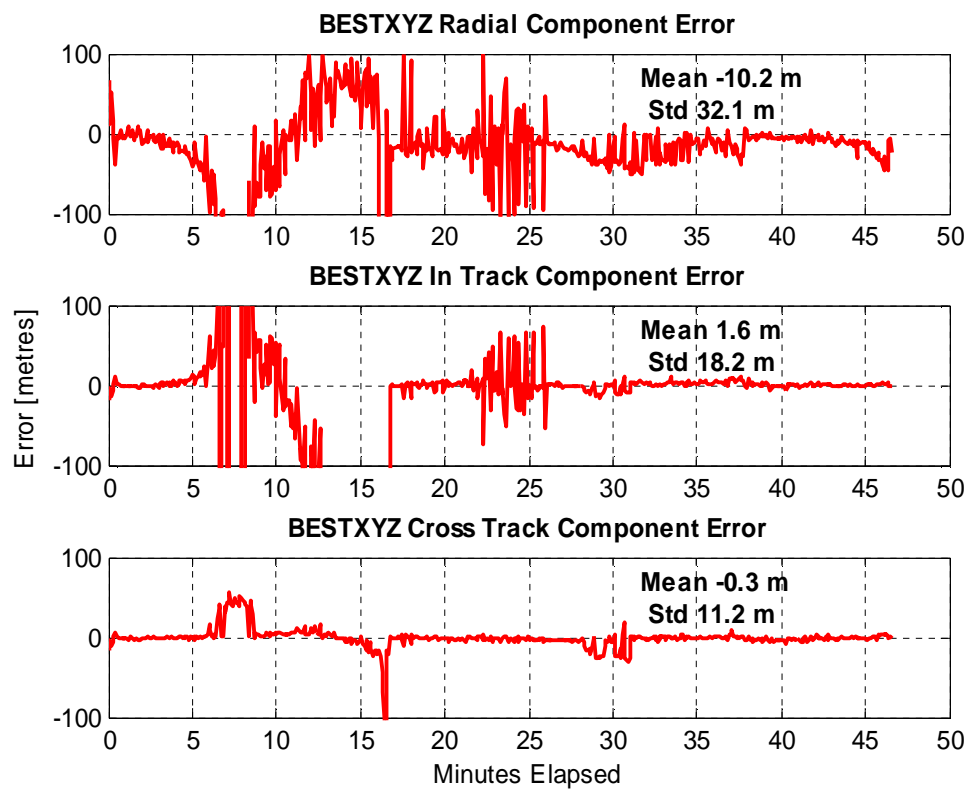


Figure 4.6: Error in the receiver's BESTXYZ position during the August 6, 2010 data collection, logged every 2 seconds

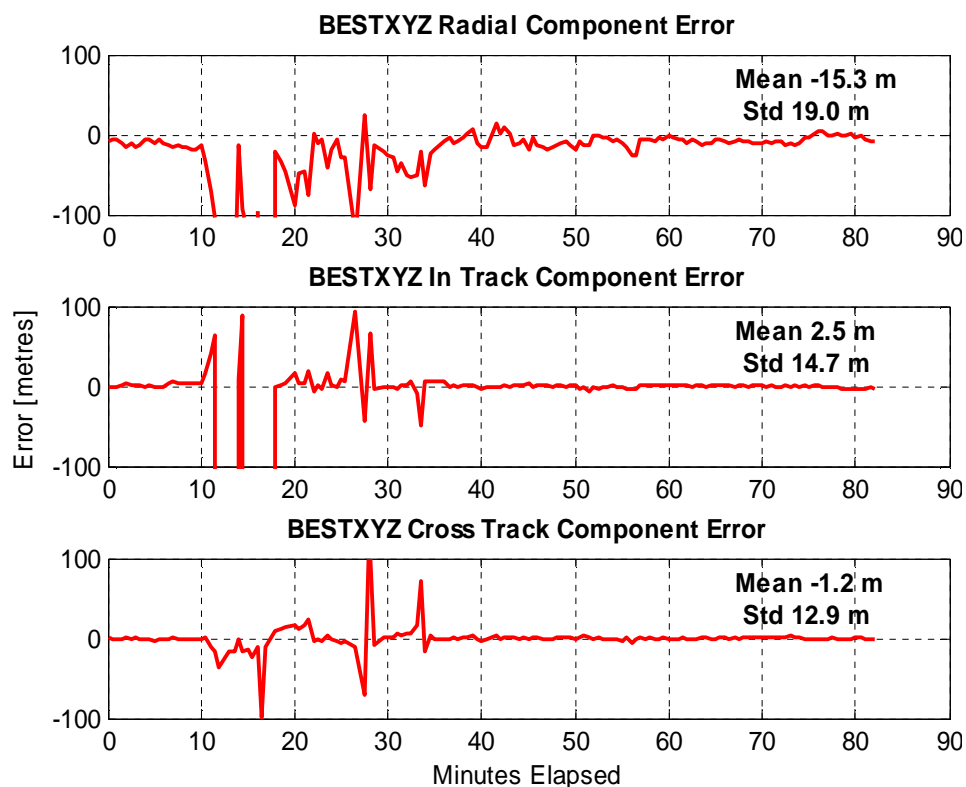


Figure 4.7: Error in the receiver's BESTXYZ position during the second November 25, 2010 data collection, logged every 30 seconds

It can be seen from the figures that the receiver's internal navigation solution generally agrees quite well with the precise orbits, but is characterised by significant levels of noise resulting in large spikes of error in the position solution, particularly during epochs with poor geometry during the first 20 minutes of the data collections.

Another source of error apparent in the BESTXYZ data is a systematic bias in the radial component of the position typically lying between -20 and -10 metres. Epochs with an error greater than 100 m are considered outliers and have been excluded from the bias calculation. This observed bias is not entirely unexpected, as it matches with simulator test results for the OEM4 receiver presented in (Montenbruck 2003). As explained in Chapter 2, the bias is assumed to be the result of tropospheric modelling in the receiver's firmware incorrectly dealing with orbital height.

4.3.3.3 Coordinate Systems

In order to estimate orbital elements, an inertial coordinate system is required. The system used for the SGP4 orbital model is a TEME, or true equator mean equinox, system. The TEME system neglects nutation (or in other words the entire system nutates with the earth, as all NORAD's tracking stations are on the earth's surface and this simplifies orbital element estimation) but takes into account the gradual precession of the mean vernal equinox. (Hoots & Roehrich 1980, Kelso 1998) An illustration of TEME as compared to an earth centred earth fixed coordinate frame is presented in Figure 4.8 below.

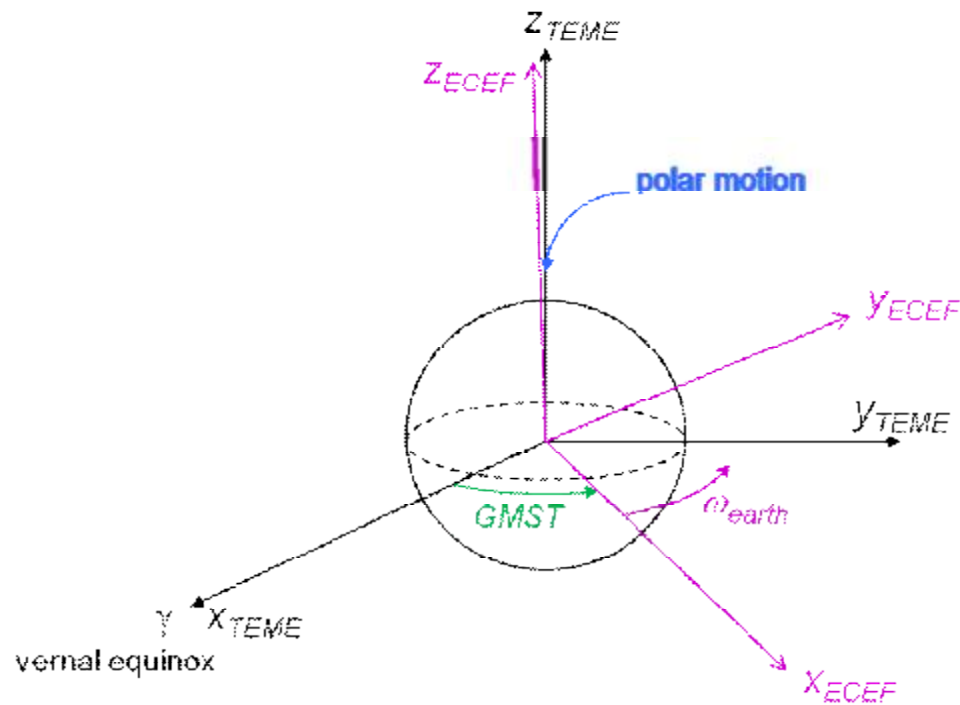


Figure 4.8: Relation between the TEME and ECEF coordinate frames

Because the output of SGP4 is in TEME, and the GPS data is logged in earth centred earth fixed (ECEF) Cartesian coordinates, a conversion between the two systems is required. It was decided to rotate all the GPS data into the TEME frame at the beginning

of the program, in order to avoid repeatedly converting the SGP4 output to an earth fixed frame at each iteration of the least squares as part of the misclosure vector calculation. Mathematically these two approaches are identical in terms of estimating the TLE.

In order to rigorously convert from WGS84 into TEME, several steps are required:

1. WGS84 coordinates are converted to the current International Terrestrial Reference Frame (ITRF) coordinate frame
2. Julian date is calculated based on the UT1 time scale, using the UTI-UTC information published by the International Earth Rotation and Reference System Service (IERS) in bulletin b

$$JD_{UT1} = JD_{UTC} + (UT1 - UTC)_{decimaldays} \quad \text{eq. 4.12}$$

3. The earth fixed frame is rotated into the instantaneous terrestrial frame (IT) using the polar motion parameters x_p and y_p , also published by the IERS in bulletin b

$$r_{IT} = R_1(y_p)R_2(x_p)r_{ITRF} \quad \text{eq. 4.13}$$

4. The UT1 Julian date is used to calculate the Greenwich Mean Siderial Time (GMST) in closed form, using equations from (Vallado et al 2006)

$$T_{UT1} = (JD_{UT1} - 2451545.0) / 36525 \quad \text{eq. 4.14}$$

$$GMST = 67310.54841 + (3.15576 * 10^9 + 8640184.812866)T_{UT1} + 0.093104T_{UT1}^2 - 6.2 * 10^{-6}T_{UT1}^3 \quad \text{eq. 4.15}$$

5. The instantaneous terrestrial frame is rotated into the TEME frame using GMST

$$r_{TEME} = R_3(-GMST)r_{IT} \quad \text{eq. 4.16}$$

$$v_{earthfixedTEME} = R_3(-GMST)v_{IT} \quad \text{eq. 4.17}$$

6. For the conversion of velocities, the magnitude of the earth fixed velocity must be adjusted for the earth's rotation in order to obtain the correct magnitude for the inertial velocity

$$v_{inertialTEME} = v_{earthfixedTEME} + w_{earth} \times r_{TEME} \quad \text{eq. 4.18}$$

The rotation matrices, R_1 , R_2 and R_3 , describe a positive rotation of angle θ about the first, second and third axis of the coordinate frame. They are defined as:

$$R_1 = \begin{pmatrix} 1 & 0 & 0 \\ 0 & \cos q & \sin q \\ 0 & -\sin q & \cos q \end{pmatrix}, R_2 = \begin{pmatrix} \cos q & 0 & -\sin q \\ 0 & 1 & 0 \\ \sin q & 0 & \cos q \end{pmatrix}, R_3 = \begin{pmatrix} \cos q & \sin q & 0 \\ -\sin q & \cos q & 0 \\ 0 & 0 & 1 \end{pmatrix} \quad \text{eq. 4.19}$$

Because the accuracy of the SGP4 model is only on the order of kilometres, and because the required accuracy for warm starting the receiver is not particularly stringent, a simplified approach to the conversion from WGS84 is also possible. This approach is less accurate:

1. The UTC Julian date is used to calculate the Greenwich Mean Siderial Time (GMST) in closed form, using the same equation as step 4 above

2. The earth centred earth fixed frame is rotated into the TEME frame using GMST (slight differences between ECEF frames are neglected, as is polar motion)

$$r_{TEME} = R_3(-GMST)r_{ECEF} \quad \text{eq. 4.20}$$

$$v_{earthfixedTEME} = R_3(-GMST)v_{ECEF} \quad \text{eq. 4.21}$$

3. For the conversion of velocities, the magnitude of the earth fixed velocity must be adjusted for the earth's rotation in order to obtain the correct magnitude for the inertial velocity

$$v_{inertialTEME} = v_{earthfixedTEME} + w_{earth} \times r_{TEME} \quad \text{eq. 4.22}$$

The simplified approach has been applied for all the results presented in this thesis. While the least squares algorithm has been programmed such that it is able to read in bulletin b information and correct the UTC Julian date to UT1, and the functionality could easily be extended to also account for polar motion, bulletin b is only published once per month retroactively (IERS 2010, Montenbruck & Gill 2000). In order to implement onboard estimation using the rigorous coordinate transformation, the predicted values for the UT1-UTC and polar motion corrections would have to be transmitted to the satellite on a regular basis, reducing the autonomy of warm starting the receiver in space. Because autonomous operation is the ultimate goal of this work, the simplified coordinate transformation would be more realistic operationally and therefore has been used in generating the results. This allows for an assessment of its viability in place of the rigorous coordinate transformation, and leaves the use of the rigorous transformation as a possible future improvement.

4.3.3.4 Weight Matrix

The weight matrix is formed using the estimated standard deviations of the single point GPS positions, obtained from the BESTXYZ log. Figure 4.9 and Figure 4.10 below show comparisons between the true error (calculated by differencing the receiver's navigation solution and the precise orbit) and the one and three standard deviation envelopes obtained from the BESTXYZ log. The plots establish that the receiver's estimated standard deviations do generally follow the actual trend of the error in the orbital GPS solutions, and are therefore suitable for weighting the GPS data in the least squares TLE estimation.

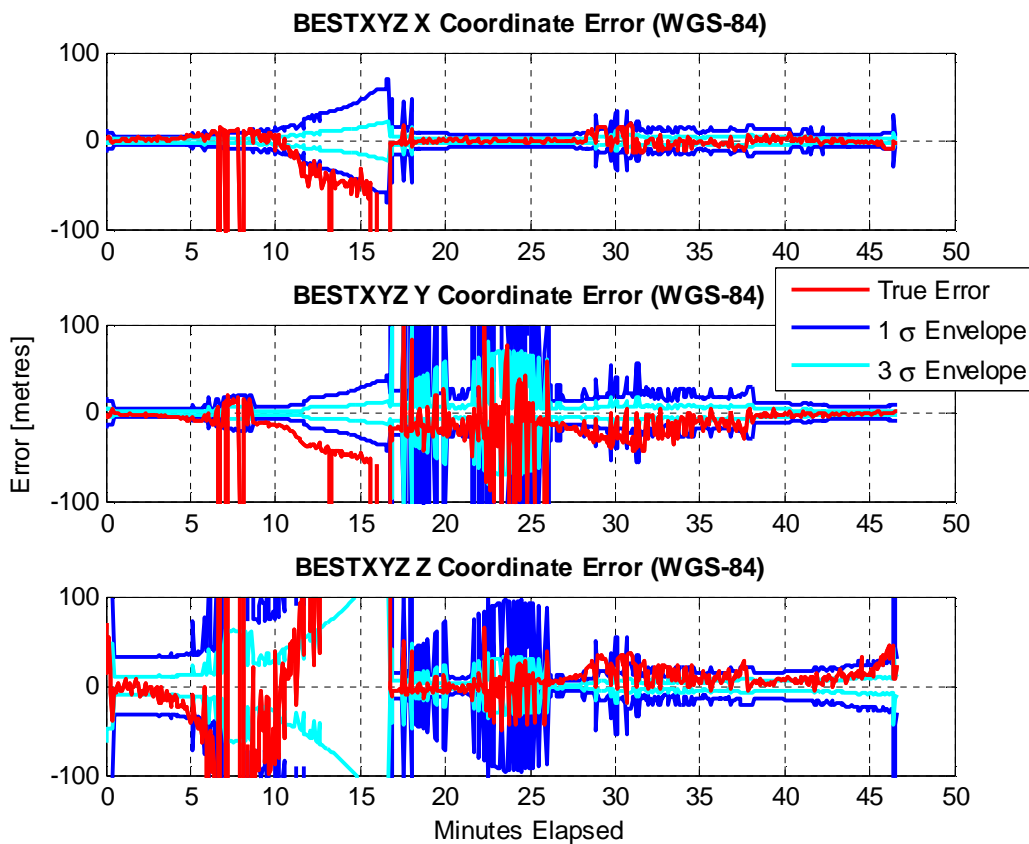


Figure 4.9: Comparison between the receiver's BESTXYZ standard deviations and true position error during the August 6, 2010 data collection, logged every 2 seconds

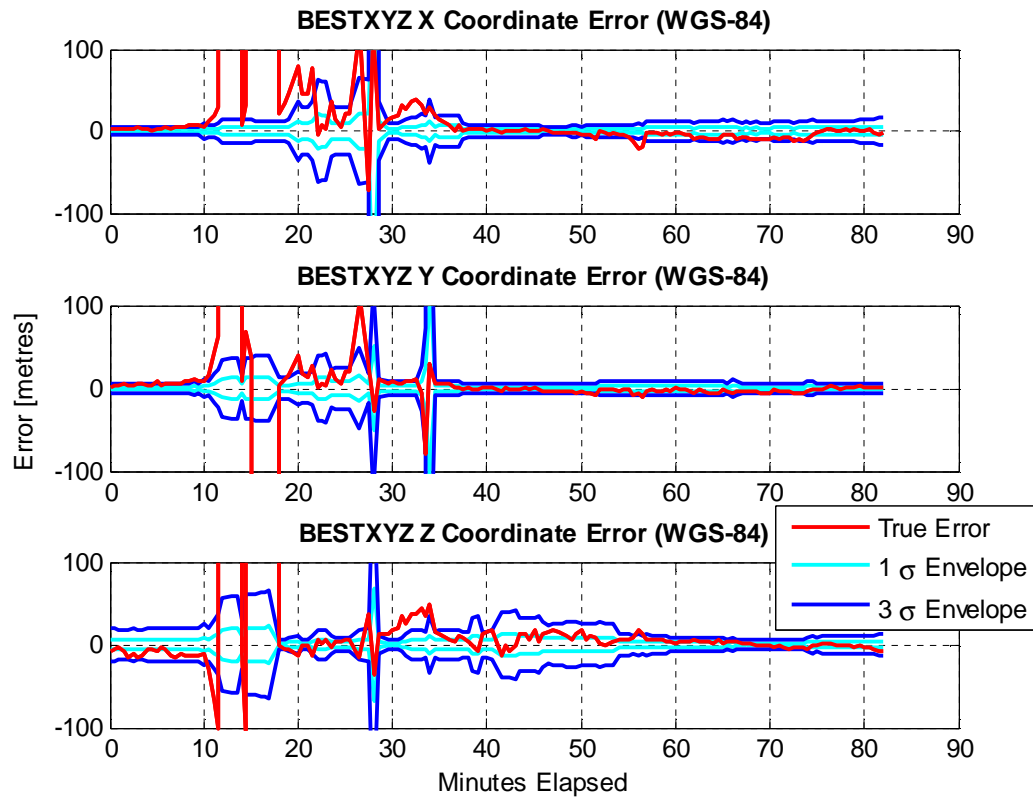


Figure 4.10: Comparison between the receiver's BESTXYZ standard deviations and true position error during the November 25, 2010 data collection, logged every 30 seconds

Converting the GPS measurements into TEME requires making the same conversion for the standard deviations. In order to accomplish this, the standard deviations are squared and used to populate the diagonal of a variance covariance matrix in WGS84. The matrix is then rotated into TEME, preserving the full covariance information and resulting in a cross-correlation in x and y. Unfortunately, no cross-correlations from the receiver's original navigation solution have been recorded, so the use of the full covariance information remains a source of future improvement. The weight matrix at each least square epoch, P , is the inverse of the TEME variance covariance matrix.

4.3.3.5 Outlier Detection

Because the simplified orbital model does not perfectly describe the trajectory of the satellite as previously explained in section 4.3.1 and shown in Figure 4.5, it is not possible to implement blunder detection. Blunder detection assumes a normal distribution of the errors (Petovello 2009), while in this case much of the valid data can actually lie quite far from the best fit trajectory due to systematic differences between SGP4 and the satellite's true position. However, some method was desired in order to eliminate the GPS measurement epochs with large spikes in error.

A cut off mean radial spherical error (MRSE) of 20 metres was used. The 20 m threshold was determined empirically, based on a comparison of the true 3D error obtained by differencing the receiver's internal navigation solution (x_{OEM4} , y_{OEM4} , z_{OEM4}) and precise orbit determination results (x_{POD} , y_{POD} , z_{POD}), to the MRSE calculated using the estimated standard deviations from the BESTXYZ log (S_{xOEM4} , S_{yOEM4} , S_{zOEM4}).

$$TrueError = \sqrt{(x_{OEM4} - x_{POD})^2 + (y_{OEM4} - y_{POD})^2 + (z_{OEM4} - z_{POD})^2} \quad \text{eq. 4.23}$$

$$MRSE = \sqrt{S_{xOEM4}^2 + S_{yOEM4}^2 + S_{zOEM4}^2} \quad \text{eq. 4.24}$$

Figure 4.11 and Figure 4.12 below depict the MRSE (in cyan), the true 3D error (in red), and the 20 metre cut off applied instead of blunder detection (in black) for the same sample data sets as above. The majority of epochs of GPS data have an estimated RMS falling below the 20 metre threshold, while many of the worst GPS outliers occur in epoch with an estimated RMS above 20 metres. These plots are representative of all the data sets investigated.

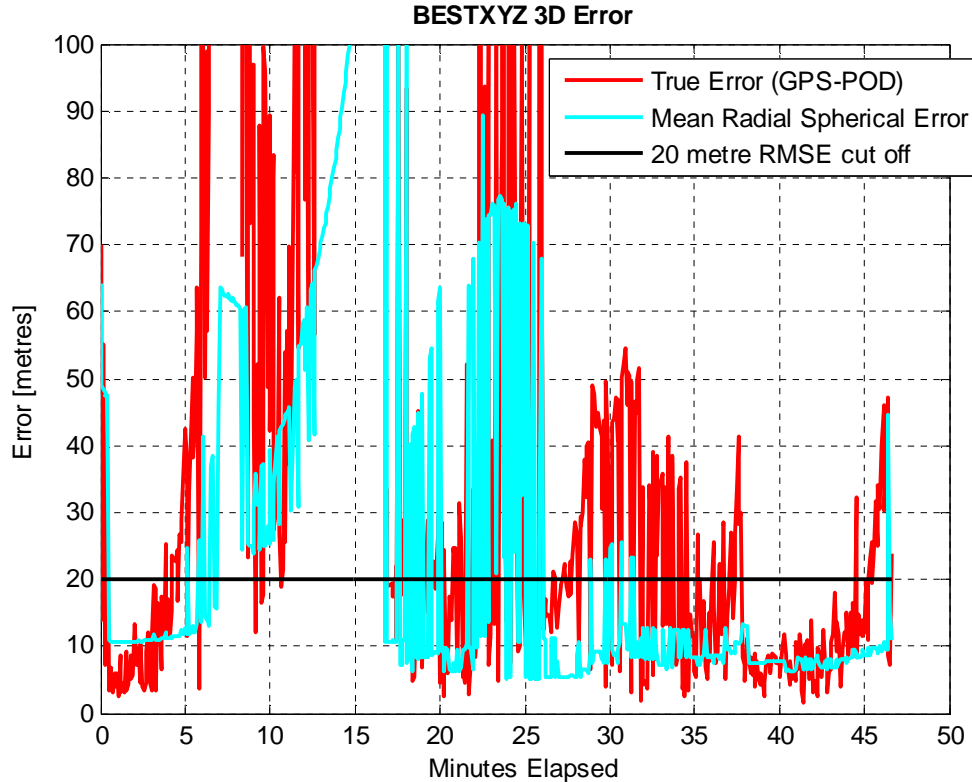


Figure 4.11: Positioning errors (red) are eliminated if the estimated errors (cyan) are above the 20 m threshold. August 6, 2010 data collection, logged every 2 seconds

Epochs of GPS data where the true error spikes but there is still a conservative standard deviation estimate, for example at 20 minutes in Figure 4.12 below, are unfortunately still included as input to the least squares solution. Lowering the cut off threshold would eliminate more of these outliers, but in cases such as a rear pointing GPS antenna, where the PDOP is almost certainly going to be high, having a conservative threshold would run the risk of not including enough data to estimate the TLE.

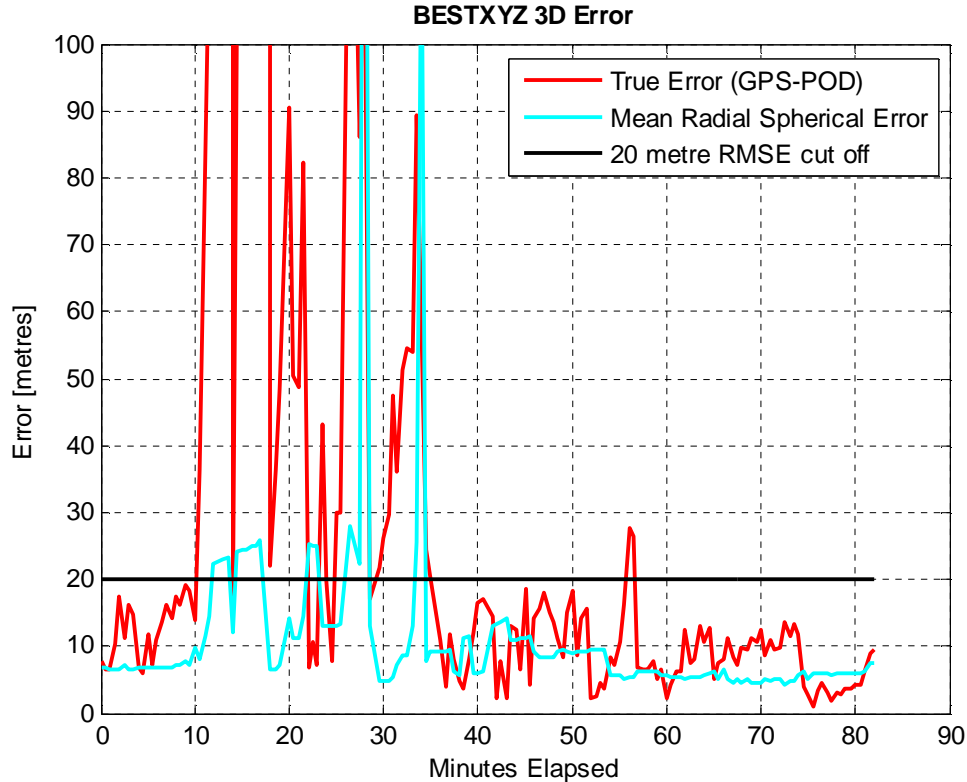


Figure 4.12: Positioning errors (red) are eliminated if the estimated errors (cyan) are above the 20 m threshold. November 25, 2010 data collection, logged every 30 seconds

4.3.3.6 Design Matrix

The design matrix is populated by the partial derivatives of the observations with respect to the unknowns. Partial derivatives are formed analytically through finite differencing. The current point of expansion is run through the SGP4 algorithm, and one by one each of the input Keplerian elements is modified by a small percentage to calculate the corresponding change in output SGP4 coordinates. The change in output coordinates is divided by the change in input parameters to form approximate derivatives.

The percentage change used in the finite differencing calculation is 0.0075%. This value was obtained by testing different percentages and observing what occurred in the estimation process. If too small of a percent change was applied a relatively large number

of iterations would be required before the least squares converged to a solution, while if too large a percent change was applied the estimated parameters would often oscillate between two sets of values but never converge. The optimum value of 0.0075% is on the same order of magnitude as the value of 0.001 % used in TLE estimation by Vallado and Crawford (2008). The use of finite differencing avoids calculating closed form derivatives from the highly nonlinear SGP4 algorithm, but presents a potential source of instability in the least squares estimation.

4.3.3.7 Misclosure Vector

The misclosure vector is calculated by propagating the current best estimate of the TLE through SGP4 to each epoch of available GPS measurements, and differencing the calculated SGP4 positions from the GPS measured positions.

4.3.3.8 SGP4 Version

As previously mentioned, there exist a large number of different versions of the SGP4 algorithm. One point which is often repeated is the necessity of using the same orbital propagator to estimate elements as is used to propagate the satellite's position forward. For this work, a Matlab version of SGP4 was programmed directly from the original Spacetrack Report 3 publication (Hoots & Roehrich 1980). Output of this newly programmed version of SGP4 was then compared to the Matlab implementation from the Revisiting Spacetrack source code, which is both rigorously documented and the version most likely to coincide with the official program used in generating the official two line element sets (Vallado et al 2006). Using TLE for CanX-2 as input, the two versions agreed to 10^{-8} over six weeks of propagation.

In spite of this agreement, the least squares algorithm has been given a switch which allows either of the Matlab versions of SGP4 to be used in TLE generation. The newly programmed version is tailored to CanX-2's orbit and takes full advantage of shortcuts in the Matlab programming language, and therefore runs faster. Vallado's version takes into

account a far greater range of satellite orbits, includes the deep space SDP4 algorithm, and has been tested for a large range of problems that may come up in special cases (Vallado et al 2006). While the faster version tailored to CanX-2's orbit has been used to generate the results presented here, the more rigorous version should certainly be used for other cases.

4.3.3.9 Convergence Criteria

In order to establish when the least squares had converged, the a posteriori variance factor is calculated at each iteration, using the equation

$$S^2 = \frac{v^T P v}{(n_{obs} - n_{unknowns})} \quad \text{eq. 4.25}$$

Where P is the weight matrix for the observations, v is the vector of residuals, n_{obs} is the number of observations, and $n_{unknowns}$ is the number of unknowns. When the a posteriori variance factor is changing by less than 0.0001 m^2 , corresponding to a change of less than 1 cm in the residuals, the least squares is considered to have converged.

4.3.3.10 Point of Expansion

Because the observation equation for the least squares estimation is so non-linear, and because most GPS measurements will not fall directly on the SGP4 trajectory, finding an appropriate point of expansion is both difficult and critical to the success of the estimation.

The point of expansion was originally found by taking in a single epoch of GPS data, and either using it as the point of expansion directly for the Cartesian parameterization or converting the position and velocity to osculating Keplerian elements using the relations given in Montenbruck & Gill (2000). The initial estimate of the drag value is always set

to $2.7E-5$, which is the mean drag value for CanX-2 from two years of published TLE sets.

It was quickly discovered that using a single continuous GPS data set as input, the final estimate of the drag value would be too large by several orders of magnitude, but by using multiple GPS data sets collected a few days apart the least squares algorithm would diverge in most cases. Another difficulty was comparison of the final TLE elements to published values, as the elements drift over time and only a comparison at exactly the same time of ephemeris (TOE) is valid.

In order to solve the difficulty with the point of expansion and drag estimation, the least squares estimation is now carried out over several steps. First, the desired time of ephemeris is input to the program, and the nearest epoch of GPS data (which may be days away from the TOE) is found. The time stamp on this GPS seed point is used as the preliminary time of ephemeris, and the GPS position and velocity are used as the point of expansion. Least squares is carried out using only the data set containing the GPS seed point, and the drag parameter is constrained to the mean value.

Once the initial estimate of the TLE is obtained, it is modified to have the desired time of ephemeris. The mean anomaly, which describes the position of the satellite along its orbit, is updated by taking the time difference between the desired TOE and the initial TOE, and calculating the angular change based on the estimated number of revolutions per day. This modified TLE is then used as the point of expansion for a second orbit determination process, using all available GPS data sets as input and no drag constraint. Because the point of expansion is much more accurate, the second estimation is stable even with input data spanning a week. Figure 4.13 is a flowchart of the final least squares algorithm.

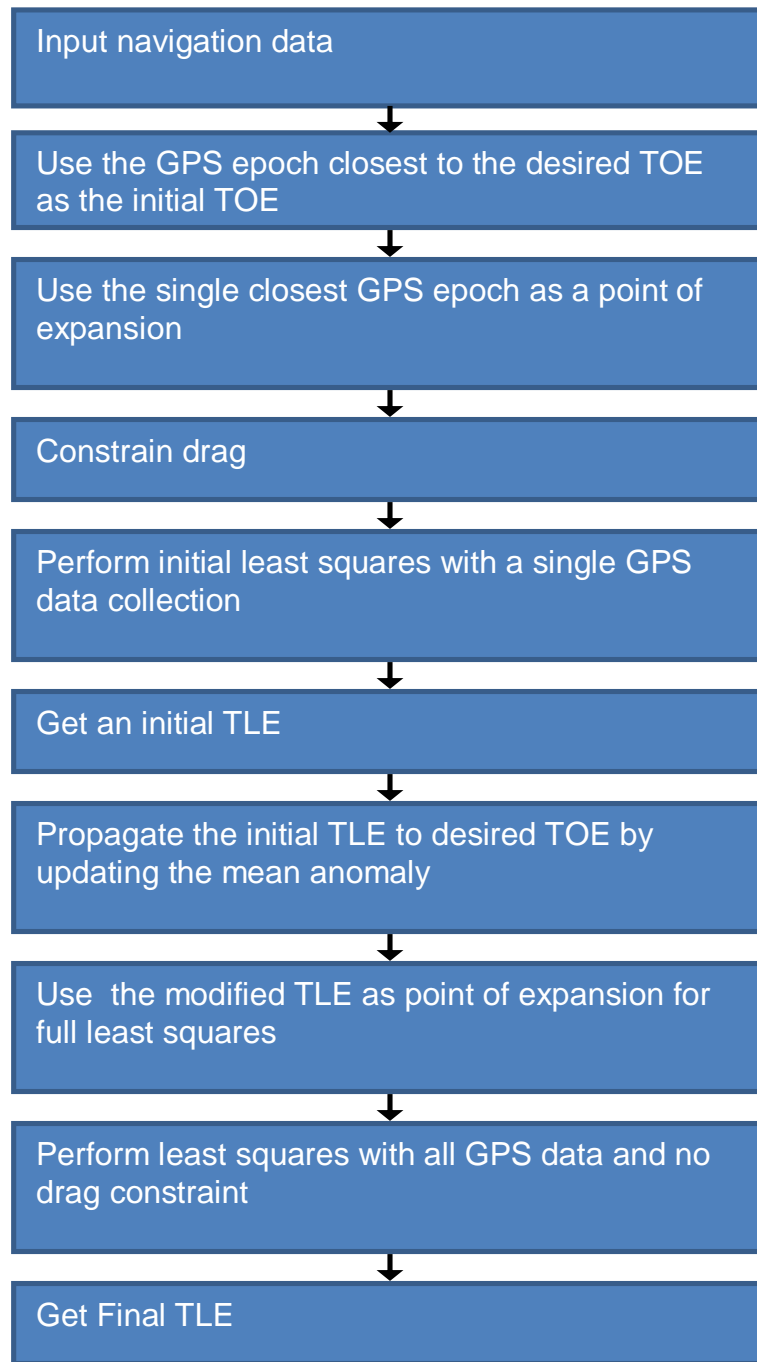


Figure 4.13: Flow chart of the least squares estimation

4.4 Preliminary Results

The least squares algorithm produces two line elements which, at the same time of ephemeris, agree closely with both NORAD TLE and with TLE formed using DLR's least squares estimator with CanX-2 GPS data as input. There are slight differences in the estimated orbital parameters, due to either differences in the algorithm (the DLR algorithm appears not to make use of GPS covariance information to weight the GPS measurements) or to differences in the input data (NORAD uses their own tracking network and the DLR algorithm was run with post-processed GPS positions as input rather than BESTXYZ results). Below are two sample TLE created using the least squares estimator, compared to a NORAD TLE and to a DLR TLE. Elements in bold were estimated through the least squares adjustment, while the remaining fields were padded with appropriate information to maintain the proper ascii format for the two lines.

Least Squares Estimator:

```
1 32790U 08021H 10211.66515121 .00000000 00000-0 +78583-4 0 44
2 32790 97.8918 275.8814 0016690 140.6101 219.6295 14.8165510 0
```

NORAD:

```
1 32790U 08021H 10211.66515121 -.00000063 00000-0 -12642-5 0 7331
2 32790 97.8918 275.8894 0015989 140.3639 219.8760 14.81654755121908
```

Least Squares Estimator:

```
1 32790U 08021H 10211.74982639 .00000000 00000-0 +78583-4 0 44
2 32790 97.8918 275.9648 0016690 140.3351 311.2829 14.8165520 0
```

DLR Estimator:

```
1 32790U 08021H 10211.74982639 0.00000673 00000-0 +85400-4 0 05
2 32790 097.8924 275.9813 0016721 140.2493 311.3674 14.81654916 07
```

There is greater agreement with the DLR element set than with the NORAD element set, due no doubt to the greater similarity in the estimation process and the use of the same GPS data arcs as input, in spite of the different pre-processing steps.

Figure 4.14 below is a sample plot of the residuals obtained from a best fit TLE through five days of GPS data collections. The distribution of the residuals is highly systematic due to the un-modelled forces, but the overall disagreement between the GPS and SGP4 trajectories is quite good, well within the 2 km suggested by Montenbruck (2000). The bias in individual data collections (continuous short arcs in the figure) relative to the best fit trajectory can be clearly seen, for example in the along-track component of the data set at -1000 minutes past epoch. These biases are an indication that individually, short GPS data arcs are unlikely to produce TLE sets with good long term propagation accuracy.

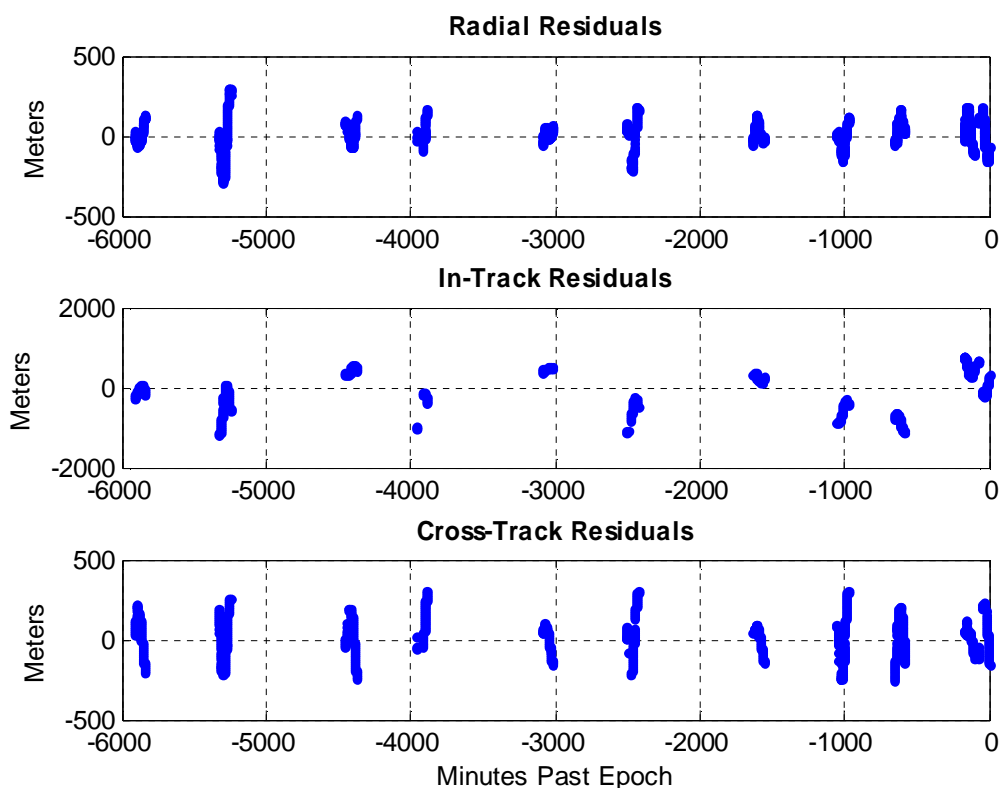


Figure 4.14: Residuals in the fit of five days of GPS data to an SGP4 trajectory

The following chapter provides an in depth analysis of the ability of the estimated TLE sets to accurately represent the trajectory of CanX-2 into the future, based on comparisons with subsequent GPS data arcs. It addresses the suitability of this method for autonomously warm starting the receiver.

Chapter Five: Results

The previous chapter developed a method for autonomously determining input parameters for the SGP4 orbital propagator using only information readily available from a NovAtel OEM4 GPS receiver operating on board a low earth orbiting satellite. The goal of this chapter is to determine whether the estimated parameters are able to predict the position of the satellite with sufficient accuracy to be helpful in warm starting the GPS receiver after an outage. In order for the propagated position to be of use, it must be sufficiently accurate to predict which GPS satellites will be visible to the low earth orbiting receiver on start up, and to predict the Doppler shift of each visible GPS satellite with sufficient accuracy for rapid acquisition.

This chapter compares the accuracy of the propagated trajectory to precise orbit determination results for CanX-2, compares the quality of estimated elements to the quality of NORAD elements with and without holding the drag parameter fixed, establishes the optimal operation scheme for maintaining a good TLE estimate, and discusses the required position accuracy for successful Doppler channel assignment.

5.1 Experimental Setup

Data collected during November and December 2010 was used as input to the TLE estimator in order to test it. The data was collected at a 30 second sampling rate for 85 minutes, and both raw RANGECPB data and BESTXYZB navigation data were collected. The data sets provide the opportunity for precise orbit processing for use as truth trajectories, and also provide receiver navigation solutions for use as input to the TLE estimator. Data collection followed a pattern of two data sets daily, one immediately following the morning pass block and one immediately following the evening pass block. Generally no data was collected over the weekends, and occasional poor contacts with the ground station or crashes of the satellite's operating system caused missed data collections as well. The exception was November 19th, 2010 (day of year 323) during

which four long arcs were collected, providing a few data sets with shorter temporal separations. Table 5.1 below is a listing of all the November long arc data sets collected.

Table 5.1: November-December 2010 data collection campaign

<i>Year</i>	<i>Day</i>	<i>Date</i>	<i>Day of week</i>	<i>Start UTC</i>	<i>End UTC</i>	<i>Antenna FOV</i>
2010	313.2	09-Nov-10	Tuesday	4:23:57	5:16:37	zenith
2010	313.8	09-Nov-10	Tuesday	18:59:07	19:51:47	zenith
2010	317.2	13-Nov-10	Saturday	5:38:45	7:03:45	zenith
2010	317.8	13-Nov-10	Saturday	18:36:45	20:01:45	zenith
2010	319.8	15-Nov-10	Monday	19:14:11	20:39:11	zenith
2010	320.2	16-Nov-10	Tuesday	4:57:39	6:22:39	zenith
2010	320.8	16-Nov-10	Tuesday	19:32:53	20:57:53	zenith
2010	321.2	17-Nov-10	Wednesday	3:39:09	5:04:09	zenith
2010	321.8	17-Nov-10	Wednesday	18:14:23	19:39:23	zenith
2010	322.2	18-Nov-10	Thursday	3:57:51	5:22:51	zenith
2010	322.8	18-Nov-10	Thursday	18:33:05	19:58:05	zenith
2010	323.2	19-Nov-10	Friday	4:16:35	5:41:35	zenith
2010	323.4	19-Nov-10	Friday	10:45:35	12:10:35	zenith
2010	323.8	19-Nov-10	Friday	18:51:49	20:16:49	zenith
2010	323.9	19-Nov-10	Friday	20:29:03	21:54:03	zenith
2010	329.2	25-Nov-10	Thursday	4:31:29	5:56:29	zenith
2010	329.8	25-Nov-10	Thursday	19:07:01	20:32:01	zenith
2010	330.2	26-Nov-10	Friday	4:50:29	6:15:29	zenith
2010	330.8	26-Nov-10	Friday	19:25:41	20:50:41	zenith
2010	331.2	27-Nov-10	Saturday	5:09:09	6:34:09	zenith
2010	334.2	30-Nov-10	Tuesday	4:28:01	5:53:01	zenith
2010	335.2	01-Dec-10	Wednesday	4:46:41	6:11:41	zenith
2010	335.8	01-Dec-10	Wednesday	19:21:53	20:46:53	zenith
2010	336.2	02-Dec-10	Thursday	5:05:35	6:30:35	zenith
2010	337.2	03-Dec-10	Friday	5:24:15	6:49:15	zenith
2010	337.8	03-Dec-10	Friday	19:59:27	21:24:27	zenith

In order to assess the long term propagation of the estimated TLE sets, data from November 13th to 19th was used to form TLE, leaving data from November 9th and from November 25th to December 3rd for validation.

Subsets of the data from the 13th to the 19th were input to the estimator, representing spreads of input data from three hours in duration to a full week in duration, in order to determine how much time separation between data sets would be required in order to get a good estimate of the drag parameter. The combinations used are summarized in Table 5.2 below, and consist of either the first and last data set for a given time span, or all the data sets collected within a particular time span.

Table 5.2: Data combinations used for TLE estimation

<i>Time Span</i>	<i>Data Sets</i>
3 hours	323.8, 323.9
6 hours	323.2, 323.4
12 hours	323.2, 323.8
12 hours	323.2, 323.4, 323.8
18 hours	323.2, 323.9
18 hours	323.2, 323.4, 323.8, 323.9
24 hours	322.8, 323.8
24 hours	322.8, 323.2, 323.4, 323.8
48 hours	321.8, 323.8
48 hours	321.8, 322.2, 322.8, 323.2, 323.4, 323.8
72 hours	320.8, 323.8
72 hours	320.8, 321.2, 321.8, 322.2, 322.8, 323.2, 323.4, 323.8
96 hours	319.8, 323.8
96 hours	319.8, 320.2, 320.8, 321.2, 321.8, 322.2, 322.8, 323.2, 323.4, 323.8
1 week	317.2, 323.9
1 week	317.2, 317.8, 319.8, 320.2, 320.8, 321.2, 321.8, 322.2, 322.8, 323.2, 323.4, 323.8, 323.9

5.2 Initial Results

Figure 5.1 to Figure 5.4 below are samples of the results obtained using the various combinations of input data, and propagating the estimated TLE through SGP4 to compare them to the precise orbit trajectories. An analysis of the precise orbits is in Appendix C, but they are assumed to be accurate at the one meter level where there are GPS measurements. Figures have only been included for TLE created using all available GPS

data in the specified time span, the results for using only the start and end GPS data sets are generally worse.

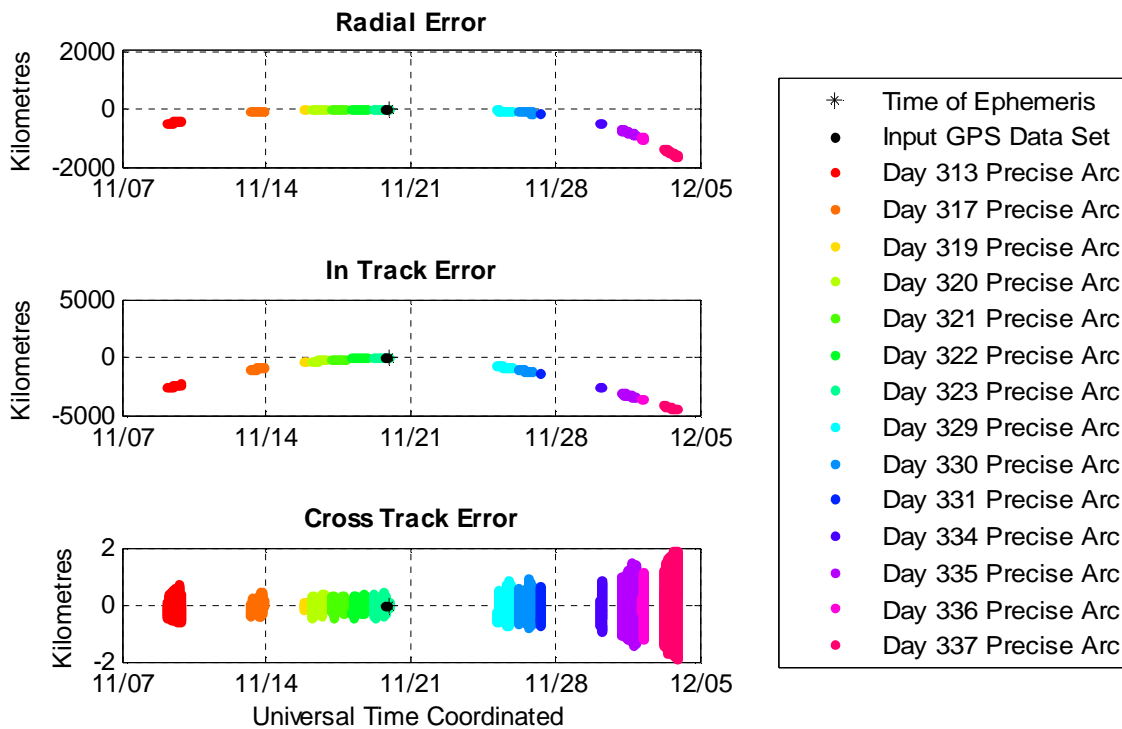


Figure 5.1: Long term propagation accuracy of a TLE estimated from all GPS data collected over a 3 hour span, relative to the precise orbit trajectories

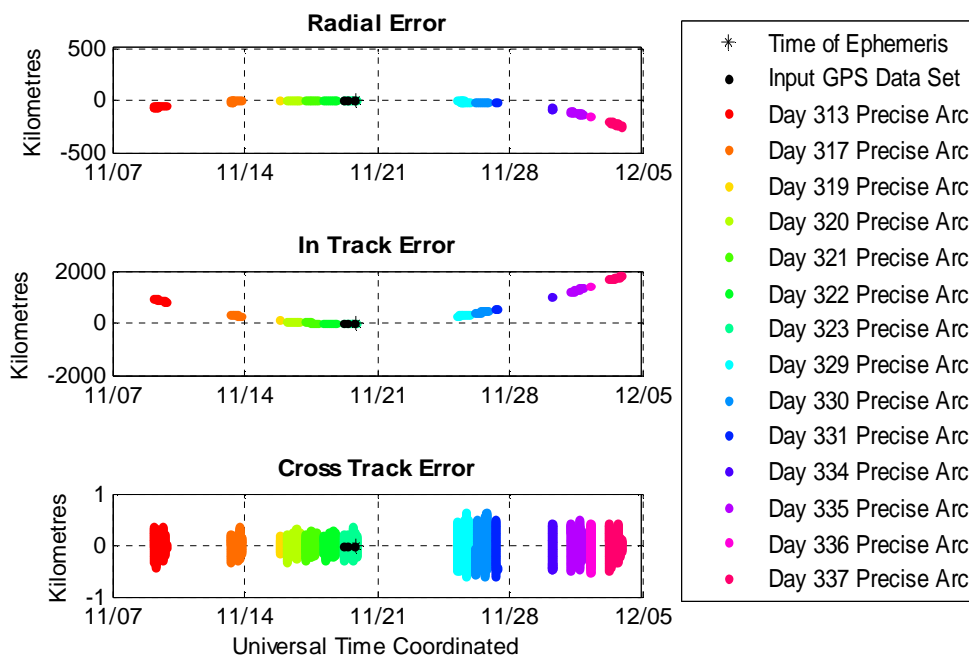


Figure 5.2: Long term propagation accuracy of a TLE estimated from all GPS data collected over a 12 hour span, relative to the precise orbit trajectories

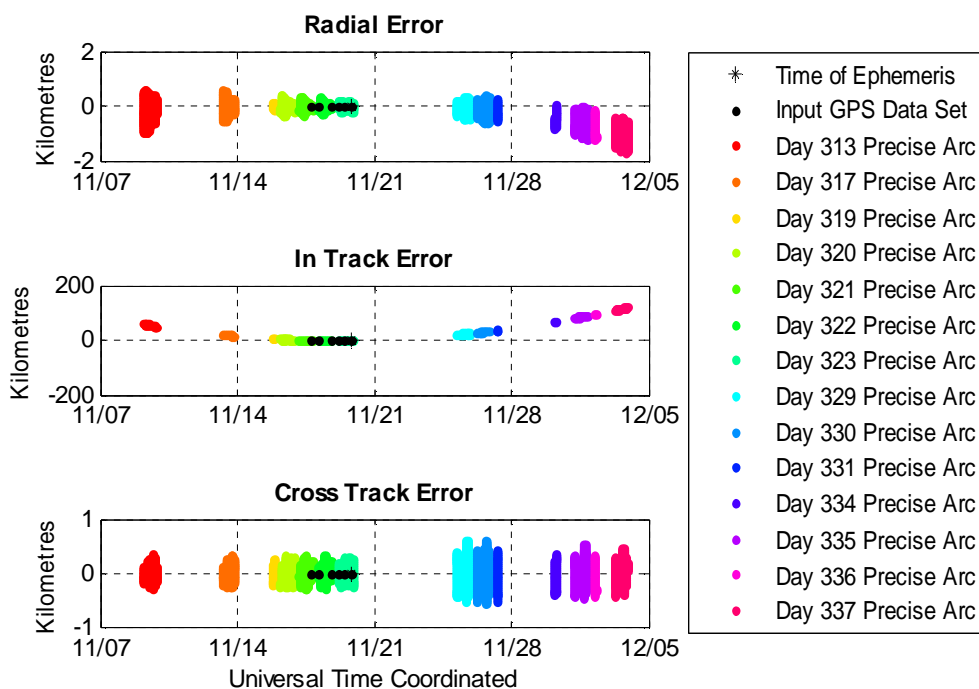


Figure 5.3: Long term propagation accuracy of a TLE estimated from all GPS data collected over a 48 hour span, relative to the precise orbit trajectories

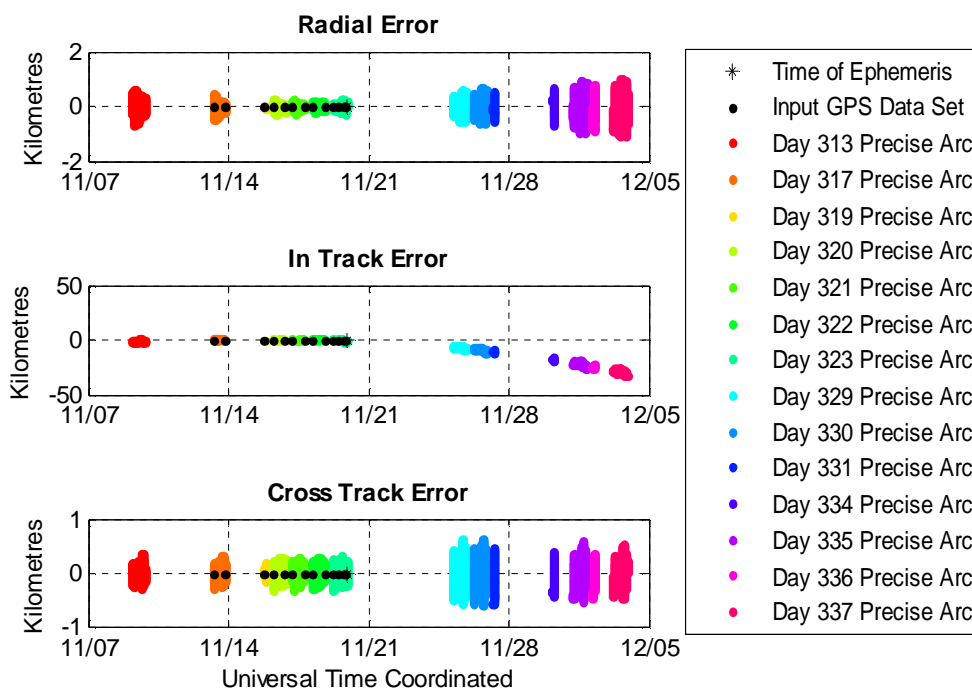


Figure 5.4: Long term propagation accuracy of a TLE estimated from all GPS data collected over a week span, relative to the precise orbit trajectories

It can be seen from the plots that shorter data collections lead to elements which very quickly develop a large along track error, and the general trend that more data is better is clearly visible. Only the week long data collection, consisting of generally two 85 minute data collections daily, provides reasonably good along track accuracy, on the order of 40 km after two weeks.

5.3 NORAD Assessment

In order to get an idea of whether the initial GPS results had similar propagation accuracies to the NORAD TLE, the NORAD TLE set with the same time of ephemeris as the GPS results was similarly compared to the precise orbit trajectories. The result is shown in Figure 5.5 below. It can be seen that the NORAD result, with an along track error of 20 km after two weeks of propagation, is significantly better than the GPS results of 40 km or worse after two weeks.

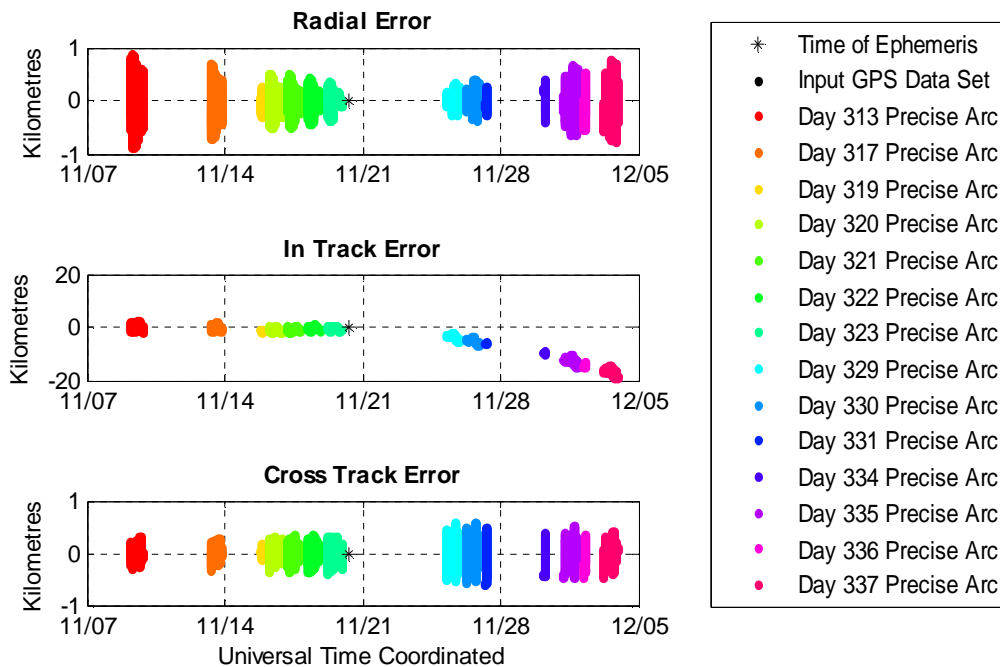


Figure 5.5: Long term propagation accuracy of the November 20th, 2010 (day 324) NORAD TLE, relative to the precise orbit trajectories

In order to assess whether all the NORAD data sets were similarly accurate over long time spans, all TLE published by NORAD between November 9th and December 3rd were similarly compared to the precise orbit solutions for CanX-2. The combined plot of the long term accuracies is displayed in Figure 5.6.

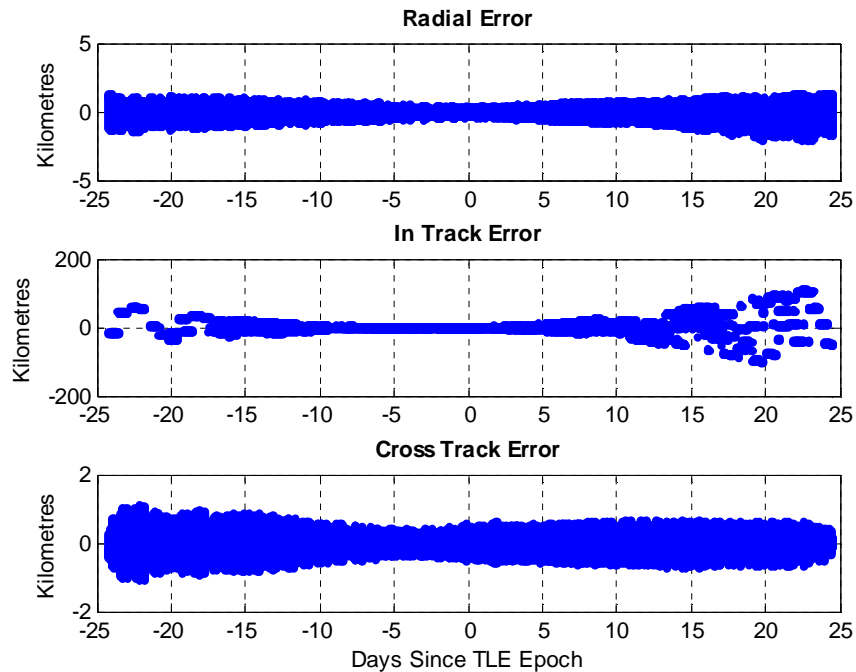


Figure 5.6: Long term propagation accuracy of all NORAD TLE sets published from November 9th to December 3rd 2010 (days 313 to 337), relative to the precise orbits

Based on the figure, after one week all the NORAD trajectories are within 20 km in along track, and after two weeks all the NORAD trajectories are within 50 km, similar to the GPS one week result. In nearly all cases the NORAD radial and cross track errors fall within a 2 km envelope of the precise trajectory. Some of the NORAD trajectories were found to have excellent long term accuracy, as depicted in the example in Figure 5.7 below.

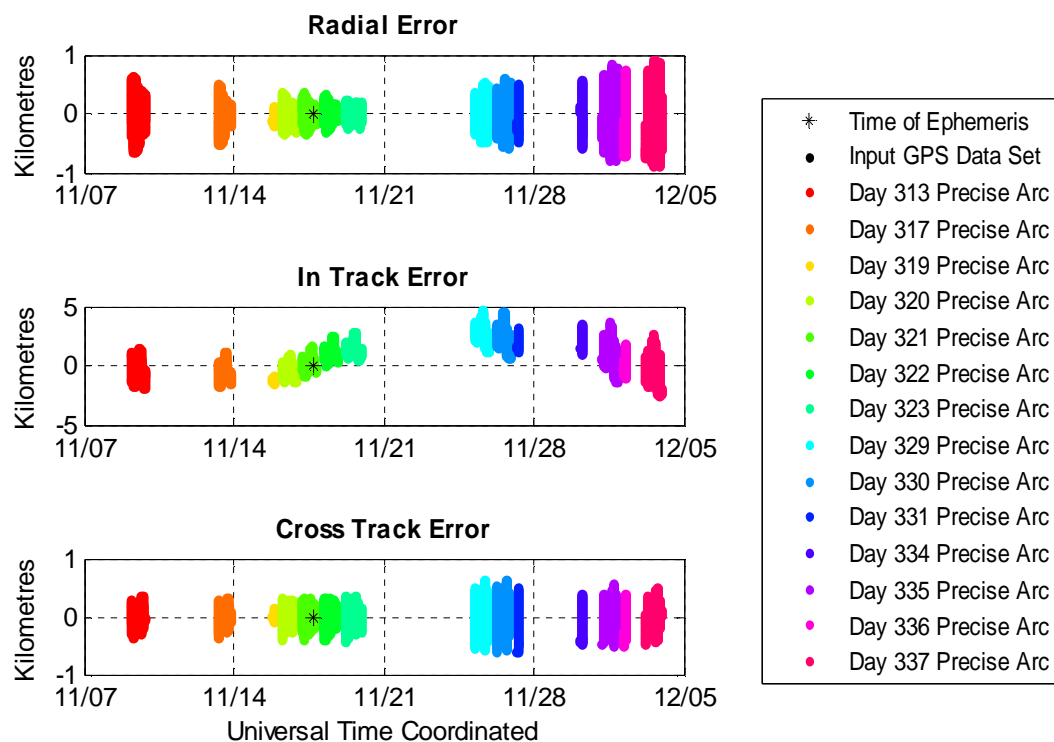


Figure 5.7: Long term propagation accuracy of the third November 17th, 2010 (day 321) NORAD TLE, relative to the precise orbit trajectories

The trend in the NORAD TLE is that the long term accuracy is highly dependent on the drag value. Analysis of the drag values for the best published TLE sets showed that a value near 5×10^{-5} earth radii⁻¹ consistently gave very good results, while significantly higher or lower drag estimates were not as accurate after a few weeks.

5.4 Fixed Drag Results

Although a week of GPS data collection was shown to get similar accuracy to NORAD, in over two years of nanosatellite operation the required density of data was only collected over a single week. Also, an operating scheme in which a TLE could be estimated after a single data set would be operationally much simpler to manage. The ability to estimate similarly accurate TLE with less input data is therefore highly desirable. In order to achieve this, TLE were estimated with drag constrained to the ideal

NORAD value of 5×10^{-5} earth radii⁻¹. Figure 5.8 to Figure 5.12 below are samples of the resulting accuracy achievable with fixed drag.

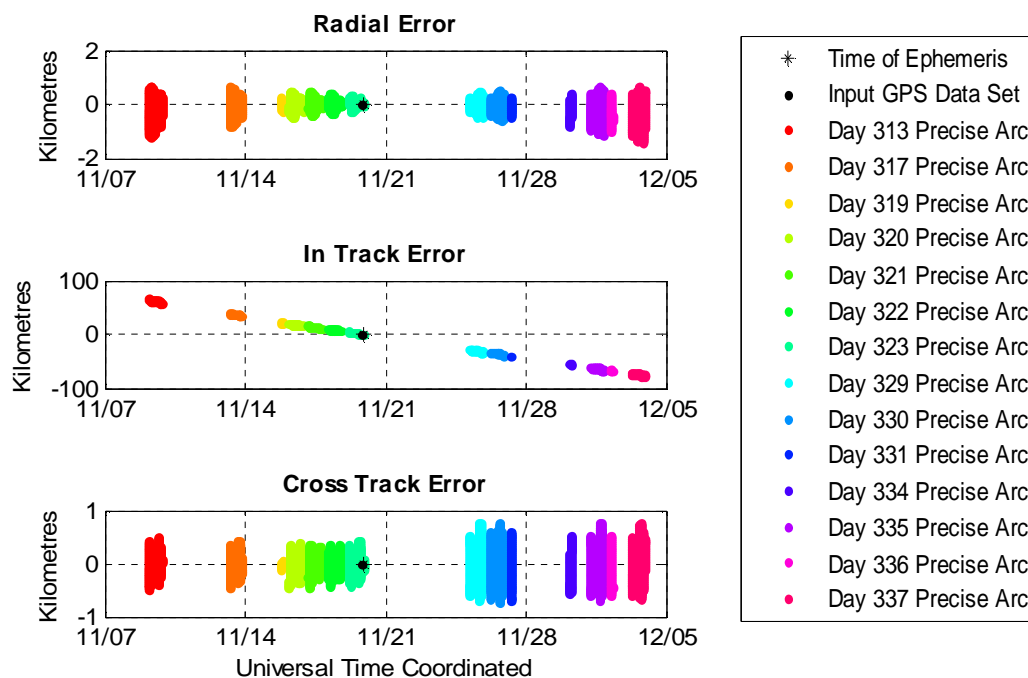


Figure 5.8: Long term propagation accuracy of a TLE estimated from GPS data collected over a 3 hour span and fixed drag, relative to the precise orbits

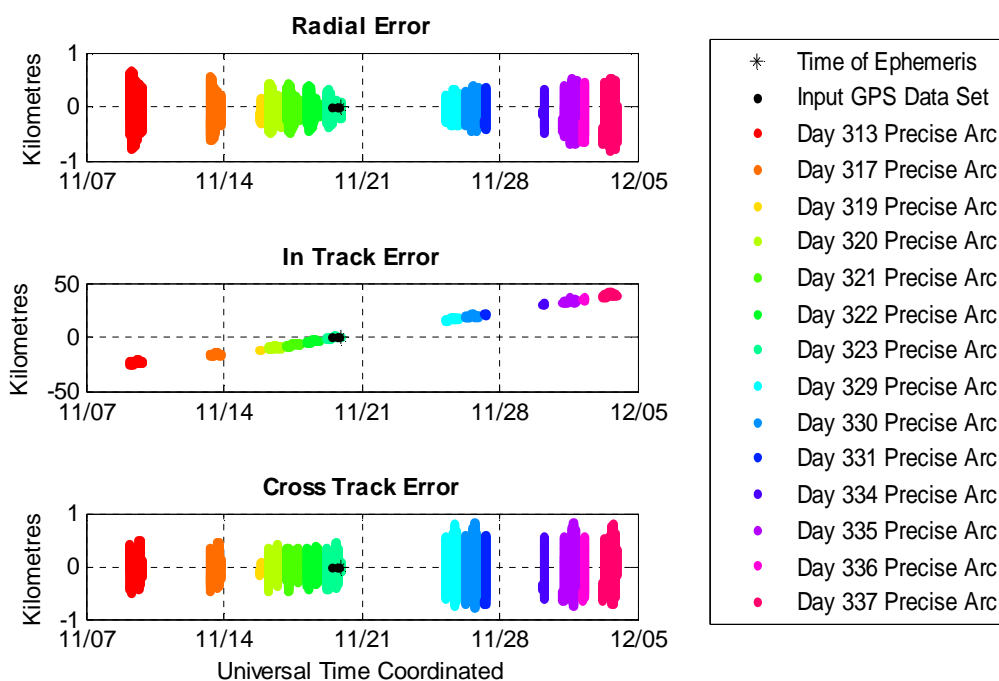


Figure 5.9: Long term propagation accuracy of a TLE estimated from GPS data collected over a 12 hour span and fixed drag, relative to the precise orbits

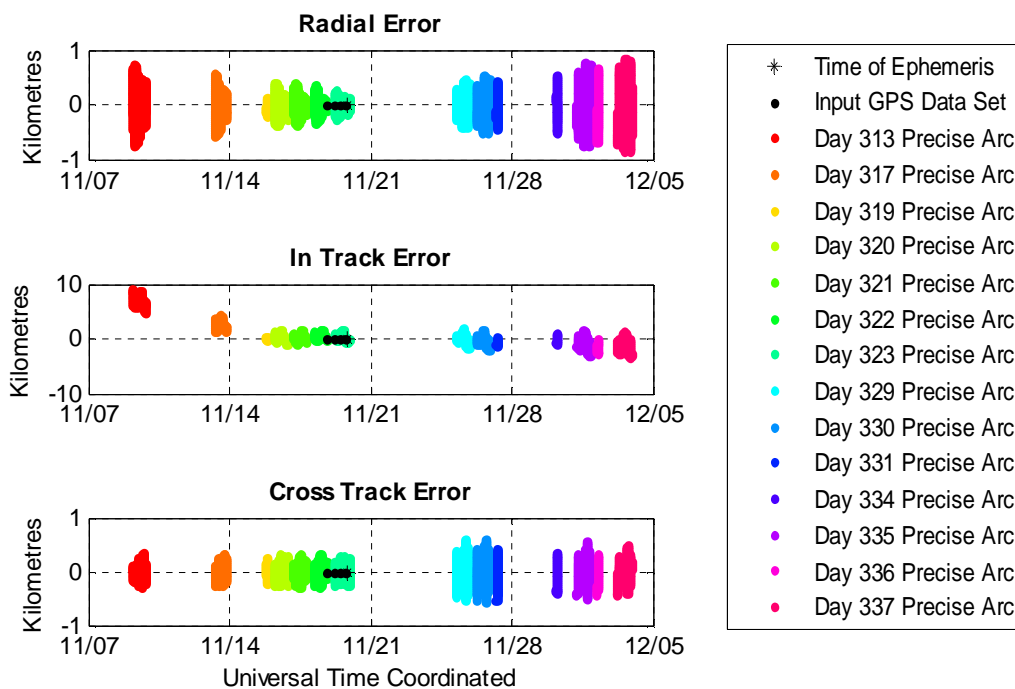


Figure 5.10: Long term propagation accuracy of a TLE estimated from GPS data collected over a 24 hour span and fixed drag, relative to the precise orbits

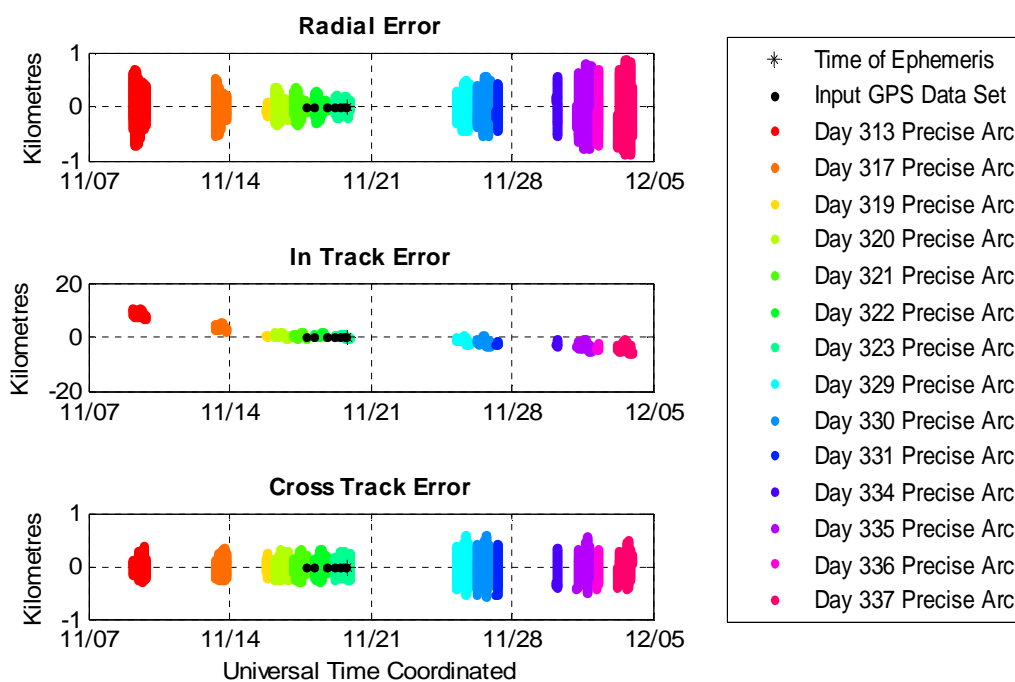


Figure 5.11: Long term propagation accuracy of a TLE estimated from GPS data collected over a 48 hour span and fixed drag, relative to the precise orbits

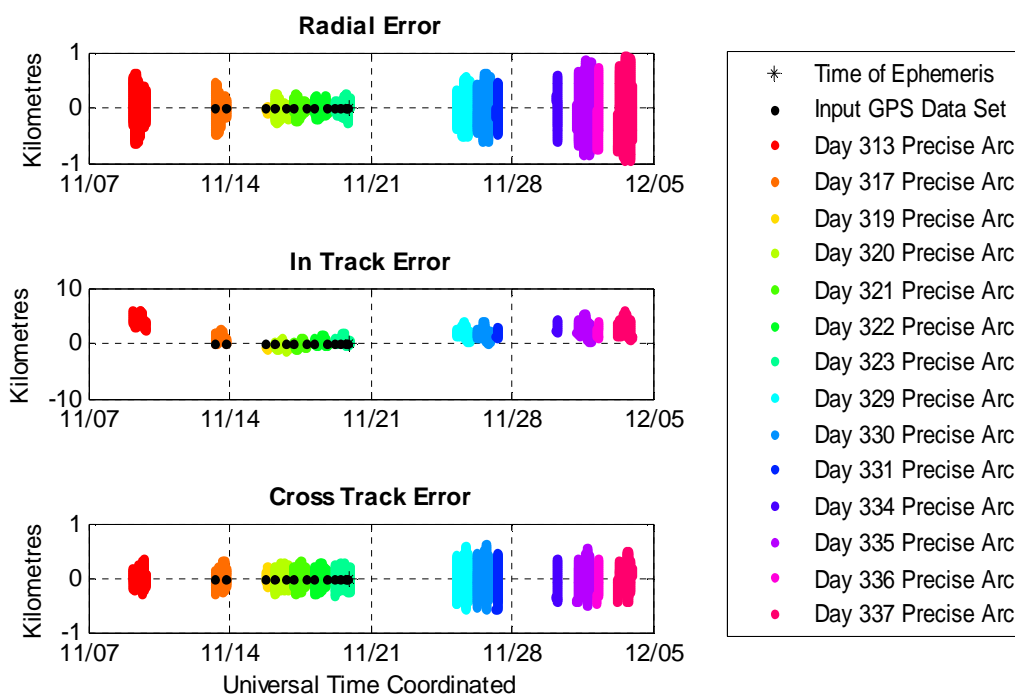


Figure 5.12: Long term propagation accuracy of a TLE estimated from GPS data collected over a week span and fixed drag, relative to the precise orbits

The figures again depict that there is a strong correlation between more input data and more accurate propagation results, but the difference is far less dramatic because overall the results are far more accurate. With three hours of input GPS data the in track error is less than 100 km two weeks later, which represents an error of only one degree. With 12 hours of input data the along-track error after two weeks is less than 50 km, on par with NORAD TLE.

5.5 Optimum Operating Scheme

The results from section 5.4 suggest that with more data optimal results are achieved, but that when drag is fixed the results are very good with 24 hours, reasonable with 12 hours of data, and may still be acceptable with only a single data set. In order to assess whether the behaviour was specific to a few good GPS collections or is universally applicable, all possible combination of the data from the week of November 13th to 19th spanning 12 and 24 hours were used to create TLE and the results were assessed. An assessment was also done using each individual 85 minute collection to form a TLE. Figure 5.13 to Figure 5.15 below show the results.

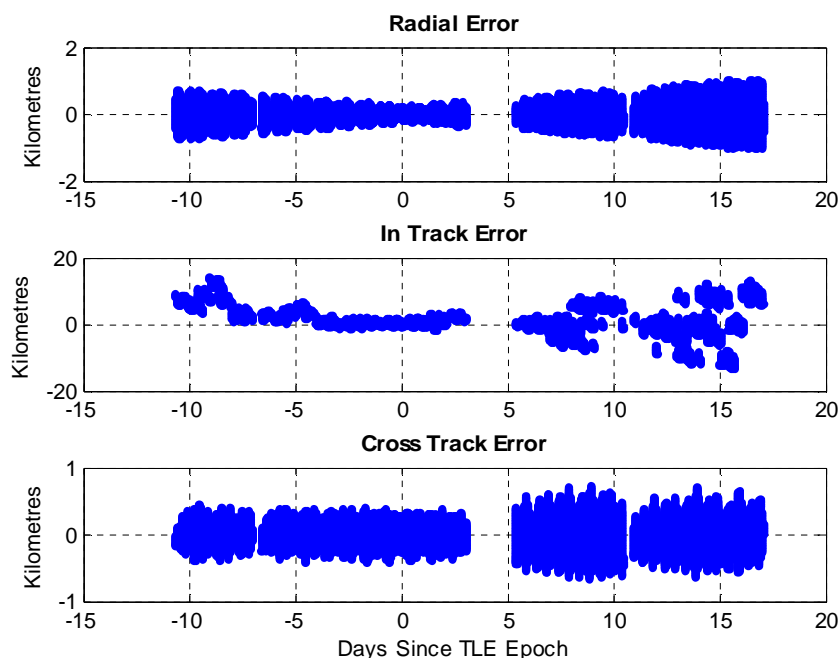


Figure 5.13: Long term propagation accuracy of all TLE estimated from 24 hour spans of GPS data and fixed drag, relative to the precise orbits

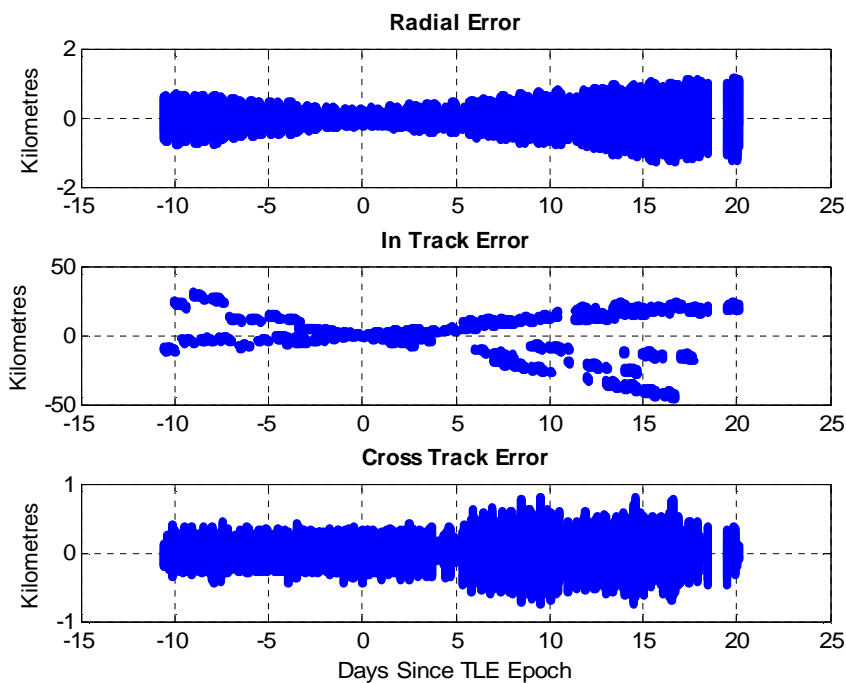


Figure 5.14: Long term propagation accuracy of all TLE estimated from 12 hour spans of GPS data and fixed drag, relative to the precise orbits

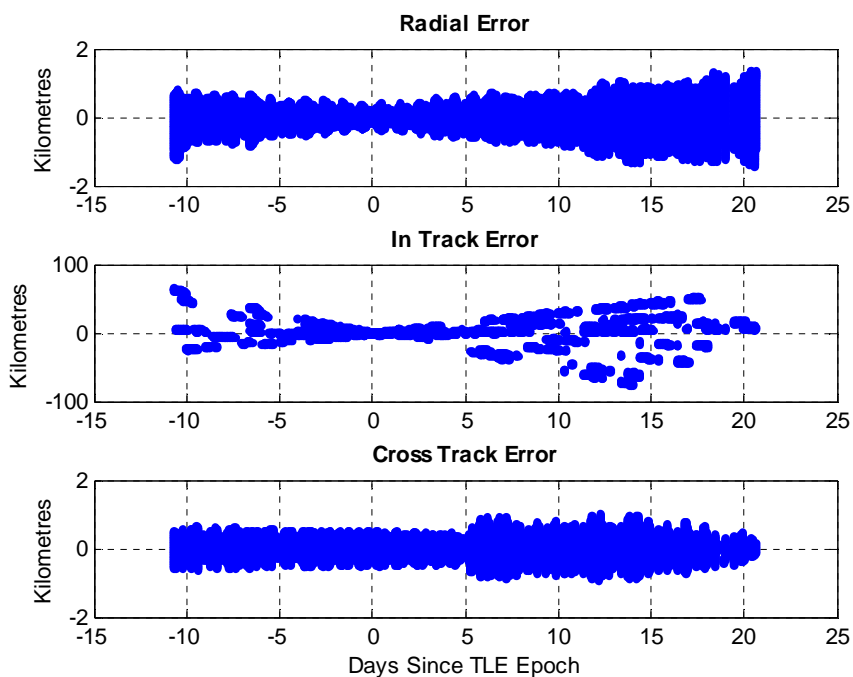


Figure 5.15: Long term propagation accuracy of all TLE estimated from single GPS data sets and fixed drag, relative to the precise orbits

It can be seen from Figure 5.13 that for 24 hours of input data and fixed drag the results were consistently below 20 km of in track error even after two weeks, which outperforms the in track error of 20 km after one week achieved by the NORAD TLE.

Figure 5.14 shows that using input data spanning 12 hours and fixed drag similar results to NORAD were achieved, with nearly all combinations having in-track errors below 20 km after one week, and below 50 km after two weeks.

Finally, Figure 5.15 shows that the individual data sets were worse than the NORAD results, with in-track errors within 50 km for one week and within 100 km within two weeks. Even this error level of error is quite small, when considering that a significant bias can exist in an 85 minute data arc when compared to the general trend in the data over several orbits or days.

5.6 Suitability of Onboard TLE Estimation for Rapid Acquisition

It has been shown that under the right conditions estimated TLE from GPS data can match or even improve on the performance of NORAD's published TLE. Based on two years of successful data collection onboard CanX-2 using NORAD TLE to aid acquisition, that result alone is enough to prove that, in terms of accuracy, onboard TLE estimation is a viable way to improve the warm start capability of the receiver.

However, in an attempt to actually determine the trade off between error in CanX-2's position and the receiver's ability to acquire, experiments were carried out in orbit, where the time of ephemeris of the TLE used for script generation was intentionally adjusted by values of -35 seconds, -17.5 seconds, +17.5 seconds, +20 seconds, and +35 seconds, corresponding to along track errors for CanX-2 of +/-1 degree, 1.125 degrees, and +/-2 degrees. The motivation for one degree as the starting point was that according to Montenbruck (2010), one degree corresponds to approximately a 500 Hz error in Doppler, which is the "interval in which a 1ms C/A code correlation can successfully be

performed,” and is therefore the point at which the receiver would be expected to first run into acquisition problems. The motivation for only simulating an along track error is that the along track error is dominant in SGP4 propagation, and rapidly outweighs cross track and radial errors by orders of magnitude.

Figure 5.16 below displays the standard Doppler shifts seen in various parts of the satellite’s field of view. Signals from GPS satellites at zenith experience the smallest Doppler shift (Doppler goes to zero when the satellite trajectories are briefly parallel), but the highest rate of change in the Doppler shift (As the LEO passes beneath the GPS satellite the Doppler changes from positive to negative).

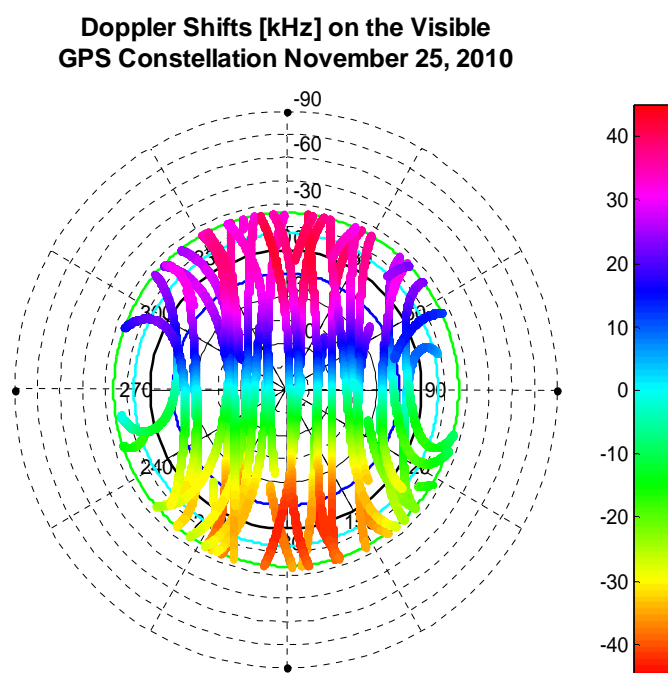


Figure 5.16: Predicted Doppler shifts on the visible GPS constellation November 25, 2010 from 19:07 to 20:32 UTC

Figure 5.17 to Figure 5.21 display the errors in Doppler induced by each of the changes to the times of ephemeris. The values were calculated by differencing the predicted Dopplers obtained using the unaltered and altered NORAD element sets.

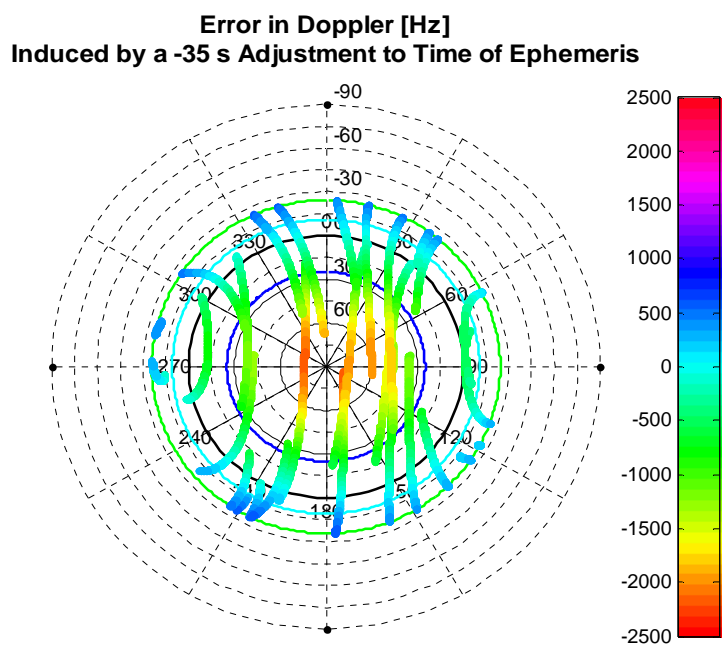


Figure 5.17: Error in Doppler induced by a -35 second adjustment to the time of ephemeris

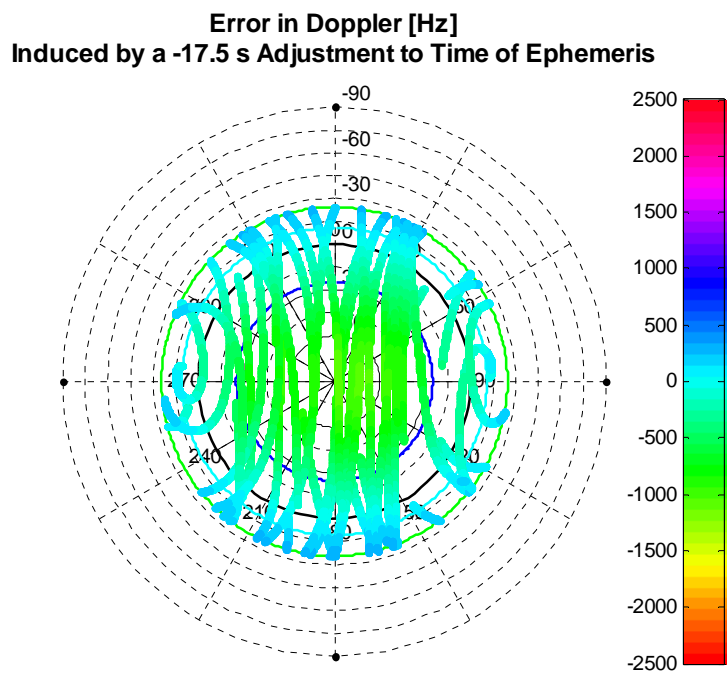


Figure 5.18: Error in Doppler induced by a -17.5 second adjustment to the time of ephemeris

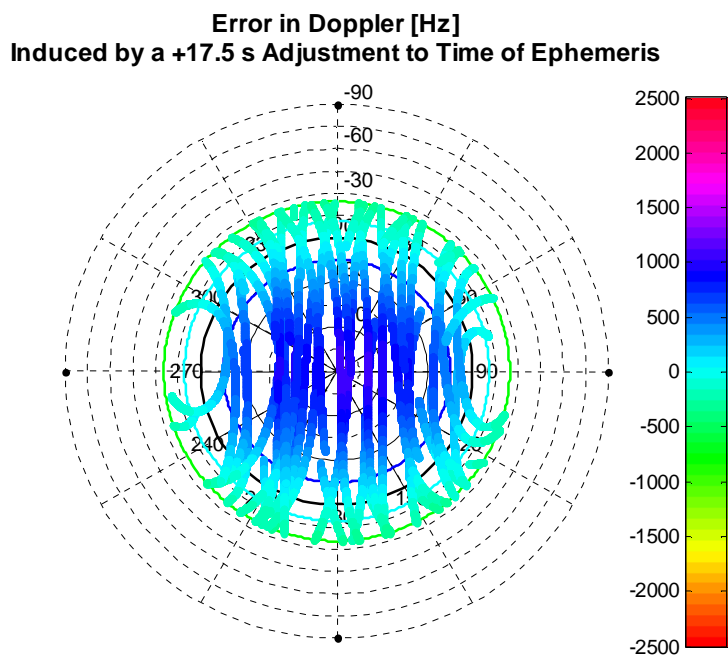


Figure 5.19: Error in Doppler induced by a 17.5 second adjustment to the time of ephemeris

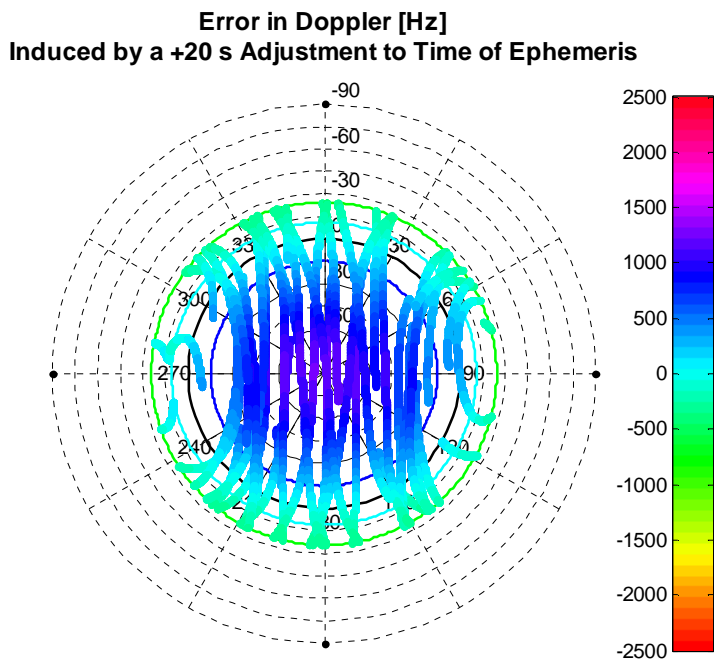


Figure 5.20: Error in Doppler induced by a 20 second adjustment to the time of ephemeris

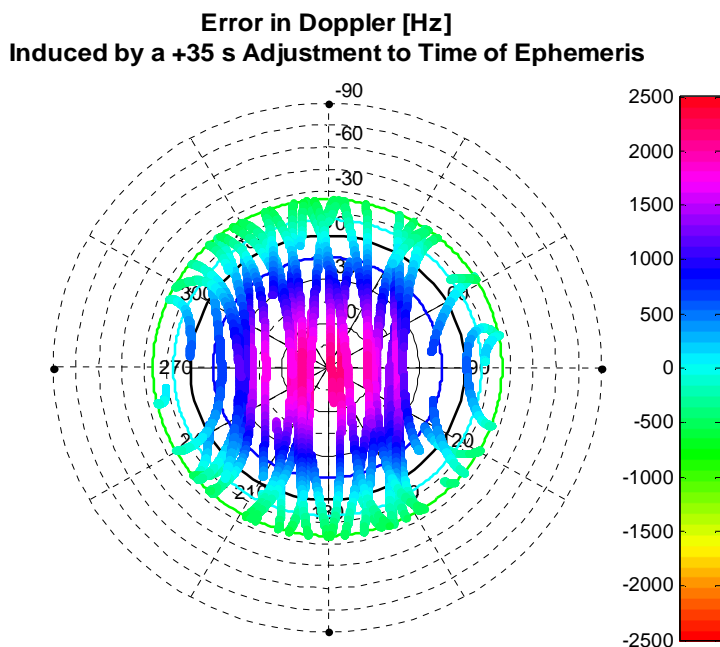


Figure 5.21: Error in Doppler induced by a 35 second adjustment to the time of ephemeris

The trend in the plots shows that the GPS satellites at zenith experience the greatest error in Doppler, in part because the values are already changing rapidly. The maximum error at zenith induced by a +/-17.5 second along track error is approximately +/-1100 Hz, by a 20 second advance is 1300 Hz and by a +/-35 second along track error is +/-2200 Hz.

The pattern of Doppler error caused by an along track error in the LEO satellite's position is quite encouraging. GPS satellites at the horizon, which experience the maximum Doppler shift and therefore are most dependent on the channel assignment, are barely impacted by an along track error caused by a poor TLE estimate. Satellites overhead with Dopplers near zero are most likely to be acquired even without channels assigned to them, and so as long as a receiver in orbit has some channels left for default search at low Doppler shifts they too could be acquired even with a poor TLE estimate. As long as the along track error is not so large as to impact the constellation visible to the LEO satellite, Doppler channel assignment should be quite robust.

Table 5.3 below shows the time to first fix obtained using scripts generated with the various along track errors, as well as using a standard unaltered NORAD TLE. It can be seen from the table that there is a high degree of variability in time to first fix, but overall it appears that, as predicted, the warm start process is in fact very insensitive to along track error in the input TLE.

Table 5.3: Variability in Time to First Fix at various level of in-track orbit error

<i>statistic</i>	<i>simulated position error</i>	<i>Time from receiver on to</i>				
		<i>first L1</i>	<i>first four L1</i>	<i>four L1 + L2</i>	<i>position soln.</i>	<i>clock soln.</i>
Mean	-35s	45	60	89	155	192
	-17.5s	41	87	105	179	216
	none	39	106	121	191	234
	17.5s	30	81	95	163	208
	20s	28	78	93	151	191
	35s	42	91	106	173	218
	all	38	97	113	181	224
Std	-35s	1	18	14	32	12
	-17.5s	8	36	32	45	45
	none	13	69	68	86	64
	17.5s	5	53	53	55	68
	20s	3	10	11	9	28
	35s	18	32	32	31	50
	all	12	54	53	65	58
Min	-35s	44	49	70	117	177
	-17.5s	36	44	64	136	173
	none	30	39	56	104	164
	17.5s	26	38	50	122	144
	20s	24	71	86	142	160
	35s	23	65	83	148	156
	all	23	38	50	104	144
Max	-35s	46	86	100	193	207
	-17.5s	38	46	64	173	173
	none	74	281	293	408	408
	17.5s	37	159	171	244	304
	20s	30	89	106	160	212
	35s	57	137	153	218	278
	all	74	281	293	408	408

One interesting outcome from the experiment, based on the mean TTFF values in the above table, is that it appears advancing the time of ephemeris actually provides an

improvement to TTFF. An along track delay of 20 seconds appears to be the optimal value, with a mean TTFF of 151 seconds. With only three or four trials run at each orbital error there is, however, insufficient data to draw firm conclusions, as the 35 second advance had the second best result.

The potential improvement in TTFF at 20 seconds can be explained by the geometry of the situation, as shown in Figure 5.22. Adding time had the result that the true position of CanX-2 was behind the predicted position. The end result was that 20 seconds later CanX-2 had reached almost exactly the signal environment that was predicted, and was therefore easily able to acquire a position fix.

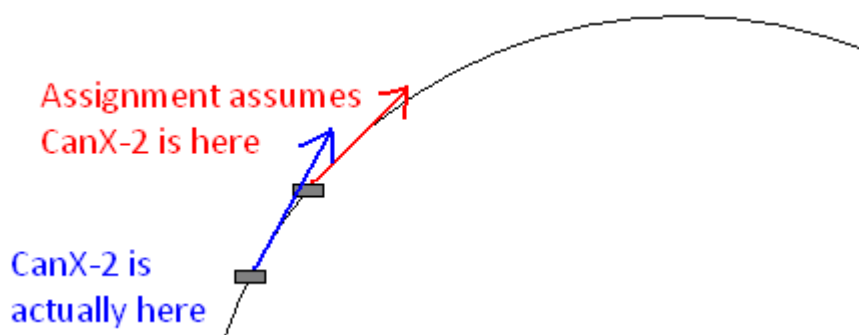


Figure 5.22: Effect of advancing the time of ephemeris on channel assignment

The experimental results confirm that warm starting the receiver is still easily possible with along track errors of two degrees or 200 km in either direction. This allowable error is at least twice as big as the achieved error in the propagated position after two weeks, even when the TLE was estimated from a single 85 minute arc of GPS data and a fixed drag value. The results also suggest that if the actual position of the LEO satellite lags the estimated position the receiver is even less sensitive to orbital errors, because the satellite will eventually reach the predicted signal environment. It has therefore been confirmed that using GPS data to estimate a TLE is a viable solution for warm starting a receiver in low earth orbit.

Chapter Six: Conclusions and Future Work

The launch of CanX-2 on April 28, 2008 marked the first time the commercial off the shelf OEM4-G2L GPS receiver, or any NovAtel GPS receiver, flew in space. The flight heritage obtained onboard CanX-2 and the previously demonstrated suitability of the receiver for orbital use have resulted in it and several other NovAtel receivers being incorporated into satellite missions, both nanosatellites such as CanX-4/5, and larger missions such as JC2Sat. After nearly three years in space the GPS receiver is still fully functional and collecting scientific data.

6.1 Conclusions from Operation in Orbit

The constraints associated with operating onboard a nanosatellite have dictated that an intermittent operation scheme for the GPS receiver is required. Probably the most significant challenge for the collection of GPS data in space is rapidly acquiring sufficient GPS signals for positioning. This challenge prompted the adoption of an operation scheme in which receiver channels were pre-assigned with PRNs and Doppler shifts at which to begin the search. Channel assignment scripts for CanX-2 are generated on the ground ahead of time, and must be transmitted to the satellite for each data collection.

The GPS data collections run to date have occurred in five time windows. From November 2008 to February 2009 the trials met with no success in acquiring a position fix, but provided a wealth of information which was used for debugging. From April to June of 2009 the first positioning data was collected and the channel assignment scripts were refined in order to better suit the needs of the radio occultation experiment. In the period from December 2009 to July 2010 radio occultation data was successfully collected. In the period from July to April of 2010, the focus of GPS data collection shifted to longer arcs at lower logging rates, suitable for orbit determination work. Finally experimentation is returning to radio occultation trials. Figure 6.1 below illustrates the timeline of data collection.

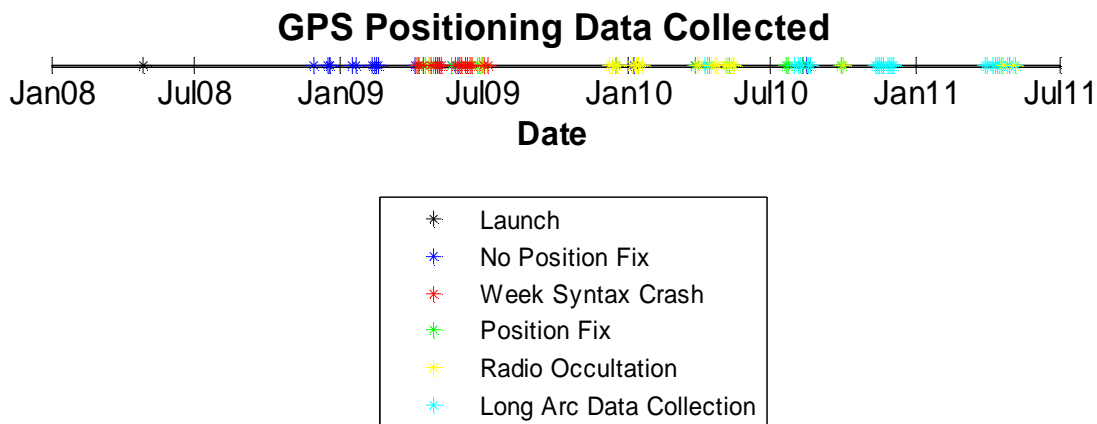


Figure 6.1: Timeline of GPS data collection on board CanX-2

The average time to first fix using channel assignment, calculated as the time span from when the receiver is powered on until it has calculated a position solution, was just under 3.5 minutes calculated over both radio occultation trials and long arc data collection. This value marks a significant improvement over the 20 minutes required to cold start CanX-2's COTS receiver, and is comparable to the performance of specialized space receivers in cold start. The most important lesson to come out of the experience with the channel assignment scripts was that the four requirements for effective channel assignment are knowledge of the current time, knowledge of the antenna field of view, knowledge of how the receiver clock drifts in the space environment, and knowledge of the low earth orbit (LEO) and GPS satellites' positions in order to predict Doppler shifts.

6.2 Suitability of the Proposed Operating Scheme

Based on the experience with the ground generated channel assignment scripts, a method was devised to propagate the position of the LEO satellite forward in time, in order for the receiver to ultimately be able to generate a channel assignment script "on the fly" and acquire quickly without ground contact. In order to provide this capability, the GPS data is fed into a least squares estimator, and the best fit two line element set (TLE) for the satellite's orbit is estimated. The SGP4 orbital model can then be used together with the

TLE to propagate the LEO satellite's position through a GPS outage, enabling the autonomous calculation of the GPS constellation visibility and expected Doppler shifts for a warm start.

The results of estimating two line element sets using the GPS data is promising, but unexpected challenges were encountered. The difficulty in estimating TLE from the receiver's internal navigation solution is the estimation of the drag parameter, which has a significant impact in the along-track error. It was found that the data collected over 85 minute arcs every 12 hours only provided sufficient information for a good drag estimate after a week of data collection. This may in part be as a result of the data being collected over the same two parts of the earth's surface for each of the two daily trials, giving a poor look at the overall satellite motion during an extended time period.

Constraining the drag value proved to have excellent results. It was shown that with drag constrained to an appropriate value and two 85 minutes periods of receiver operation separated by 12 hours, results on the same level of accuracy as NORAD's published values were consistently achieved. The operationally simpler scenario of using a single 85 minute data arc with constrained drag to estimate the TLE was less accurate than NORAD's results, but the consistently achieved 100 km or less of error after two weeks is more than accurate enough for a warm start based on empirical tests run on CanX-2.

The ongoing difficulty of using constrained drag, both for the initial calculation of a point of expansion at the desired epoch and for the final solution, is finding an appropriate drag value to use as a constraint. In the absence of an outside source of drag information it would still be necessary to operate the receiver as frequently as possible for at least a week in order to get a good estimate. Over the lifetime of the satellite it is expected that the drag will change, as the satellite slowly drops closer to the earth. For this reason an occasional update to the constrained drag value would likely be required. Coordinating the necessary week long data collections to feed into the TLE estimates, particularly with

an intermittent and irregular receiver operation schedule such as CanX-2's, would be complex at best.

The results underline the fundamental trade off associated with predicting the position of a satellite. Either a large amount of observations are required in order to estimate mean elements for use with a simplified orbital model, such as the case illustrated here, or alternately a much shorter span of observations may be used to get an osculating orbital position, which requires a high fidelity orbital dynamics model in order to propagate it forward. For an operating scheme as limited as CanX-2's, neither option is ideal because neither long stretches of receiver power nor highly complex computations demand resources are readily available on board a nanosatellite.

In conclusion, sufficient accuracy to warm start the receiver autonomously is achievable, but requires the operationally difficult step of estimating drag.

6.3 Current Work

This thesis has dealt almost exclusively with the acquisition behaviour of CanX-2's GPS receiver, with little to no analysis of the other measures of GPS performance such as noise, ability to track continuously, and positioning accuracy. A broader analysis of the performance of the NovAtel OEM4-G2L in space is currently being prepared under the title "GPS Tracking on a Nanosatellite – The CanX-2 Flight Experience" (Kahr et al 2011). It will be presented at the ESA GNC 2011 conference.

6.4 Future Work

CanX-2 is only one of a vast number of satellites, and SGP4 is only one of numerous possible orbital models. While the proposed operating scheme was shown to be viable for this combination of sun-synchronous low earth orbit and orbital model, far more work should be carried out in order to test the widespread reliability of the method. The early days of debugging CanX-2's channel assignment highlighted the extent to which

unpredicted, satellite specific “features” can prevent a methodology that has been proven to work in simulations on the ground from being effective after launch. The difficulty of remote debugging and inaccessibility of faulty systems if a problem is discovered make using a system which has not been tested as extensively as possible onboard a satellite extremely risky, in particular when the cost and rarity of opportunities for operating in space are considered.

Recommended future work is therefore a more widespread test of the algorithm, using input GPS data from other satellite missions if possible, preferably with different orbital configurations. Particular attention should be paid to missions with potential singularities in the Keplerian orbital elements, such as equatorial orbits with poorly defined ascending nodes and circular orbits with poorly defined arguments of perigee. These orbits are likely to run into numerical problems during the least squares estimation of orbital elements.

Testing the algorithm with continuous GPS data would also be extremely beneficial, providing the ability to simulate various periods of receiver operation and providing continuous arcs for long term assessment of the propagator results, rather than the brief windows in time provided by CanX-2 data. The chapter five assessment of how much input data is required for a good TLE estimate was restricted by the availability of the CanX-2 data sets, but many of the other missions carrying NovAtel receivers could potentially afford longer periods of continuous receiver operation, yielding better estimated orbital parameters. CanX-2 data collection is extremely sporadic, and therefore not representative of most satellite missions.

Another important test which has not been carried out is an assessment of the error in the predicted GPS satellites’ orbits, which contributes just as significantly to the Doppler calculations as the LEO satellite’s position error. In this work it has been assumed that the receiver’s storage of GPS almanacs for future acquisition is fully available, and that the resulting predicted positions of the GPS satellites are error free or nearly so.

A final practical consideration is on board memory. While the motivation for choosing an analytical orbital model was to reduce the computational complexity, no work has been carried out to quantitatively assess the computational resources required for the least squares estimation, TLE propagation or Doppler shift computation. It has been assumed that it could easily be run either internally in the GPS receiver or on some future satellite's onboard computer, based on the similar estimation and orbit propagation algorithms already existing as part of the GPS receiver's functionality.

Finally, this research has focused on real orbital experience and developing an algorithm for use in space. The ultimate goal is therefore to implement the algorithm and to fly it!

References

- AeroAntenna (2003) *Low Profile L1/L2 Antenna*, Drawing No. AT2775-103, Revision C.
- Ashby, N. and J.J. Spilker, Jr. (1995) "Introduction to Relativistic Effects in the Global Positioning System," Ch. 18 in *The Global Positioning System--Theory and Applications Volume 1*, Progress in Astronautics and Aeronautics, vol 163, American Institute of Aeronautics and Astronautics.
- Birmingham, W. P., B. L. Miller and W. L. Stein (1983) "Experimental Results of Using the GPS for Landsat 4 Onboard Navigation," *Navigation: Journal of the Institute of Navigation*, vol 30, no 3, Fall, pp. 244-251.
- Bradbury, L. (2011) Personal Communication, UTIAS SFL.
- Bradbury, L. (2010) *CanX-2 and NTS (CanX-6) - Combined Predicted Pass Times*, University of Toronto Institute of Aerospace Studies, Space Flight Laboratory.
- Celestrak Website (2011) *NORAD Two-Line Element Sets Current Data*, <http://celestrak.com/NORAD/elements/>, last accessed March 15, 2011.
- Celestrak Website (2004) *NORAD Two-Line Element Set Format*, <http://celestrak.com/NORAD/documentation/tle-fmt.asp>, last accessed March 15, 2011.
- DeGroot, L. (2008) *Use of the Global Environmental Multiscale Model for Atmospheric Retrieval from Radio Occultation for Canadian Events*, MSc Thesis, Department of Geomatics Engineering, University of Calgary, Canada. (Available at <http://www.geomatics.ucalgary.ca/graduatetheses>)
- De Jong, C. D., G. Lachapelle, S. Skone and I. A. Elema (2002) *Hydrography*, Delft University Press, the Netherlands.
- De Rooter, A., J. Lee, K. Yoshihara, and A. Ng (2009) *GPS-Based Orbital Determination and Relative Navigation for JC2Sat*, Technical Report No JCF-000112, Canadian Space Agency, 261 pages.
- Ebinuma, T., E. Rooney, S. Gleason and M. Unwin (2005) "GPS Receiver Operations on the Disaster Monitoring Constellation Satellites" *The Journal of Navigation*, vol. 58, p 227.

El Sheimy, N. (2000) *Adjustment of Observations*, ENGO 361 Course Notes, Geomatics Engineering, University of Calgary.

Ernandes, K. (1996) Vector to Two-Line Elements (VEC2TLE) *Software User Manual*, Version 9648, Flushing NY.

Feng, Y., N. Zhou and W. Enderle (2003) “FedSat Orbit Determination: Results From Daily GPS Flight Code Observations” Proceedings of SatNav 2003: The 6th International Symposium of Satellite Navigation Technology Including Mobile Positioning & Location Services, Melbourne, Australia.

Fjeldbo, G., V. R. Eshleman, K. Garriott, and F. L. Smith III (1965) The two-frequency Bistatic Radar Occultation Method for the Study of Planetary Ionospheres, *Journal of Geophysical Research*, vol. 70, pp 3701-3710.

Fleeter, R. (2000) *The Logic of Microspace*, Microcosm Inc. and Kluwer Academic Publishers, USA.

Fortescue, P. W., J. Stark and G. Swinerd (2004) *Spacecraft Systems Engineering*, Third Edition, John Wiley and sons, pp. 63 – 71.

Garcia-Fernández, M. and O. Montenbruck (2006) “Low Earth orbit satellite navigation errors and the vertical total electron content in single-frequency GPS tracking,” in *Radio Science*, vol. 41, RS5001.

GENESIS (2011) *GPS/MET*, Global Environmental & Earth Sciences Information System, NASA JPL, <http://genesis.jpl.nasa.gov/zope/GENESIS/Missions/GPSMET>, last accessed May 9, 2011.

Gerner, J. L., J. L. Issler, D. Laurichesse, C. Mehlen, and N. Wilhelm (2002) “TOPSTAR 3000 – An Enhanced GPS Receiver for Space Applications,” *ESA Bulletin*, no 104, November, pp. 86-91.

Gill, E., and O. Montenbruck (2002) *The Onboard Navigation System for the BIRD Small Satellite*, Technical Report, German Space Operations Centre, DLR.

Gleason, S., S. Hodgart, Y. Sun, C. Gommenginger, S. Mackin, M. Adjrak and M. Unwin (2005) “Detection and Processing of Bistatically Reflected GPS Signals from

Low Earth Orbit for the Purpose of Ocean Remote Sensing,” in *IEEE Transactions on Geoscience and Remote Sensing*, vol 43, no 6, June, pp. 1229-1241.

GPS World (2011) *GPS World Antenna Survey 2011*,
<http://www.gpsworld.com/professional-oem/component-technologies/2011-antenna-survey-11044>, last accessed May 4, 2011.

Greene, M. and R. Zee (2009) “Increasing the Accuracy of Orbital Position Information from NORAD SGP4 Using Intermittent GPS Readings,” *Proceedings of the 23rd Annual AIAA/USU Conference on Small Satellites*, SSC09-X-7.

Guitteau, J. (2010) Email communication with AeroAntenna, Nov 29.

Hajj, G., C. Ao, B. Iijima, D. Kuang, E. Kursinski, A. Mannucci, T. Meehan, L. Romans, M. Juarez, and T. Yunck, (2002) CHAMP and SAC-C atmospheric occultation results and intercomparisons, *Journal of Geophysical Research*, vol. 109, p. 45.

Hoots, F. R., and R. L. Roehrich (1980) *Spacetrack Report #3: Models for Propagation of the NORAD Element Sets*, U.S. Air Force Aerospace Defense Command, Colorado Springs, CO.

Hoots, F., P. Schumacher, and R. Glover (2004) “History of Analytical Orbit Modeling in the U. S. Space Surveillance System,” *Journal of Guidance, Control, and Dynamics*, vol. 27, no.2, pp. 174–185.

Hwang, C., T. Tseng, T. Lin, D. Svehla, and B. Schreiner (2009) Precise Orbit Determination for the FORMOSAT-3/COSMIC Satellite Mission using GPS. *Journal of Geodesy*, vol. 83, no. 5, pp. 477-489.

International Earth Rotation and Reference System Service (IERS) (2010) *Bulletin B – Product Metadata*,
http://www.iers.org/nn_11252/IERS/EN/DataProducts/EarthOrientationData/bulB_MD.html, last accessed March 15, 2011.

Jochim, E. F., E. Gill, O. Montenbruck, and M. Kirschner (1996) “GPS Based onboard and on Ground Orbit Operations for Small Satellites,” *Acta Astronautica*, vol. 39, no. 9, pp. 917-922.

Kahr, E. (2007) *CanX-2 Occultation Determination*, ENGO 500 Course Report, Department of Geomatics Engineering, University of Calgary.

Kahr E., O. Montenbruck, K. O’Keefe, S. Skone, J. Urbanek, L. Bradbury, and P. Fenton (2011) “GPS Tracking of a Nanosatellite – the CanX-2 Flight Experience”, in *Proceedings of the 8th International ESA Conference on Guidance, Navigation and Control Systems*, June 5-11, Carlsbad, Czech Republic.

Kahr, E., S. Skone and K. O’Keefe (2010) “Orbit Determination for the CanX-2 Nanosatellite Using Intermittent GPS Data,” *Proceedings of ION GNSS 2010*, September 21-24, Portland, Oregon.

Kramer, H. J. (2002) “Observation of the earth and its environment: survey of missions and sensors,” 4th Edition, Springer-Verlag, Berlin.

Kelso, T. S. (1998) “More Frequently Asked Questions,” *Satellite Times*, 4(3), <http://celestrak.com/columns/v04n05/#FAQ08>, last accessed March 15, 2011.

König, R., S. Zhu, C. Reigber, K.H. Neumayer, H. Meixner, R. Galas, G. Baustert & P. Schwintzer (2002) “CHAMP rapid orbit determination for GPS atmospheric limb sounding” *Advances in Space Research*, vol. 30, no. 2, p 289.

Kroes, R. (2006) *Precise Relative Positioning of Formation Flying Spacecraft using GPS*, Publications on Geodesy 61, Delft, The Netherlands.

Lachapelle, G. (2009) *Advanced GNSS Theory and Applications*, ENGO 625 Course Notes, Department of Geomatics Engineering, University of Calgary, Canada.

Langer, J. V., W. A. Feess, K. M. Harrington, M. R. Bacigalupi, R. G. Mach, P. A. M. Abusali, and M. A. Cardoza (1994) “RADCAL: Precision Orbit Determination with a Commercial Grade GPS Receiver,” in *Proceedings of the 1994 National Technical Meeting of The Institute of Navigation*, San Diego, CA, January, pp. 421-431.

Langley, R. B., O. Montenbruck, M. Markgraf, and D. Kim (2004) “Qualification of a Commercial Dual-Frequency GPS Receiver for the e-POP Platform onboard the Canadian CASSIOPE Spacecraft” in *Proceedings of NAVITEC 2004, the 2nd ESA Workshop on Satellite Navigation User Equipment Technologies*, ESTEC, Noordwijk, The Netherlands, pp. 397-405.

Leick, A. (2004) *GPS Satellite Surveying*, John Wiley & Sons, New Jersey.

Markgraf M. and O. Montenbruck (2004) *Total Ionizing Dose Testing of the NovAtel OEM4-G2L GPS Receiver*, DLR Document TN 04-04, version 1.0.

Montenbruck, O. (2010) Personal Communication.

Montenbruck, O. (2003) *Performance Assessment of the NovAtel OEM4-G2 Receiver for LEO Satellite Tracking*, DLR Document TN 03-05, version 1.1.

Montenbruck, O. (2000) “An Epoch State Filter for use with Analytical Orbit Models of Low Earth,” *Aerospace Science Technology*, 4, pp. 277–287.

Montenbruck, O. and E. Gill, (2000) *Satellite Orbits Models, Methods, and Applications*, Springer, Berlin.

Montenbruck, O. and R. Kroes (2003) “In-flight performance analysis of the CHAMP BlackJack GPS Receiver,” *GPS Solutions*, vol. 7, p 74.

Montenbruck, O., M. Garcia-Fernandez and J. Williams (2006) “Performance comparison of semicodeless GPS receivers for LEO satellites,” *GPS Solutions*, vol. 10, p 249.

Montenbruck, O., E. Gill, and J. M. Fraile-Ordonez (1996) “Orbit Determination of the MIR Space Station Using MOMSNAV GPS Measurements,” in *Proceedings of the 20th International Symposium on Space Technology and Science*, May 19-25, Gifu, Japan.

Montenbruck, O., M. Markgraf, M. Garcia-Fernandez and A. Helm (2007) “GPS for Microsatellites – Status and Perspectives,” in *6th IAA Symposium on Small Satellites for Earth Observation*, Berlin, April, 23-26.

NovAtel Inc. (2006) *OEM4-G2L Data Sheet*, <http://www.novatel.ca/Documents/Papers/oem4g2.pdf> , last accessed Feb12, 2011.

NovAtel Inc. (2005). *OEM4 Family of Receivers, User Manual - Volume 2 Command and Log Reference*, Publication No. OM-20000047, Canada.

NovAtel Inc. (2003). *OEM4 Family of Receivers, User Manual - Volume 1 Installation and Operation*, Publication No. OM-20000046, Canada.

Orr, N. (2009) Personal Communication, UTIAS SFL.

Orr, N. G., J. K. Eyer, B. P. Larouche, and R. Zee (2007) “Precision Formation Flight: The CanX-4 and CanX-5 Dual Nanosatellite Mission,” in *Proceedings of the 21st Annual AIAA/USU Conference on Small Satellites*, August 13-16, Logan, UT.

Page, S., M. Harlacher and L. Haas (2003) “Test Results From The Communications And Navigation Demonstration On Shuttle (CANDOS) Experiment,” in *Proceedings of the International Symposium on GPS/GNSS*, November 15-18, Tokyo, Japan.

Pail, R. (2005) *Satellitengeodäsie*, Satellitengeodäsie Course Notes, Institut für Navigation und Satellitengeodäsie, Technische Universität Graz, Graz, Austria.

Petovello, M. (2009) *Estimation for Navigation*, ENGO 699.18 Course Notes, Geomatics Engineering, University of Calgary.

Rankin, D., D. D. Kekez, R. E. Zee, F. M. Pranajaya, D. G. Foisy, and A. M. Beattie (2005) “The CanX-2 Nanosatellite: Expanding the Science Abilities of Nanosatellites,” *Acta Astronautica*, 57, pp.167-174.

Rocken, C., R. Anthes, M. Exner, D. Hunt, S. Sokolovskiy, R. Ware, M. Gorbunov, W. Schreiner, D. Feng, B. Herman, Y. -H. Kuo, and X. Zou (1997) “Analysis and Validation of GPS/MET Data in the Neutral Atmosphere,” *Journal of Geophysical Research*, vol 102, no D25, December, pp 29849-29866.

Sarda, K. (2010) Personal Communication, UTIAS SFL.

Sarda K., S. Eagleson, E. Caillibot, C. Grant, D. Kekez, F. Pranajaya, and R. E. Zee (2006) “Canadian Advanced Nanospace Experiment 2: Scientific and Technological Innovation on a Three-Kilogram Satellite,” *Acta Astronautica*, vol. 59, pp. 236 – 245.

Sarda, K., C. Grant, S. Eagleson and D. Kekez A. Shah and R. Zee (2009) “Canadian Advanced Nanospace Experiment 2 Orbit Operations: One Year of Pushing the Nanosatellite Performance Envelope” *Proceedings of the 23rd Annual AIAA/USU Conference on Small Satellites*, SSC09-IV-6.

Sneeuw, N. (2006) *Dynamic Satellite Geodesy*, Analytische Bahnrechnung Künstlicher Satelliten Course Notes, Institute of Geodesy, Universität Stuttgart, Germany.

Spangelo, S., A. Klesh, and J. Cutler (2010) “Position and Time System for the RAX Small Satellite Mission,” in *Proceedings of AIAA Guidance, Navigation, and Control Conference*, 2 - 5 August, Toronto, Ontario, Canada.

University of Toronto Institute for Aerospace Studies Space Flight Laboratory
(2011) The AISSat-1 Mission, <http://www.utias-sfl.net/nanosatellites/AISSat-1/> last accessed March 15, 2011.

Unwin, M. J. and M. Oldfield (2000) "The Design and Operation of a COTS Space GPS Receiver," *Advances in the Astronautical Sciences, Guidance and Control*, p 465.

Unwin, M. and M. Sweeting (1995) "A Practical Demonstration of Low Cost Autonomous Orbit Determination Using GPS" in *Proceedings of ION GPS – 95: 8th International Technical Meeting of the Satellite Division of the Institute of Navigation*, p 579.

Urbanek, J (2010) Personal Communication, UTIAS SFL.

Valdes, S. (2010) Personal Communication, AeroAntenna.

Vallado, D. A., and P. Crawford (2008) "SGP4 Orbit Determination," in *Proceedings of AIAA/AAS Astrodynamics Specialist Conference and Exhibit*, August 18 - 21, Honolulu, Hawaii.

Vallado, D., P. Crawford, R. Hujsak and T. Kelso (2006) "Revisiting Spacetrack Report #3," in *Proceedings of the AIAA/AAS Astrodynamics Specialist Conference*, August 21-24, Keystone, CO.

Vig, J. R. (2008) Quartz Crystal Resonators and Oscillators for Frequency Control and Timing Applications – A Tutorial, Rev 8.5.3.9, http://www.ieee-uffc.org/frequency_control/teaching.asp, last accessed May 3, 2011.

Zhou, Y. F. (2003) *A Study for Orbit Representation and Simplified Orbit Determination Methods*, MSc Thesis, Department, Queensland University of Technology, Brisbane, Australia.

APPENDIX A: RECEIVER CONFIGURATION ON BOARD CANX-2

Option	Setting
#ADJUST1PPSA	OFF,ONCE,0
#ANTENNAPOWERA	ON
#CLOCKADJUSTA	ENABLE
#CLOCKOFFSETA	0
#COMA	COM1,115200,N,8,1,N,OFF,ON
#COMA	COM2,9600,N,8,1,N,OFF,ON
#COMA	COM3,9600,N,8,1,N,OFF,ON
#COMA	USB1,9600,N,8,1,N,OFF,ON
#COMA	USB2,9600,N,8,1,N,OFF,ON
#COMA	USB3,9600,N,8,1,N,OFF,ON
#COMCONTROLA	COM1,RTS,DEFAULT
#COMCONTROLA	COM2,RTS,DEFAULT
#COMCONTROLA	COM3,RTS,DEFAULT
#CSMOOTHA	2,5
#DATUMA	WGS84
#DGPSEPHEMDELAYA	120
#DGPSTIMEOUTA	300
#DGPSTXIDA	AUTO,"ANY"
#DYNAMICSA	AIR
#ECUTOFFA	-45
#EXTERNALCLOCKA	DISABLE,5MHZ,1.000000000e-21,1.000000000e-20,1.000000000e-20
#FIXA	NONE,-10000.00000000000,-10000.00000000000,-10000.0000
#FREQUENCYOUTA	DISABLE,0,0
#INTERFACEMODEA	COM1,NOVATEL,NOVATEL,ON
#INTERFACEMODEA	COM2,NOVATEL,NOVATEL,ON
#INTERFACEMODEA	COM3,NOVATEL,NOVATEL,ON
#INTERFACEMODEA	XCOM1,NOVATEL,NOVATEL,ON
#INTERFACEMODEA	XCOM2,NOVATEL,NOVATEL,ON
#INTERFACEMODEA	USB1,NOVATEL,NOVATEL,ON
#INTERFACEMODEA	USB2,NOVATEL,NOVATEL,ON
#INTERFACEMODEA	USB3,NOVATEL,NOVATEL,ON
#LOGA	COM1,RXSTATUSEVENTA,ONNEW,0.000000,0.000000,HOLD
#LOGA	COM2,RXSTATUSEVENTA,ONNEW,0.000000,0.000000,HOLD
#LOGA	COM3,RXSTATUSEVENTA,ONNEW,0.000000,0.000000,HOLD
#LOGA	USB1,RXSTATUSEVENTA,ONNEW,0.000000,0.000000,HOLD
#LOGA	USB2,RXSTATUSEVENTA,ONNEW,0.000000,0.000000,HOLD
#LOGA	USB3,RXSTATUSEVENTA,ONNEW,0.000000,0.000000,HOLD
#MAGVARA	CORRECTION,0.000000000,0.000000000
#MARKCONTROLA	MARK1,ENABLE,NEGATIVE,0,0
#MARKCONTROLA	MARK2,ENABLE,NEGATIVE,0,0
#PASSTOPASSMODEA	DISABLE,OFF,OFF,DEFAULT,1.000000000
#POSAVEA	OFF,0.00,0.0,0.0

Option	Setting
#POSTIMEOUTA	600
#PPSCONTROLA	ENABLE,NEGATIVE,1.000000000,0
#PSRDIFFSOURCEA	AUTO,"ANY"
#RTKCOMMANDA	USE_DEFAULTS
#RTKSOLUTIONA	AUTO
#RTKBASELINEA	UNKNOWN,0.0000000000000000,0.0000000000000000,0.0000000000000000,0.000000000
#RTKDYNAMICSA	DYNAMIC
#RTKELEVMASKA	AUTO,0.000000000
#RTKSVENTRIESA	12
#RTKIFTHRESHA	7000
#RTKFIXRATEA	1.25
#RTKSOURCEA	AUTO,"ANY"
#SETNAVA	90.000000000,0.000000000,90.000000000,0.000000000,0.000000000,"from","to"
#STATUSCONFIGA	PRIORITY,STATUS,0
#STATUSCONFIGA	PRIORITY,AUX1,8
#STATUSCONFIGA	PRIORITY,AUX2,0
#STATUSCONFIGA	SET,STATUS,0
#STATUSCONFIGA	SET,AUX1,0
#STATUSCONFIGA	SET,AUX2,0
#STATUSCONFIGA	CLEAR,STATUS,0
#STATUSCONFIGA	CLEAR,AUX1,0
#STATUSCONFIGA	CLEAR,AUX2,0
#USERDATUMA	6378137.000,298.25722356280,0.0000,0.0000,0.0000,0.0000,0.0000,0.0000,0.000000000
#UNDULATIONA	TABLE,0.000000000
#HEIGHTMODELA	DISABLE,0.000000000,1.000000000
#WAASCORRECTIONA	DISABLE,0,NONE
#SBASCONTROLA	DISABLE,NONE,0,NONE
#WAASECUTOFFA	-5
#LOGA	COM1,BESTXYZB,ONTIME,30.000000,0.000000,NOHOLD
#LOGA	COM1,RANGECMPB,ONTIME,30.000000,0.000000,NOHOLD
#LOGA	COM1,RXCONFIGB,ONTIME,5.000000,0.000000,NOHOLD
#LOGA	COM1,VERSIONB,ONTIME,5.000000,0.000000,NOHOLD

These receiver configurations were logged in December 2010 following the long arc data collection. The logging shown in the above table for the #LOGA option reflects settings used for specific experiments but is changed often via scripts based on the needs of particular data collection.

APPENDIX B: CANX-2 DATA COLLECTIONS

Legend

	Sufficient data for radio occultation work
	Position fix but insufficient data for radio occultation work
	Long arc data collection
	Receiver crash (due to script syntax problems)
	No position fix, receiver configuration, other data collection

<i>Date</i>	<i>Week Day</i>	<i>GPS Week</i>	<i>Logging</i>	<i>Antenna FOV</i>
21-Nov-08	Friday	1506	bestpos	zenith
28-Nov-08	Friday	1507	rangecmpb	forward
16-Dec-08	Tuesday	1510	ascii	forward
18-Dec-08	Thursday	1510	rangecmpb	forward
19-Dec-08	Friday	1510	rangecmpb	no control
<i>*Changed the predictor output format, and corrected time for 10s pause and missing UTC offset</i>				
16-Jan-09	Friday	1514	rangecmpb, 50Hz	forward
21-Jan-09	Wednesday	1515	rangecmpb, 50Hz	forward
<i>*At this point we changed logging to 1Hz, took out the assigned dopplers, and increased acquisition time to 600s</i>				
11-Feb-09	Wednesday	1518	rangecmpb, 1Hz	forward
12-Feb-09	Thursday	1518	rangecmpb, 1Hz	no control
<i>*At this point we add antennapower on command from 494 Friday until the 495 Wednesday</i>				
13-Feb-09	Friday	1518	rangecmpb, 1Hz	forward
14-Feb-09	Saturday	1518	rangecmpb, 1Hz	forward
15-Feb-09	Sunday	1519	rangecmpb, 1Hz	forward
16-Feb-09	Monday	1519	rangecmpb, 1Hz	forward
16-Feb-09	Monday	1519	rangecmpb, 1Hz	forward
17-Feb-09	Tuesday	1519	rangecmpb, 1Hz	forward
17-Feb-09	Tuesday	1519	rangecmpb, 1Hz	forward
18-Feb-09	Wednesday	1519	rangecmpb, 1Hz	forward
18-Feb-09	Wednesday	1519	rangecmpb, 1Hz	forward
<i>*Next (thurs-sat week 495) we add a doppler search window of 10000 instead of 1500 and put the dopplers back in</i>				
19-Feb-09	Thursday	1519	rangecmpb, 1Hz	forward
19-Feb-09	Thursday	1519	rangecmpb, 1Hz	forward

*Still not working, week 496 we try all channels on auto(sun and tues) or add doppler offsets of 5522 to all assigned dopplers (mon and wed) and use logging at 1s for acquisition and 0.02s for event				
nothing was run, we traded our week for April				
*April 6 was run with only a time and position assigned, no channel assignments, and pointing towards zenith for a "do nothing" case				
6-Apr-09	Monday	1526	rangecmpb, 1Hz	zenith
*April 7 & 11 were run with doppler assignments based on a 5815Hz predicted shift in doppler, zenith pointing, elevation mask set to -90				
7-Apr-09	Tuesday	1526	rangecmpb, 1Hz	zenith
11-Apr-09	Saturday	1526	rangecmpb, 1Hz & 50Hz	zenith
11-Apr-09	Saturday	1526	rangecmpb, 1Hz	zenith
*Satellite turned to rear pointing for the first time				
15-Apr-09	Wednesday	1527	rangecmpb, 1Hz	rear
*Satellite Zenith pointing				
16-Apr-09	Thursday	1527	rangecmpb, 1Hz & 50Hz	zenith
16-Apr-09	Thursday	1527	rangecmpb, 1Hz & 50Hz	zenith
*Satellite anti-velocity pointing, scripts with -10 degree elevation mask				
18-Apr-09	Saturday	1527	rangecmpb, 1Hz & 50Hz	rear
*May have been zenith not negative velocity				
23-Apr-09	Thursday	1528	rangecmpb, 1Hz & 50Hz	zenith
*Anti-velocity, -10 elev mask, still 5815 doppler shift				
24-Apr-09	Friday	1528	rangecmpb, 1Hz & 50Hz	rear
24-Apr-09	Friday	1528	rangecmpb, 1Hz & 50Hz	rear
*Changed to 10s logging for startup and smaller atmosphere				
28-Apr-09	Tuesday	1529	rangecmpb, 0.1Hz & 50Hz	rear
*20Hz during occultation, with bending, back to large doppler window, set some channels to auto				
1-May-09	Friday	1529	rangecmpb 0.1Hz	rear
3-May-09	Sunday	1530	rangecmpb 0.1Hz & 20Hz	rear
3-May-09	Sunday	1530	rangecmpb 0.1Hz & 20Hz	rear
4-May-09	Monday	1530	rangecmpb 0.1Hz & 20Hz	rear
*Problem occured and 0 data was logged, all these files are copies of data logged in May 4th trial				
5-May-09	Tuesday	1530		rear
*Requested all future experiments be run with antenna pointing 45 degrees between zenith and rear				
5-May-09	Tuesday	1530		rear 45 degrees
6-May-09	Wednesday	1530		rear 45 degrees
* Engineering test script is run and results are logged				
6-May-09	Wednesday	1530	bestxyza 0.5Hz	unknown
*Toronto rebooted entire satellite and reloaded their software				
7-May-09	Thursday	1530	rangecmpb 0.1Hz & 20Hz	no control
8-May-09	Friday	1530		rear 45 degrees
*After a week of ground station outage problem seems to have fixed itself				
21-May-09	Thursday	1532	rangecmpb 0.1Hz & 20Hz	no control
22-May-09	Friday	1532	rangecmpb 0.1Hz & 20Hz	rear 45 degrees
*Sent new scripts with the startup time set to 5 minutes and the elevation mask set to 25				

26-May-09	Tuesday	1533		rear 45 degrees
27-May-09	Wednesday	1533	rxconfig ontime 1	no control
27-May-09	Wednesday	1533	bestxyza ontime2	zenith
28-May-09	Thursday	1533		rear 45 degrees
29-May-09	Friday	1533	rangecmpb ontime 10	no control
1-Jun-09	Monday	1534	rangecmpb 0.1Hz & 20Hz	rear 45 degrees
1-Jun-09	Monday	1534	rangecmpb 0.1Hz & 20Hz	rear 45 degrees
2-Jun-09	Tuesday	1534	rangecmpb 20Hz	rear 45 degrees
2-Jun-09	Tuesday	1534	rangecmpb 0.1Hz	no control
2-Jun-09	Tuesday	1534	rangecmpb 20Hz	rear 45 degrees
3-Jun-09	Wednesday	1534	rangecmpb 20Hz	rear 45 degrees
3-Jun-09	Wednesday	1534	rangecmpb 20Hz	rear 45 degrees
4-Jun-09	Thursday	1534	rangecmpb 20Hz	rear 45 degrees
*Changed doppler offset to 5840 for week 511 based on most recent successful trial				
8-Jun-09	Monday	1535	rangecmpb 0.1Hz & 20Hz	rear 45 degrees
11-Jun-09	Thursday	1535	rangecmpb 0.1Hz & 20Hz	rear 45 degrees
12-Jun-09	Thursday	1535	rangecmpb 20Hz	rear 45 degrees
12-Jun-09	Friday	1535	rangecmpb 0.1Hz & 20Hz	rear 45 degrees
*Predictor modified to have correct off time with an elevation mask that does not touch the earth's surface				
14-Jun-09	Sunday	1536	rangecmpb 0.1Hz & 20Hz	rear 45 degrees
15-Jun-09	Monday	1536	rangecmpb 20Hz	rear 45 degrees
*Pauses are added between each pair of lines in the script in Toronto				
16-Jun-09	Tuesday	1536	rangecmpb 20Hz	rear 45 degrees
16-Jun-09	Tuesday	1536	rangecmpb 0.1Hz & 20Hz	rear 45 degrees
*Extra logs are added by Mike to find out which commands the receiver is seeing				
23-Jun-09	Tuesday	1537	rangecmbb 0.1Hz	rear 45 degrees
24-Jun-09	Wednesday	1537	rangecmbb 0.1Hz	rear 45 degrees
*Patch applied which should fix anomaly state bug, also incorrect number of lines appears to have been fixed				
25-Jun-09	Thursday	1537	rangecmbb 0.1Hz	rear 45 degrees
27-Jun-09	Saturday	1537	rangecmpb 0.1Hz & 20Hz	rear 45 degrees
*Rxstatus and trackstat logged to binary instead... Can't decode trackstat				
30-Jun-09	Tuesday	1538	rangecmpb 0.1Hz & 20Hz	rear 45 degrees
3-Jul-09	Friday	1538	rangecmpb 0.1Hz & 20Hz	rear 45 degrees
7-Jul-09	Tuesday	1539	rangecmpb 20Hz	rear 45 degrees
*Week number changed to 1023+week, pauses between all commands, doppler offset changed to 6500				
7-Dec-09	Monday	1561	rxconfig	unknown
8-Dec-09	Tuesday	1561		rear 45 degrees
9-Dec-09	Wednesday	1561	rangecmpb 0.1 and 20 Hz	rear 45 degrees
10-Dec-09	Thursday	1561	rangecmpb 0.1 and 20 Hz	rear 45 degrees
11-Dec-09	Friday	1561	rangecmpb 0.1 and 20 Hz	rear 45 degrees
11-Dec-09	Friday	1561	rangecmpb 0.1 and 20 Hz	rear 45 degrees

15-Dec-09	Tuesday	1562	rangecmpb 0.1 and 20 Hz	rear 45 degrees
15-Dec-09	Tuesday	1562	rangecmpb 0.1 and 20 Hz	rear 45 degrees
16-Dec-09	Wednesday	1562	rangecmpb 0.1 and 20 Hz	rear 45 degrees
17-Dec-09	Thursday	1562	rangecmpb 0.1 and 20 Hz	rear 45 degrees
17-Dec-09	Thursday	1562	rangecmpb 0.1	rear 45 degrees
17-Dec-09	Thursday	1562	rangecmpb 0.1 and 20 Hz	rear 45 degrees
18-Dec-09	Friday	1562	rangecmpb 0.1 and 20 Hz	rear 45 degrees
* Leave doppler offset at 6500 (probably should be 6400 but close enough) and change auto channels to idle channels to try and reduce redundant data				
6-Jan-10	Wednesday	1565	rangecmpb 0.1 and 20 Hz	rear 45 degrees
7-Jan-10	Thursday	1565	rangecmpb 0.1 and 20 Hz	no control
8-Jan-10	Friday	1565	rangecmpb 0.1 and 20 Hz	no control
9-Jan-10	Saturday	1565	rangecmpb 0.1 and 20 Hz	no control
* Generated scripts using 'auto' not 'idle' for Sunday-Tuesday due to undiagnosed lack of attitude control, changed to 'idle' for Wednesday's scripts				
11-Jan-10	Monday	1566	rangecmpb 0.1 and 20 Hz	rear 45 degrees
12-Jan-10	Tuesday	1566	rangecmpb 0.1 and 20 Hz	rear 45 degrees
13-Jan-10	Wednesday	1566	rangecmpb 0.1 and 20 Hz	rear 45 degrees
14-Jan-10	Thursday	1566	rangecmpb 0.1 and 20 Hz	rear 45 degrees
18-Jan-10	Monday	1567	rangecmpb 0.1 and 20 Hz	rear 45 degrees
*Some cold start data from U of T				
20-Jan-10	Wednesday	1567	bestxyza ontime 2	zenith?
20-Jan-10	Wednesday	1567	bestxyza ontime 2	zenith?
*Back to occultation experiments				
26-Mar-10	Friday	1576	rangecmpb 0.1 and 20 Hz	rear 45 degrees
26-Mar-10	Friday	1576	rangecmpb 0.1 and 20 Hz	rear 45 degrees
* Beginning March 29th 2010 week, all occultation scripts generated to run with the antenna pointing 60 degrees off zenith instead of 45 degrees				
29-Mar-10	Monday	1577	rangecmpb 0.1 and 20 Hz	rear 60 degrees
30-Mar-10	Tuesday	1577	rangecmpb 0.1 and 20 Hz	rear 60 degrees
*Doppler offset increased to 6550 Hz in April 5 week 554 scripts. Week 554 scripts are set up to do outage experiments rather than RO trials				
8-Apr-10	Thursday	1578	rangecmpb 0.5 Hz and satvisb 0.1 Hz	rear 60 degrees
10-Apr-10	Saturday	1578	rangecmpb 0.5 Hz and satvisb 0.1 Hz	rear 60 degrees
*Back to occultation experiments				
12-Apr-10	Monday	1579	rangecmpb 0.1 and 20 Hz	rear 60 degrees
15-Apr-10	Thursday	1579	rangecmpb 0.1 and 20 Hz	rear 60 degrees
20-Apr-10	Tuesday	1580	rangecmpb 0.1 and 20 Hz	rear 60 degrees
22-Apr-10	Thursday	1580	rangecmpb 0.1 and 20 Hz	rear 60 degrees
4-May-10	Tuesday	1582	rangecmpb 0.1 and 20 Hz	rear 60 degrees
4-May-10	Tuesday	1582	rangecmpb 0.1 and 20 Hz	rear 60 degrees
5-May-10	Wednesday	1582	rangecmpb 0.1 and 20 Hz	rear 60 degrees
6-May-10	Thursday	1582	rangecmpb 0.1 and 20 Hz	rear 60 degrees
7-May-10	Friday	1582	rangecmpb 0.1 and 20 Hz	rear 60 degrees
7-May-10	Friday	1582	rangecmpb 0.1 and 20 Hz	rear 60 degrees
10-May-10	Monday	1583	rangecmpb 0.1 and 20 Hz	rear 60 degrees

11-May-10	Tuesday	1583	rangecmpb 0.1 and 20 Hz	rear 60 degrees
12-May-10	Wednesday	1583	rangecmpb 0.1 and 20 Hz	rear 60 degrees
13-May-10	Thursday	1583	rangecmpb 0.1 and 20 Hz	rear 60 degrees
13-May-10	Thursday	1583	rangecmpb 0.1 and 20 Hz	rear 60 degrees
14-May-10	Friday	1583	rangecmpb 0.1 and 20 Hz	rear 60 degrees
*One more cold start data set from U of T				
		1584	trackstatb ontime 10	zenith?
*Changed dop offset to 6600, logging rate to 1Hz then 10 Hz, acquisition time longer by 2 minutes, anywhere globally, spare channels auto, logging bestxyz as well				
20-Jul-10	Tuesday	1593	rangecmpb 1 and 10 Hz, bestxyzb 0.5 Hz	rear 60 degrees
21-Jul-10	Wednesday	1593	rangecmpb 1 and 10 Hz, bestxyzb 0.5 Hz	rear 60 degrees
*Changed dop offset to 6800, 50 minute data sets to cover particular ascending node longitudes, may not start exactly in sunlight				
30-Jul-10	Friday	1594	rangecmpb 0.5 Hz bestxyz 0.2 Hz	zenith
*Approximately 50 minute data sets to cover particular ascending node longitudes, uses 5 minute sunlight buffer for startup at correct attitude				
5-Aug-10	Thursday	1595	rangecmpb 0.5 Hz bestxyz 0.2 Hz	zenith
6-Aug-10	Friday	1595	rangecmpb 0.5 Hz bestxyz 0.2 Hz	zenith
*Occultation scripts, anywhere globally, generated with an older predictor version?				
9-Aug-10	Monday	1596	rangecmpb 1 and 10 Hz	rear 60 degrees
10-Aug-10	Tuesday	1596	rangecmpb 1 and 10 Hz	rear 60 degrees
11-Aug-10	Wednesday	1596	rangecmpb 1 and 10 Hz	rear 60 degrees
13-Aug-10	Friday	1596		rear 60 degrees
*Approximately 50 minute data sets to cover particular ascending node longitudes, uses 5 minute sunlight buffer for startup at correct attitude				
16-Aug-10	Monday	1597	rangecmpb ontime 2 bestxyz ontime 5	zenith
18-Aug-10	Wednesday	1597	rangecmpb ontime 2 bestxyz ontime 5	zenith
19-Aug-10	Thursday	1597	rangecmpb ontime 2 bestxyz ontime 5	zenith
19-Aug-10	Thursday	1597	rangecmpb ontime 2 bestxyz ontime 5	zenith
21-Aug-10	Saturday	1597	rangecmpb ontime 2 bestxyz ontime 5	zenith
*Attempted occultation scripts with various doppler offsets to test required accuracy, all run at 7300 and last two in same file				
28-Sep-10	Tuesday	1603	rangecmpb 1 and 10 Hz	rear 60 degrees
29-Sep-10	Wednesday	1603	rangecmpb 1 and 10 Hz	rear 60 degrees
29-Sep-10	Wednesday	1603	rangecmpb 1 and 10 Hz	rear 60 degrees
*Attemp to collect the most GPS data possible in order to have a good data set for the visit to Munich's POD work				
week of Nov 1 nothing collected due to drop to bootloader status				
*Sent scripts to work around sunlight and not overlap with passes, as well as unassigning channels as the experiment progresses.				

9-Nov-10	Tuesday	1609	rangecmpb and bestxyz 30 s	zenith
9-Nov-10	Tuesday	1609	rangecmpb and bestxyz 30 s	zenith
*Tuesday dropped to bootloader, and I redesigned the experiment scripts to use less lines by configuring the receiver to log 30 second bestxyz and rangecmp by default, taking out the first 9600 baud rate commands, taking out approxpos and approxtime, taking out assinging individual channels to auto, and leaving only assign and unassign commands.				
*Thursday redesigned scripts to work around pass times and sunlight if the orbit has a pass, and to start 5 minutes into sunlight and end 85 minutes later if there is no pass				
13-Nov-10	Saturday	1609	rangecmpb and bestxyz 30 s	zenith
13-Nov-10	Saturday	1609	rangecmpb and bestxyz 30 s	zenith
15-Nov-10	Monday	1610	rangecmpb and bestxyz 30 s	zenith
16-Nov-10	Tuesday	1610	rangecmpb and bestxyz 30 s	zenith
16-Nov-10	Tuesday	1610	rangecmpb and bestxyz 30 s	zenith
17-Nov-10	Wednesday	1610	rangecmpb and bestxyz 30 s	zenith
17-Nov-10	Wednesday	1610	rangecmpb and bestxyz 30 s	zenith
18-Nov-10	Thursday	1610	rangecmpb and bestxyz 30 s	zenith
18-Nov-10	Thursday	1610	rangecmpb and bestxyz 30 s	zenith
19-Nov-10	Friday	1610	rangecmpb and bestxyz 30 s	zenith
19-Nov-10	Friday	1610	rangecmpb and bestxyz 30 s	zenith
19-Nov-10	Friday	1610	rangecmpb and bestxyz 30 s	zenith
19-Nov-10	Friday	1610	rangecmpb and bestxyz 30 s	zenith
25-Nov-10	Thursday	1611	rangecmpb and bestxyz 30 s	zenith
*Thursday and Friday added an offset to the TLE time of +17.5 seconds in order to simulate a 1 degree error in position for CanX-2 and test the acquisition properties				
25-Nov-10	Thursday	1611	rangecmpb and bestxyz 30s	zenith
26-Nov-10	Friday	1611	rangecmpb and bestxyz 30s	zenith
26-Nov-10	Friday	1611	rangecmpb and bestxyz 30s	zenith
27-Nov-10	Saturday	1611	rangecmpb and bestxyz 30s	zenith
Week 588 added an offset to the TLE time of +20 seconds				
30-Nov-10	Tuesday	1612	rangecmpb and bestxyz 30s	zenith
1-Dec-10	Wednesday	1612	rangecmpb and bestxyz 30s	zenith
1-Dec-10	Wednesday	1612	rangecmpb and bestxyz 30s	zenith
Increased the offset to +35 seconds				
2-Dec-10	Thursday	1612	rangecmpb and bestxyz 30s	zenith
3-Dec-10	Friday	1612	rangecmpb and bestxyz 30s	zenith
3-Dec-10	Friday	1612	rangecmpb and bestxyz 30s	zenith
4-Dec-10	Saturday	1612	rangecmpb and bestxyz 30s	zenith
*Undid the default logging of bestxyz and rangecmp data				
7-Dec-10	Tuesday	1613	rxconfig and version ontime 5	unknown
*Redid the default logging of bestxyzb and rangecmpb as well as satxyzb and psrdopb				
nothing logged from the configuration script, log commands and saveconfig were added to the first data collection script itself				
*Subtracted an offset from the TLE time of 17.5 seconds to simulate an advance in position				
29-Mar-11	Tuesday	1629	rangecmpb, bestxyz, satxyz, psrdop 30s	zenith
*Subtracted an offset from the TLE time of 35 seconds to simulate an advance in position				
30-Mar-11	Wednesday	1629	rangecmpb, bestxyz, satxyz, psrdop 30s	zenith

*Subtracted an offset from the TLE time of 17.5 seconds to simulate an advance in position				
8-Apr-11	Friday	1630	rangecmpb, bestxyz, satxyz, psrdop 30s	zenith
8-Apr-11	Friday	1630	rangecmpb, bestxyz, satxyz, psrdop 30s	zenith
11-Apr-11	Monday	1631	rangecmpb, bestxyz, satxyz, psrdop 30s	zenith
11-Apr-11	Monday	1631	rangecmpb, bestxyz, satxyz, psrdop 30s	zenith
12-Apr-11	Tuesday	1631	rangecmpb, bestxyz, satxyz, psrdop 30s	zenith
12-Apr-11	Tuesday	1631	rangecmpb, bestxyz, satxyz, psrdop 30s	zenith
13-Apr-11	Wednesday	1631	rangecmpb, bestxyz, satxyz, psrdop 30s	zenith
14-Apr-11	Thursday	1631	rangecmpb, bestxyz, satxyz, psrdop 30s	zenith
15-Apr-11	Friday	1631	rangecmpb, bestxyz, satxyz, psrdop 30s	zenith
*Long arcs run sandwiching an occultation. Long arcs were generated with a TLE from last week's data, occultation with a normal NORAD TLE				
19-Apr-11	Tuesday	1632	bestxyz, rangecmpb 4s	zenith
20-Apr-11	Wednesday	1632	bestxyz, rangecmpb 4s	zenith
20-Apr-11	Wednesday	1632	rangecmpb 1 and 10 Hz	rear
*Long arcs and occultation generated with normal NORAD TLE				
26-Apr-11	Tuesday	1633	rangecmpb and bestxyz 30s	zenith
27-Apr-11	Wednesday	1633	rangecmpb 1 and 10 Hz	rear
29-Apr-11	Friday	1633	rangecmpb and bestxyz 30s	zenith
*Long arcs generated with a NORAD -35seconds TLE, occultation with a normal TLE				
3-May-11	Tuesday	1634	rangecmpb and bestxyz 30s	zenith
4-May-11	Wednesday	1634	rangecmpb and bestxyz 30s	zenith
4-May-11	Wednesday	1634	rangecmpb 1 and 10 Hz	rear
5-May-11	Thursday	1634	rangecmpb and bestxyz 30s	zenith

APPENDIX C: PRECISE ORBIT DETERMINATION

A visit to the German Space Centre (DLR) provided the opportunity of processing all the CanX-2 GPS data through their suite of precise orbit determination software. Precise orbits were formed from all the data collected between launch and the end of the November/December 2010 collection campaign, including data from the radio occultation experiments and the 85 minute data arcs collected with the GPS antenna pointing to zenith.

The first steps were conversion of the raw GPS data (pseudorange, phase ranges and Dopplers were logged using NovAtel's rangecmpb log) into rinex format for use with the DLR software. The data was combined into a single circular file then parsed into daily rinex files, which fixed irregularities such as single telemetry files containing data from multiple GPS experiments and also broke the data into reasonable length data arcs for processing.

Next, the data was run through a program for single point processing using the pseudorange and Doppler data, and at the same time underwent blunder detection. The output was written to an sp3 file with irregularly spaced position and velocity data points corresponding to the GPS epochs.

The sp3 file then served as input to initial orbit determination software. This step made use of the processed GPS positions along with a dynamics model to get the best fit trajectory through the data.

The initial trajectory was finally used as input to the reduced dynamic orbit determination (RDOD) software along with the raw GPS data. The initial trajectory was used in order to carry out a more robust outlier detection of the raw GPS data. The dual frequency carrier phase data, along with a dynamics model, were then used to form the final precise trajectory. A second processing option was also possible, in which an L1 single

frequency combination was formed from the pseudoranges and phase data, which experience opposite effects due to the ionosphere. In the single frequency processing option the noisier L2 data was not used.

Due to the lower signal to noise ratio, the CanX-2 data does not provide for long arcs of continuous carrier phase tracking, particularly on L2. The RDOD program carries out carrier phase ambiguity resolution for continuous arcs, therefore the abundance of cycle slips had an impact on the achievable accuracy of the orbital solution.

Assessing the accuracy of any CanX-2 positioning solution is difficult, due to the lack of a second method of positioning other than the GPS receiver. The GPS data was however processed using both the dual and single frequency techniques, as well as processing orbital arcs using different combinations of input data, yielding somewhat independent solutions. Figure C.1, Figure C.2, and Figure C.3 below show representative differences in solutions for three epochs of data collection. The December 2009 arcs were formed from radio occultation data collected with the antenna pointing 45 degrees off zenith, the spring 2010 arcs were formed from radio occultation data collected with the antenna pointing 60 degrees off zenith, and the late 2010 arcs were formed from the 85 minute zenith pointing data collections.

In the figures, the zero line represents the arc created using one day of data and the dual frequency processing technique, which was used as the reference. As such, the zero line is not necessarily the best solution among the six.

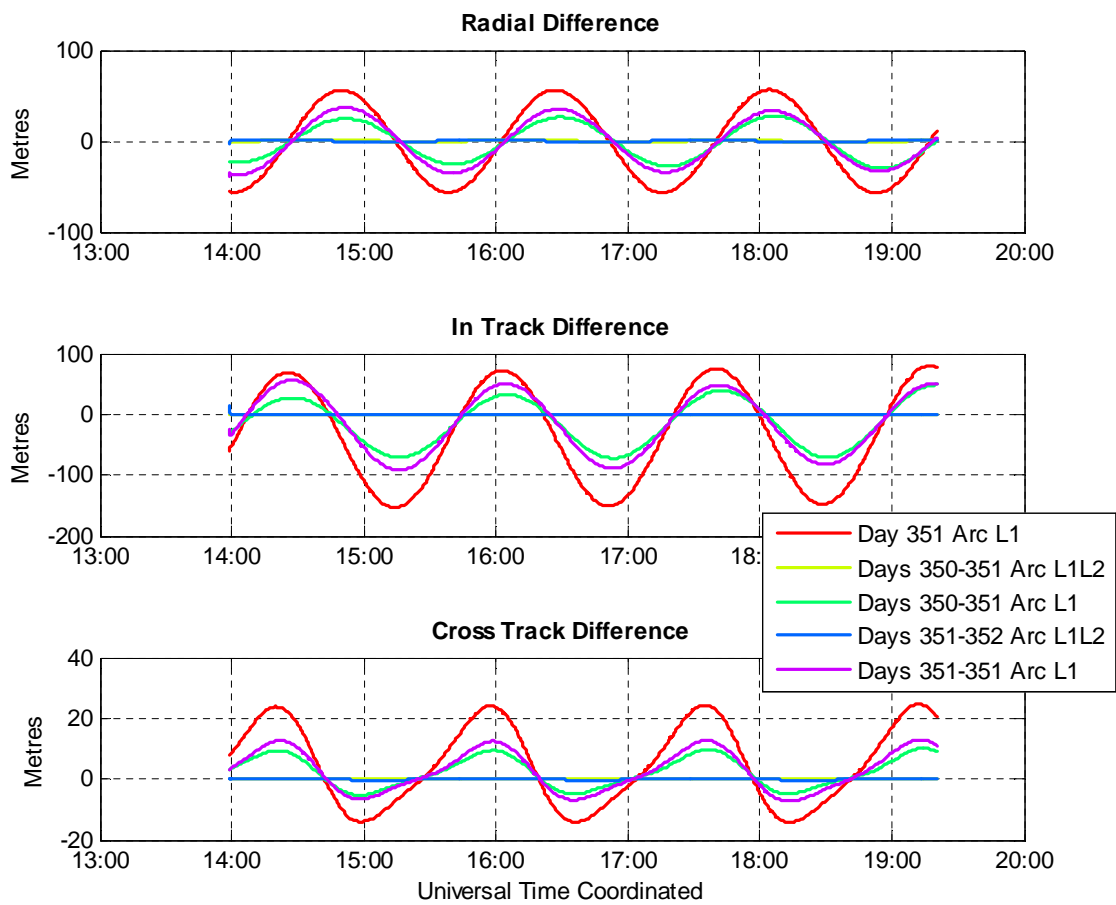


Figure C.1: Comparison with the November 17, 2009 (day 351) arc, created using L1 and L2 data

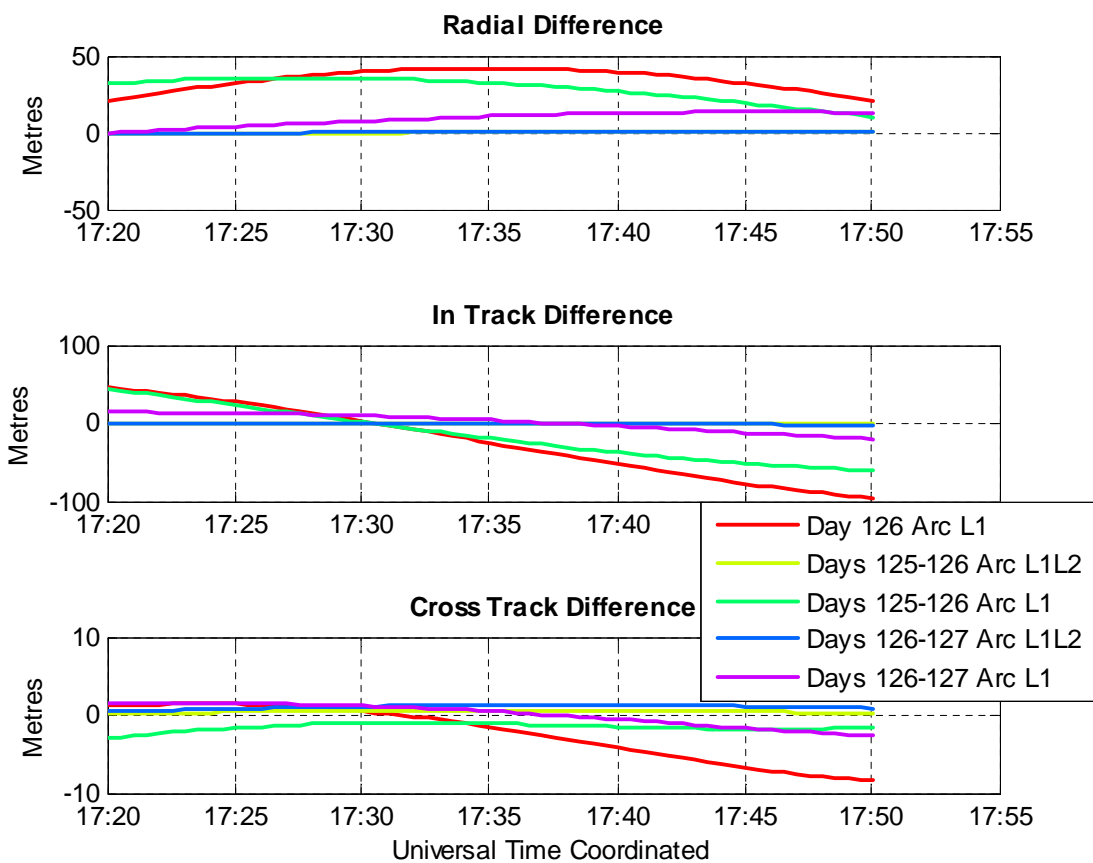


Figure C.2: Comparison with the May 6, 2010 (day 126) arc, created using L1 and L2 data

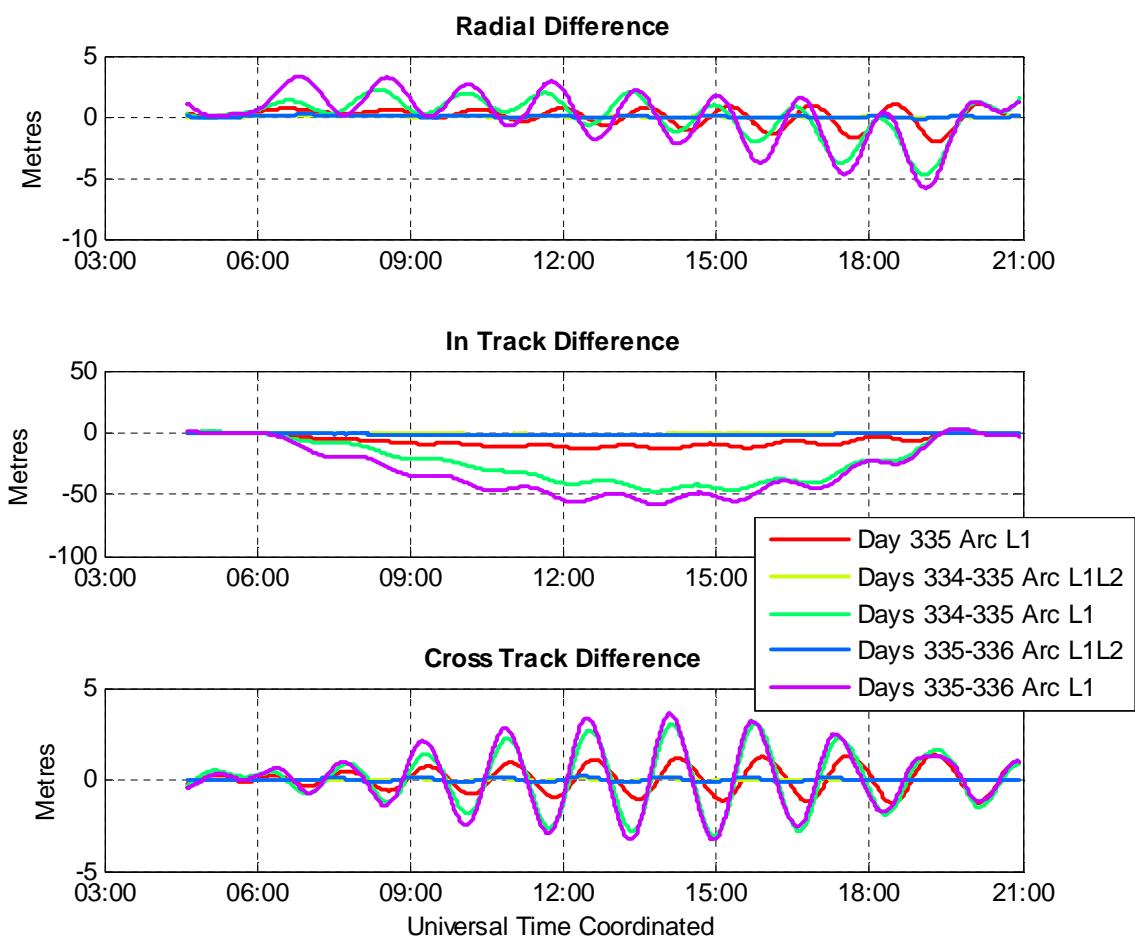


Figure C.3: Comparison with the December 1, 2010 (day 335) arc, created using L1 and L2 data

There are several patterns apparent in the data.

First, it is clear that the radio occultation data arcs suffer considerably worse accuracy than the 85 minute arcs with the antenna pointing to zenith. The worse accuracy is likely due to a combination of the poor geometry from the antenna pointing direction, the increased atmospheric effects on measurements from satellites tracked near the horizon, and above all the short measurement window providing insufficient opportunity for a good resolution of the ambiguities or observation of the satellite dynamics, as well as less time to acquire a full constellation for redundant measurements. Even when there are

measurements these short arcs appear only to be accurate to tens of meters, indicated by the poor agreement of the precise arcs processed using different strategies.

For the longer data collections, the agreement of the different processing strategies indicates that the precise orbits are accurate to approximately the 1 meter level where there are GPS measurements and to tens of meters when the position is propagated through an outage.

In both cases, it is clearly visible that the dual frequency processing option provides far greater self consistency than the single frequency processing option. Throughout the later half of the thesis the dual frequency precise orbit determination trajectories, formed with 85 minute zenith pointing GPS data sets as input, have been used as truth trajectories.